ANALYSIS OF ISLANDING DETECTION CAPABILITIES OF MULTI-INVERTER SYSTEMS

Yongzheng Zhang

A Thesis

in

The Department

of

Electrical and Computer Engineering

Presented in Partial Fulfillment of the Requirements

for the Degree of Master of Applied Science at

Concordia University

Montréal, Québec, Canada

December 2006

Copyright © Yongzheng Zhang, 2006

Library and
Archives Canada

Bibliothèque et
Archives Canada

Published Heritage
Branch

Direction du
Patrimoine de l'édition

395 Wellington Street
Ottawa ON K1A 0N4
Canada

395, rue Wellington
Ottawa ON K1A 0N4
Canada

Canada

ABSTRACT

Analysis of Islanding Detection Capabilities of Multi-Inverter Systems

Yongzheng Zhang

Islanding is one important concern for grid connected distributed resources due to personnel and equipment safety. Inverter-resident islanding detection methods (IDMs) employ locally measured parameters to detect islanding. Passive type IDMs only monitor local variables such as voltage and frequency while active IDMs inject disturbances into the supply system and detect islanding based on system responses. Although very effective in systems with a single inverter, it is believed that active frequency drifting IDMs might have their effectiveness reduced in multi-inverter systems. This thesis investigates the islanding detection capabilities of multi-inverter systems. Three possible scenarios with passive-active, different and same type of active IDMs were discussed. Their performance was assessed using the concept of non-detection zones (NDZs) in a quality factor (Q_f) vs. load resonant frequency (f_0) load parameter space extended to multi-inverter systems. This thesis also proposes the use of a small dedicated reactive power source (STATCOM) as the sole active component in a multi-inverter system. In this way, interactions between inverters with active IDMs are prevented while effective islanding detection capability is provided by the *islanding detection enhancer*. The simulation and experiment results were presented to validate the theoretical analysis and the effectiveness of the proposed techniques.

ACKNOWLEDGMENTS

The author would like to express his sincere gratitude to his supervisor, Dr. Luiz A. C. Lopes for his invaluable guidance, advice, friendship and financial support throughout the course of this study.

Special thanks to Mr. Joseph Woods for his technical support, friendship, kindness, and unconditional help.

The author would also like to thank his colleagues in the P. D. Ziogas Power Electronics Laboratory. Smart suggestions from and helpful discussions with Huili Sun, Zhixiang Luo and Neil Savio D'Souza are unforgettable.

Last but not least, the author is very grateful towards his parents whose constant support made it possible to finish the project.

To my parents

LIST OF CONTENT

LIST OF FIGURE

LIST OF TABLE

LIST OF ACRONYMS

AC   Alternating Current

AFD   Active Frequency Drift

DC   Direct Current

DG   Distributed Generation

DSP   Digital Signal Processor

HCC   Hysteresis Current Control

IDM   Islanding Detection Method

IDE   Islanding Detection Enhancer

MPPT   Maximum Power Point Tracking

NDZ   Non Detection Zone

PCC   Point of Common Coupling

PV   Photovoltaic

RMS   Root-Mean-Square value

SFS   Sandia Frequency Shift

SMS   Slip-Mode phase Shift

STATCOM   STATic synchronous COMpensator

THD   Total Harmonic Distortion

UFP/OFP   Under Frequency Protection and Over Frequency Protection

UPF   Unity Power Factor

UVP/OVP   Under Voltage Protection and Over Voltage Protection

LIST OF PRINCIPAL SYMBOLS

ω	Angular frequency
ω_0	Load resonant angular frequency
ω_g	Angular grid frequency
ω_i	Current angular frequency
ϕ_{load}	Load phase angle
ΔP	Real power mismatch
Δf_e	Frequency measurement error
ΔQ	Reactive power mismatch
C	Load Capacitance
f	Frequency
f_0	Load resonant frequency
f_{max_min}	Frequency between 59.3Hz to 60.5 Hz
f_g	Gird frequency
f_i	Current frequency
f_{is}	Islanding frequency
$f_{i(k)}$	Present current frequency
f_m	Frequency at which θ_m occurs for SMS
f_{max}	Maximum frequency
f_{min}	Minimum frequency
f_{nom}	Normal frequency that is not considered as islanding
f_{0max}	Maximum value of load resonant frequency that will result in islanding operation

f_{0min}	Minimum value of load resonant frequency that will result in islanding operation
f_{PCC}	PCC voltage frequency
f_{SMS1}	Frequency of output current of the first SMS IDM inverter with Δf_e
f_{SMS2}	Frequency of output current of the second SMS IDM inverter with Δf_e
f_v	Voltage frequency
$f_{v(k-1)}$	Voltage frequency in the previous cycle
h	Bandwidth of hysteresis control
I_{ac}	Grid ac current
i_{ac}	Instantaneous grid ac current
i_{AFD}	Instantaneous output current of PV inverter equipped with AFD IDM
I_{IDE}	RMS value of the IDE current
i_{load}	Instantaneous load current
I_{load}	Load current
I_M	Maximum magnitude of I_{IDE} with sinusoidal control method
i_{PV}	Instantaneous PV inverter output current
I_{PV}	PV inverter output current
I_{PVmax}	Maximum value of PV inverter output current
i_{PVref}	Instantaneous PV inverter reference current
i_{SMS}	Instantaneous output current of PV inverter equipped with SMS IDM
$k_{AFD\,pu}$	Ratio of the active power provided by AFD IDM inverter(s) to the total active power supplied for the load
k_{IDE}	Gain of IDE current with linear control method

xv

$k_{UPF\,pu}$	Ratio of P_{UPF} to P_{load}
L	Load inductance
L_{line}	Line equivalent inductance
P_{active}	Output power of PV inverter equipped with active IDM
P_{load}	Load real power
P_{PV}	PV inverter output real power
P_{SMS1}	Output power of the first SMS IDM inverter with Δf_e
P_{SMS2}	Output power of the second SMS IDM inverter with Δf_e
P_{UPF}	Output power of PV inverter equipped with UPF passive IDM
Q_f	Quality factor
$Q_{f\,eq}$	Equivalent quality factor
Q_{load}	Load reactive power
Q_{PV}	PV inverter output reactive power
R	Load resistance
R_{eq}	Equivalent resistance
S	Switching state
t	Time
T_s	Simulation sampling time
T_i	Period of sinusoidal part of the current
T_{PCC}	Period of PCC voltage
t_z	Dead time of PV inverter current
V_{dc}	DC side voltage of simulation
V_g	Grid voltage

v_{nom}	Normal voltage that is not considered as islanding
v_{PCC}	Instantaneous PCC voltage
V_{PCC}	PCC voltage
Z_{load_eq}	Equivalent load impedance
δf	Frequency drift
θ_{AFD}	Equivalent phase angle of current and voltage of inverter with AFD
θ_{inv}	Equivalent phase angle of inverter current and voltage
θ_{load}	Phase angle of load current and voltage ($\theta_{load} = -\phi_{load}$)
θ_{load_eq}	Equivalent phase angle of load current and voltage
θ_m	Maximum phase shift of SMS (°)
θ_{m_eq}	Equivalent maximum phase shift
θ_{SMS}	Phase angle of current and voltage of inverter with SMS
θ_{SMS1}	Maximum phase shift of the first SMS IDM inverter with Δf_e
θ_{SMS2}	Maximum phase shift of the second SMS IDM inverter with Δf_e

CHAPTER 1

INTRODUCTION

1.1 INTRODUCTION

With the current worldwide renewable energy and green power initiatives combined with the effects of the energy deregulation, Distributed Generation (DG) technologies are becoming an attractive niche supplementary energy option with reasonable profitable investment. The premise of DG is to provide electricity to a customer at a reduced cost, higher reliability and efficiency while reducing transmission and distribution losses. However the integration of DG into the main electricity networks is currently changing the paradigm which we used to live with and raises a number of issues, among which one critical concern lies in the inadvertent islanding [1, 2].

Islanding occurs when a portion of the distribution system becomes electrically isolated from the remainder of the power system, yet continues to be energized by distributed generators. The island is an unregulated power system, which may creates a safety hazard for the maintenance worker and may cause damage to power generation and power supply facilities as a result of unsynchronized re-closure [3]. In [4], it was shown that the probability of a power match is negligible with low penetration of DG in the distribution network, however the odds of islanding would increase significantly for passive inverters and very high DG penetration as what is expected to take place for the "net-zero" houses. Consequently, the ability to quickly detect and eliminate inadvertent DG supported islands is the critical safety requirement for both the distributed generators and utilities.

1

As one type of DG, the inverter-based generator is commonly connected to the secondary feeder due to its relatively small size (typically in the range of less than one kilowatt to a few megawatts) and actually works as an interface between the system and the generator, which can be photovoltaic panels, fuel cells, micro-turbines etc. Since it is the inverter that interacts with the supply system, all inverter-based DGs have operating characteristics with respect to grid interaction primarily determined by the inverter topology and controls [1]. Thus the inverter-based DGs are required to include a means to shut down when the utility source is not present in order to prevent islanding.

For successful integration of DG with utilities, clear interconnection requirements must be formulated, such as the IEEE standard 929-2000 [5] and IEEE standard 1547-2003 [6], which are meant to mandate control and protection measures to minimize the probability of an inadvertent island, and to minimize the duration of an island's existence. As a result, many inverter specific anti-islanding techniques have been proposed and a number have been implemented in actual DG projects [3] by incorporating into the controls of inverters used in utility-interactive DG applications.

However it is anticipated that the non-islanding inverters certified for independent operation can interfere with each other and yield islanding when operated in parallel. This thesis focuses on the assessment of islanding detection features of systems based on multiple photovoltaic (PV) inverters and proposes an effective way for preventing islanding in the system with multiple inverters.

1.2 ISLANDING DETECTION METHODS

Islanding detection methods (IDMs) for inverter applications may be divided into two major categories [1,3,8] shown in Fig.1-1: non inverter-resident methods and

2

inverter-resident methods. The methods not resident in the inverter are generally controlled by the utility or have communications between the inverter and the utility to cause the inverters to shut down when necessary [7]. For the relatively low power PV inverter system, it is usually not cost-effective, and there is little incentive, to communicate with utility control systems. Therefore, islanding detection and protection schemes for PV inverter systems have focused on inverter-resident methods rather than communication based techniques [1]. The inverter-resident methods can be further divided into two sub-types. One is passive methods resident in the inverter, the other is active methods resident in the inverter. In this section, we review some existing islanding detection methods resident in the inverter.
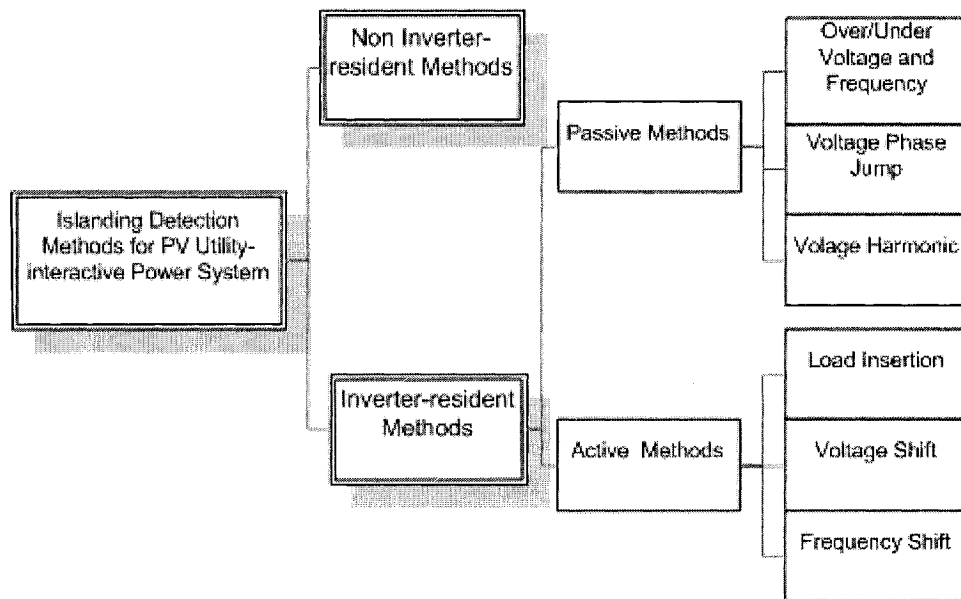
Fig. 1-1 Classification of Islanding Detection Methods for PV Utility-interactive System

3

1.2.1 PASSIVE INVERTER-RESIDENT METHODS

Passive methods for detecting an islanding condition basically monitor selected parameters such as voltage and frequency and/or their characteristics and cause the inverter to cease converting power when there is a transition from normal specified conditions [8].

1.2.1.1 Under/Over Voltage and Under/Over Frequency

The standard protections, over/under frequency protection methods (OFP/UFP) and over/under voltage protection methods (OVP/UVP), are commonly used as one passive method. All grid-connected PV inverters are required to have OFP/UFP and OVP/UVP that cause the PV inverter to stop supplying power to the utility grid if the frequency or amplitude of the voltage at the point of common coupling (PCC) between the customer and the utility strays outside of prescribed limits. Also, several other islanding prevention methods act to produce an abnormal voltage frequency or amplitude, and rely on the OFP/UFP and OVP/UVP to actually deactivate the inverter. The UVP/OVP and UFP/OFP trip thresholds and the allowed time delay are usually set according to the IEEE Std. 929-2000 shown in Table 1 [5].

Table 1-Response to abnormal voltages and frequencies [5]

Voltage (at PCC) (V)	Voltage (at PCC) of the nominal value	Frequency (Hz)	Maximum Trip Time
$V < 60$	$(V < 50\%)$	f_{nom}	6 cycles
$60 \leq V < 106$	$(50\% \leq V < 88\%)$	f_{nom}	120 cycles
$106 \leq V \leq 132$	$(88\% \leq V \leq 110\%)$	f_{nom}	Normal Operation
$132 < V < 165$	$(110\% < V < 137\%)$	f_{nom}	120 cycles
$165 \leq V$	$(137\% \leq V)$	f_{nom}	2 cycles
V_{nom}		$f < 59.3$	6 cycles
V_{nom}		$59.3 \leq f \leq 60.5$	Normal Operation
V_{nom}		$f > 60.5$	6 cycles

4

The circuit recommended in the IEEE Std. 929-2000 for assessing the islanding detection features of a given inverter is shown in Fig. 1-2 [5]. As a parallel source to a utility service, the grid-connected nonislanding PV inverter is connected to a local load, represented by a parallel RLC circuit at the PCC. The nonislanding inverter includes a means to shut down when the utility source is not present (the nonislanding feature) in order to prevent the islanding. The utility grid provides a reference ac-bus where voltage and frequency are considered to be constant. When the grid is connected, the inverter supplies active and reactive power, $P_{PV} + jQ_{PV}$, and the local load consumes active and reactive power, $P_{load} + jQ_{load}$. The utility grid supplies or absorbs the deficit or surplus of active power $\Delta P = P_{load} - P_{PV}$ and the reactive power $\Delta Q = Q_{load} - Q_{PV}$ of the local inverter-load set.
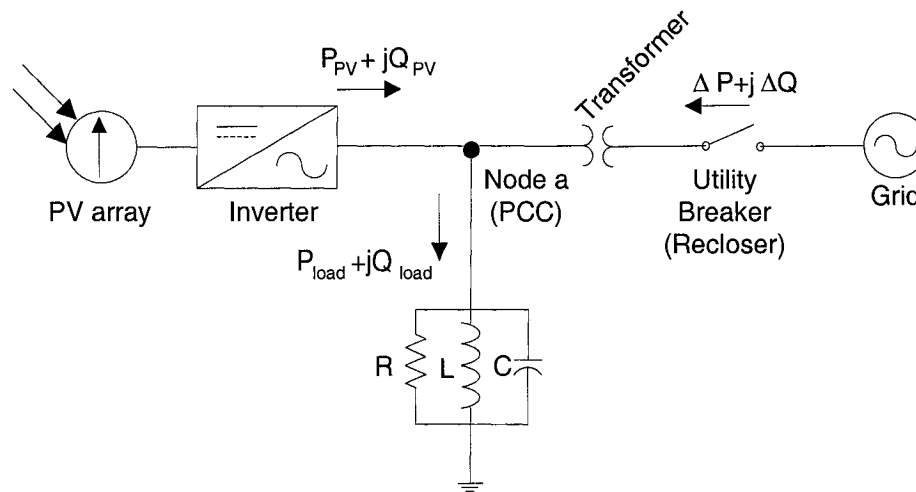
Fig. 1-2 The circuit for assessing anti-islanding features of grid-connected inverters [6]

The behavior of the system at the time of utility disconnection (islanding) will depend on ΔP and ΔQ at the instant before the switch opens to form the island. If $\Delta P \neq 0$, the RMS value of the voltage at PCC (V_{PCC}) will change, and the OVP/UVP can shut down the

5

inverter to prevent islanding, if V_{PCC} go outside of the pre-defined window. If $\Delta Q \neq 0$, the load voltage will show a sudden shift in phase, and then the inverter's control system will cause the frequency of the inverter output current, and thus the frequency of V_{PCC} to change until the reactive power balances between the PV inverter and local load occurs. This change in frequency is detected by the OFP/UFP. The OFP/UFP protection allows the inverter to disconnect if system frequency drops below or rises above pre-defined frequency values. While the method is simple, the ability of islanding detection is not guaranteed for all load conditions, especially for source-load balanced conditions when PV power penetration is high.

1.2.1.2 Voltage Phase Jump Detection

The inverter control system monitors the phase relationship of the inverter terminal voltage and output current for sudden changes. The inverter control system normally controls the output current to keep a very small phase difference between the voltage and current (unity power factor operation). A sudden change indicates that the distribution network is no longer maintaining the voltage at the inverter terminals and it has shifted in phase to match the phase angle of the local load [1,3,7]. However this method fails when the load power factor is unity.

1.2.1.3 Voltage Harmonics Detection

In this method, the inverter controller monitors the total harmonic distortion (THD) of the inverter terminal voltage and shuts down the inverter if the THD exceeds a threshold. The rationale is that, in normal operation, the distribution network acts as a stiff (low impedance) voltage source, maintaining a low distortion voltage (THD ≈ 0) on the inverter

6

terminals. Two mechanisms are expected to cause an increase in voltage THD when an island occurs. First, the impedance at the inverter terminals increases because the low impedance distribution network is disconnected and only the local load remains. As a result, current harmonics in the inverter output current will cause increased levels of voltage harmonics in the terminal voltage. Second, non-linear loads within the island, particularly distribution step-down transformers, will be excited by the output current of the inverter. The voltage response of the non-linear loads to the current excitation can be highly distorted [1,3,8]. However, setting an appropriate harmonic threshold to disconnect the inverter is nearly impossible due to presence of nonlinear loads. This renders the harmonic monitoring method as less practical.

1.2.2 ACTIVE INVERTER-RESIDENT METHODS

Active methods try to overcome the shortcomings of passive method by introducing perturbations in the inverter output. The perturbations are selected such that the response of the inverter is distinct when islanding occurs, so the active methods are generally considered more effective than the passive ones [9-19].

1.2.2.1 Load insertion techniques

The inverter can periodically connect a load impedance across its output terminals and monitor changes that occur. For example, a capacitor can be inserted across the output to increase the reactive current and the resulting phase shift in terminal voltage can be measured to calculate the effective line impedance. This has similarities to the passive phase jump detection method but since detection of the phase jump can be correlated with the insertion of the impedance, it is more resistant to false trips due to random phase jumps

7

in the grid voltage. As with other impedance measurement techniques, there are concerns about interference among multiple units and the ability to reliably detect impedance changes with practical values of the inserted load.

1.2.2.2 Voltage shift techniques

Voltage shift techniques apply positive feedback to the current or active power regulation control loop of the inverter to cause the inverter terminal voltage to rapidly shift to the under/over voltage detection threshold if the distribution network is not present to maintain the voltage. Without this positive feedback, the terminal voltage changes to a new stable operating point, largely determined by the resistance of the local load, when an island occurs and the distribution network is disconnected. This operating point may be within the under/over frequency limits of the inverter if the load is closely matched to the inverter's active and reactive power output. The positive feedback introduces instability that drives the inverter terminal voltage towards one of the voltage limits.

1.2.2.3 Frequency shift techniques

The main concept behind the operation of frequency drifting IDMs is that the frequency of an islanded system drifts until reactive power balance is achieved. That is, when the reactive power consumed by the load is equal to that produced by the local source, PV inverter. The reactive power of inverters equipped with frequency drifting IDMs is controlled as a function of the system frequency with positive feedback. It can be shown that a parallel RLC load becomes more capacitive when the system frequency increases, thus supplying more reactive power. If the inverter increases the amount of reactive power it absorbs as the frequency increases, the load of an islanded system is

8

forced to supply more reactive power and the system frequency tends to increase. Therefore, operation within the normal frequency range (59.3 Hz to 60.5 Hz for a 60Hz system) can be made unstable when the grid is disconnected by controlling the inverter with a rate of change of reactive power different with that presented by the local load. In such a case, either the UFP or the OFP of the inverter will trip preventing islanding. Following two frequently used frequency drift methods will be introduced in detail. They are the active frequency drift (AFD) method and the slip mode frequency shift (SMS) method.

In active frequency drift (AFD), the waveform of the inverter current is slightly distorted presenting a zero current segment for a drift-up operation. AFD can be implemented by forcing the current frequency to be δf (< 1.5 Hz) above the voltage frequency in the previous cycle ($f_{i(k)} = f_{v(k-1)} + \delta f$) and keeping the inverter current equal to zero from the end of its negative semi-cycle until the positive zero crossing of the voltage. When the grid is present, it maintains the voltage frequency. Otherwise, the frequency of the voltage at the PCC tends to drift upward, reaching values superior to the resonant frequency of the local RLC load (f_0). In both cases, the fundamental component of the current leads the voltage by a small angle θ_{AFD}.

For AFD implemented with a constant frequency drift, the current in each cycle is expressed by

$$i_{PV(k)} = \sqrt{2}I \sin[2\pi(f_{v(k-1)} + \delta f)]t \qquad (1\text{-}1)$$

In the steady state and under islanding conditions, from Fig. 1-3, one can see that although the PV inverter output current has the same zero crossing point with the PCC voltage, the current waveform is neither odd nor even. In order to simplify the calculation

9

of the phase angle between of the fundamental components of the voltage and the current,

the start of the fundamental current has been moved by $-t_z/2$. Thus, the fundamental

component of the inverter output current leads the PCC voltage by an angle proportional to

$-t_z/2$. the phase angle of the inverter θ_{inv} can be approximated by

$$\frac{t_z/2}{T_v} = \frac{\theta_{AFD}}{2\pi} \tag{1-2}$$

where, $t_z = \dfrac{1}{f_v} - \dfrac{1}{f_i} = \dfrac{1}{f} - \dfrac{1}{f+\delta f} = \dfrac{\delta f}{f(f+\delta f)}$.

The inverter angle for the AFD IDM is given by

$$\theta_{AFD} = \pi \, f \, t_z = \frac{\pi \delta f}{f+\delta f} \tag{1-3}$$

This phase angle plays an important role in mapping the no detection zone (NDZ),

which will be discussed in the next section.
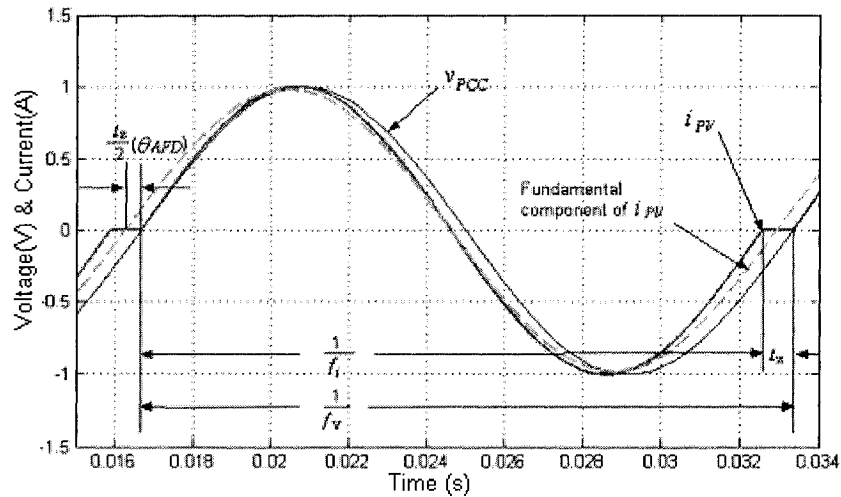
Fig. 1-3 Current and voltage waveforms of upward AFD IDM

In the slip mode frequency shift (SMS) method, the phase angle of the current is

controlled as a function of the deviation of the frequency of the voltage in the previous

cycle $f_{v(k-1)}$ from the nominal operating frequency of the utility grid f_g. By applying

10

positive feedback to the current angle, one manages to vary the short-term frequency of

the load voltage, when the grid is disconnected, until reactive power balance is achieved.

The inverter current is then defined as

$$i_{PV(k)} = \sqrt{2}I \sin\left(2\pi f_{v(k-1)}t + \theta_{SMS}\right)$$ (1-4)

The phase shift θ_{SMS} is set to be a sinusoidal function of the deviation of the

frequency from the grid frequency f_g, then

$$\theta_{SMS} = \theta_m \sin\left(\frac{\pi}{2} \frac{f_{v(k-1)} - f_g}{f_m - f_g}\right),$$ (1-5)

where f_m is the frequency at which the maximum phase shift θ_m occurs.

Comparing with the voltage shift techniques, the frequency shift techniques can

reduce the impact on the dc side of the inverters since reactive power is not reflected to the

dc side of the inverter and the amount of reactive power required for effective frequency

shifting is smaller than that of active power required for effective voltage drifting [8].

However like other active islanding detection methods, the frequency shift methods, such

as AFD and Sandia Frequency Shift (SFS), slightly degrade the power quality of the PV

system by injecting low frequency current harmonics.

1.3 ASSESSMENT OF ISLANDING DETECTION METHODS WITH NDZ

One of the main limitations with local detection schemes is that each scheme has an

operating region where islanding conditions cannot be detected. This region is called the

non-detection zone (NDZ). NDZ is one of the most important indexes to assess the

performance of islanding detection methods (IDMs). This is defined as the range of local

11

loads (that is, loads inside the potential island) for which the islanding detection methods (IDMs) under consideration can be made to fail to detect islanding [9-13].

Traditionally the effectiveness of the passive (monitoring only) IDM can be represented by a non-detection zone (NDZ) defined in a power imbalance or mismatch space (ΔP vs. ΔQ) [13]. However the use of NDZs in the power mismatch ΔP vs. ΔQ space is not adequate for assessing the performance of most of active IDMs since for a given reactive power mismatch different combinations of L and C are possible [9]. Some of these combinations result in islanding while others do not. However a new load parameter space based on the quality factor and resonant frequency of the load (Q_f vs. f_0) can be used for plotting the NDZs of these frequency drifting IDMs. The assessment of the performance of a given IDM applied to a given load can be done by inspection. One can easily identify if a given IDM design meets the design specifications and for what cases it fails. This Section is organized in three parts. At first the characteristics of the local load are presented; then the concept and the principle behind the plotting NDZ in $Q_f \times f_0$ load parameter space will be explained; at last the NDZs of the different IDMs are analyzed in the $Q_f \times f_0$ load parameter space.

1.3.1 PARALLEL RLC LOAD FREQUENCY CHARACTERISTICS

The values of the frequency and magnitude of the voltage at the PCC after grid disconnects (islanding condition) heavily depend upon the local load characteristics. It is important to derive the equations related to the load that are required to analyze the operating principles and assess the performance of common IDMs [9]. Usually the local load (the load inside the potential island) is modeled as a parallel *RLC* circuit. This is done because for most IDMs it is some type of *RLC* load that causes the most difficulty in

12

detection. In general, nonlinear loads such as harmonic-producing loads or constant-power loads do not present as much difficulty in islanding detection [10,14].

According to the IEEE Std. 929-2000 [4], the quality factor (Q_f) is defined as: two pi times the ratio of the maximum stored energy to the energy dissipated per cycle at a given frequency.

$$Q_f = 2\pi \frac{Maximum\ Energy\ Stored}{Total\ Energy\ Lost\ In\ One\ Period} \tag{1-6}$$

For a parallel RLC load

$$Q_f = \frac{2\pi\left(\frac{1}{2}CR^2I^2\right)}{\pi RI^2\Big/\omega_0} = \omega_0 RC = \frac{R}{\omega_0 L} = R\sqrt{\frac{C}{L}} \tag{1-7}$$

where, $\omega_0 = 2\pi f_0 = \dfrac{1}{\sqrt{LC}}$.

The magnitude and phase of a parallel RLC load at an arbitrary frequency (f), as a function of the quality factor (Q_f) and resonant frequency (f_0) of the load are given by:

$$|Z_{load}| = \frac{1}{\sqrt{\dfrac{1}{R^2}+\left(\dfrac{1}{\omega L}-\omega C\right)^2}} = \frac{R}{\sqrt{1+Q_f^2\left(\dfrac{f_0}{f}-\dfrac{f}{f_0}\right)^2}} \tag{1-8}$$

$$\phi_{load} = \tan^{-1}\left(R\frac{1-\omega^2 LC}{\omega L}\right) = \tan^{-1}\left[Q_f\left(\frac{f_0}{f}-\frac{f}{f_0}\right)\right] \tag{1-9}$$

The load current voltage (C-V) phase angle (θ_{load}), that represents the angle by which the current leads the voltage, is given by

$$\theta_{load} = -\phi_{load} = \tan^{-1}\left[Q_f\left(\frac{f}{f_0}-\frac{f_0}{f}\right)\right]. \tag{1-10}$$

The load phase angle θ_{load} ($\theta_{load} = -\phi_{load}$) vs. frequency characteristic curves of loads with different quality factors and different resonant frequencies f_0 are shown in Fig. 1-4. There one sees that the larger Q_f, the larger is the variation of θ_{load} for a certain variation

13

of the system frequency around f_0. In addition, the intersection of the θ_{load} vs. f curves and

the zero phase angles always takes place at f_0. Further, one can see that a load with $f_0 < f_g$

is net capacitive at grid frequency since the current leads the voltage ($\theta_{load} > 0°$).

Conversely, a load with $f_0 > f_g$ is net inductive at grid frequency.
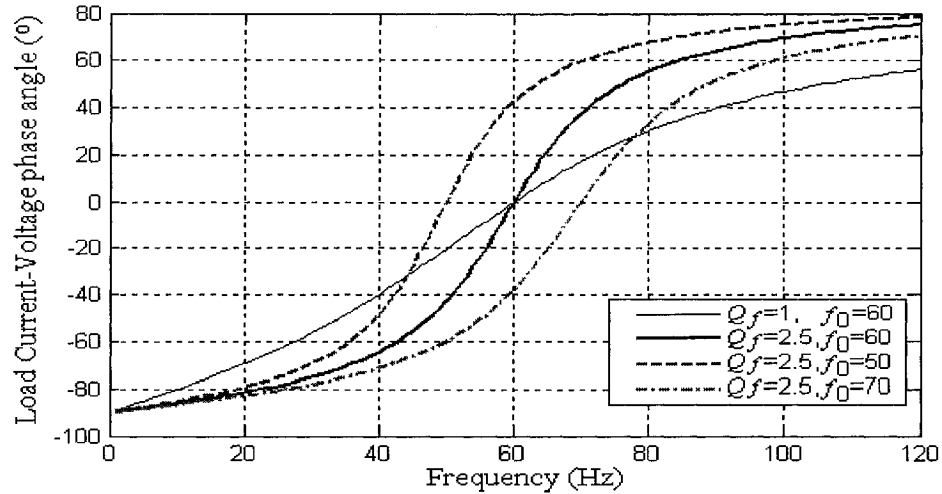
Fig. 1-4 Variation of the load angle of a RLC load with frequency for different values of

resonant frequency (f_0) and quality factor (Q_f)

1.3.2 CONCEPT BEHIND THE $Q_f \times f_0$ NDZ

The principle behind the $Q_f \times f_0$ load parameter space is called the phase criteria [10].

It says that the frequency of an islanded system in the steady-state condition is that where

the angle θ_{load} by which the load current leads the PCC voltage is equal to that of the

inverter θ_{inv}, that is

$$\theta_{load}(f) = \theta_{inv}(f) \tag{1-11}$$

In order to calculate the boundaries for islanding detection one needs to obtain an

equation that represents the steady-state frequency of the voltage across the PCC as a

function of the load parameters (Q_f and f_0) and also as a function of the main

parameters of the active IDM methods. Therefore, from (1-10) and (1-11),

14

$$\tan^{-1}\left[Q_f\left(\frac{f}{f_0}-\frac{f_0}{f}\right)\right]=\theta_{inv}(f).\tag{1-12}$$

Thus, one can get

$$f_0^{\ 2}+\frac{\tan\theta_{inv}(f)f}{Q_f}f_0-f^2=0.\tag{1-13}$$

Then the resonant frequency f_0 which will cause the islanding operation can be solved as the function of the islanding frequency f_{is} and the inverter equivalent angle, and the negative value can be neglected:

$$f_0=\frac{f_{is}}{2Q_f}\left(-\tan\theta_{inv}(f_{is})+\sqrt{\tan^2\theta_{inv}(f_{is})+4Q_f^{\ 2}}\right).\tag{1-14}$$

In order to calculate the NDZ, one imposes the islanding frequency to be a threshold frequency (f_{max} and f_{min}), varies the value of Q_f and then calculates the resonant frequency of the load at the threshold of the NDZ. Thus, if we can find equivalent inverter angle for some IDM, the NDZ for the corresponding IDM can be plotted by applying Equation (1-14) [18].

1.3.3 NDZs in The Q_f vs. f_0 Load Parameter Space

1.3.3.1 NDZ of Passive IDM

Since the passive IDM does not apply any disturbances to the current, for a stand-alone and unity power factor with current control inverter, its inverter angle is always equal to zero, that is

$$\theta_{inv}=0\tag{1-15}$$

Applying equation (1-14), one can get

$$f_0=f_{is}\tag{1-16}$$

15

So the finial frequency of the inverter system with passive IDM after grid disconnected will be the resonant frequency of the load (f_0). If $f_{min} \leq f_0 \leq f_{max}$, UFP/OFP will not trip and islanding will occur regardless of the Q_f of the load.

1.3.3.2 NDZ of Active Frequency Drift (AFD) IDM

The operation principle of this method was discussed in Section 1.2.2.3. The phase angle of the inverter with AFD IDM was calculated and shown in Equation 1-3. Applying the phase criteria ($\theta_{load} = \theta_{AFD}$),

$$- \tan^{-1} \left[Q_f \left(\frac{f_0}{f_{is}} - \frac{f_{is}}{f_0} \right) \right] = \frac{\pi \, \delta f}{f_{is} + \delta f} \tag{1-17}$$

Thus,

$$f_0^2 - \frac{f_{is} \tan[\theta_{AFD}(f_{is})]}{Q_f} f_0 - f_{is}^2 = 0 \tag{1-18}$$

In order to calculate the NDZ of the AFD IDM, one imposes the islanding frequency to be a threshold frequency (f_{min} or f_{max}), varies the value of Q_f and then calculates the resonant frequency f_0 of the load at the threshold of the NDZ.

Fig. 1-5 shows the NDZ for AFD IDM for different values of δf for a normal frequency range of 59.3Hz $\leq f \leq$ 60.5Hz. There one sees that the main effect of the AFD is to shift the NDZ to lower values of f_0 as δf increases. For $Q_f = 2.5$ and $\delta f = 0.5$ Hz the method will fail to detect islanding for loads with 58.99Hz $\leq f_0 \leq$ 60.19Hz. According to Fig.1-5, no islanding would occur for inductive loads with $Q_f < 3$ if speed-up AFD IDM with $\delta f = 1$ Hz is used. For loads with high Q_f this active IDM does not present any improvement with respect to the passive UFP/OFP because the frequency drifting capacity is significantly reduced.

16
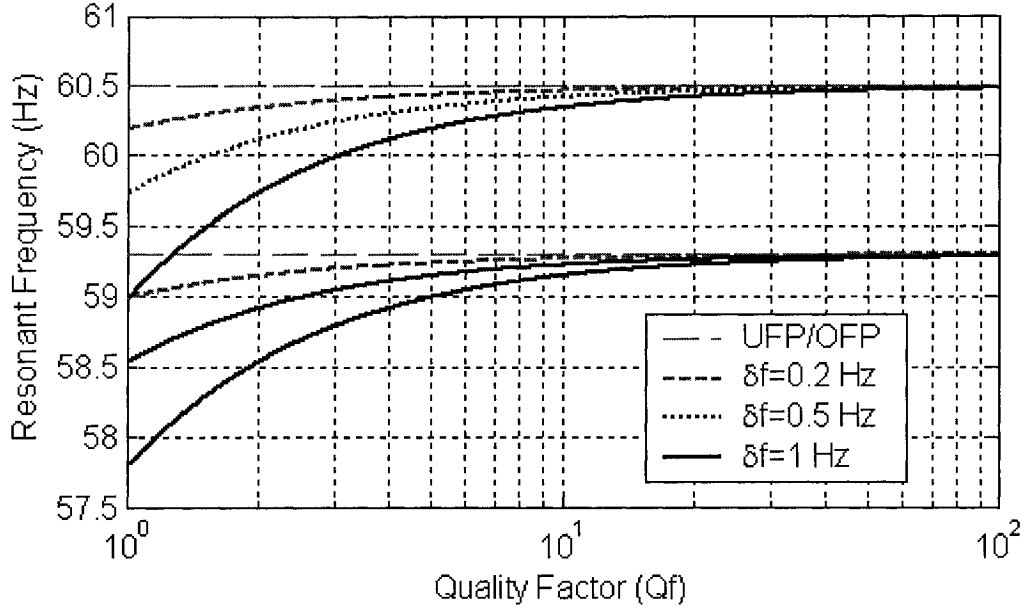
Fig. 1-5 NDZs of AFD IDM for different values of $\delta\! f$

1.3.3.3 NDZ of Slip Mode Frequency Shift (SMS) IDM

The operation principle of this method was discussed in Section 1.2.2.3. The phase angle of the inverter with AFD IDM was calculated and shown in Equation 1-5. The NDZ of the SMS IDM in the Q_f vs. f_0 space is derived using the phase criteria:

$$-\tan^{-1}\left[Q_f\left(\frac{f_0}{f_{is}}-\frac{f_{is}}{f_0}\right)\right]=\theta_m\sin\left(\frac{\pi}{2}\frac{f_{is}-f_g}{f_m-f_g}\right) \tag{1-19}$$

Thus,

$$f_0^2-\frac{f_{is}\tan[\theta_{SMS}(f_{is})]}{Q_f}f_0-f_{is}^2=0 \tag{1-20}$$

The resulting NDZ for SMS IDM in the Q_f vs. f_0 space obtained from the solution of (1-20) is shown in Fig. 1-6 for different values of θ_m. There one sees that the NDZ is null for $Q_f < 2.5$ when $\theta_m = 10°$ and $f_m - f_g = 3$Hz, as per the design specifications. Besides, as θ_m decreases, the maximum Q_f of the loads for which islanding can be prevented also decreases. It is worth mentioning that although large values of θ_m allow islanding

17

detection of loads with large Q_f, the maximum amount of active power the inverter can inject, without exceeding its rated apparent power, is reduced.
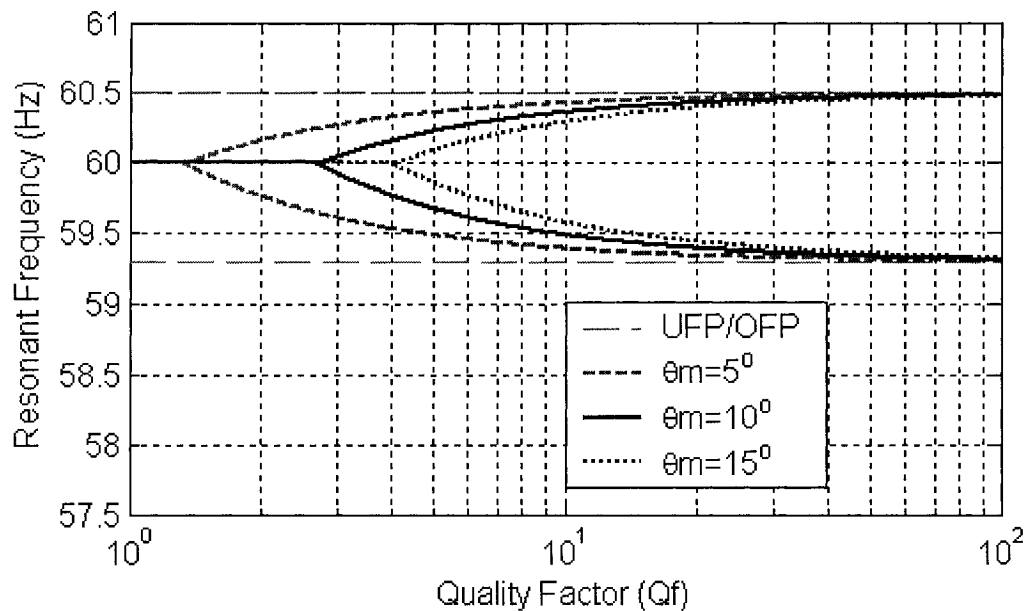
Fig. 1-6 NDZs of SMS IDM for different θ_m and with $f_m - f_g = 3$ Hz.

1.4 THESIS SCOPE AND CONTRIBUTIONS

A number of islanding detection methods have been implemented in actual project applications [3]. Although very effective in systems with a single inverter, it is believed that frequency drifting active IDMs might have their effectiveness reduced in multi-inverter systems. This thesis assesses the islanding detection capabilities of systems with multiple inverters. The main contributions of this thesis are the following:

1. Extend the concept of phase criteria used for single inverter systems to the multi-inverter systems. Based on that, the NDZs of the multi-inverter systems are deduced and used for the analysis of anti-islanding capacity of the multi-inverter systems.

18

2. Proposes a method based on the use of STATCOM to reduce or eliminate the NDZ of multi-inverter systems. In this case, all inverters can be of the passive IDM type, so that interference between active IDMs is prevented.

3. A multi-inverter system laboratory prototype was built and the experimental results verified the theoretical analysis and computer simulation.

1.5 THESIS OUTLINE

The contents of this thesis are organized in four Chapters.

The first Chapter introduces the topic of anti-islanding and some common used IDMs, also explains how to create NDZs based on the phase criteria for the single inverter systems.

The second Chapter further utilizes the phase criteria to produce the new NDZs for the assessment of multi-inverter systems. Three different case studies are presented to analyze how the frequency drifting methods can interfere with each other in the multi-inverter system. The simulation and experiment results are presented to validate the theoretical analysis.

The third Chapter proposes a method to eliminate the potential islanding in multi-inverter systems. The effectiveness of the proposed scheme is demonstrated with simulation and experimental results.

The forth Chapter summarizes the work carried out in this thesis and the final conclusions. Suggestions for future work on this topic are presented.

CHAPTER 2

ACTIVE FREQUENCY DRIFTING IDMS IN MULTI-INVERTER SYSTEMS

2.1 INTRODUCTION

From the previous chapter one can clearly find that active IDMs can effectively reduce the NDZ of the passive methods in single-inverter systems. However, it is believed that in systems with multiple inverters equipped with active IDMs, non-islanding inverters certified for independent operation can interfere with each other averaging their effects out and failing to detect islanding [21,22]. With increased deployment or even expansion of PV systems, it is very likely that actual islands will contain multiple inverters. Therefore, it is of paramount importance to investigate not only the way IDMs affect each other but also whether and when islanding becomes more likely to occur in multi-inverter systems.

This chapter discusses three possible scenarios that can be found in a system with multiple PV inverters. The first is a system with one inverter equipped with an active frequency drifting IDM while the others present standard passive IDM. A procedure for identifying how the share of power supplied by the passive IDM affects the NDZ of a nonislanding active IDM inverter (for net inductive loads with quality factor smaller or equal to 2.5) is presented. The second case concerns a system with nonislanding active IDM inverters of two different types that are very common: active frequency drift (AFD) and slip mode frequency shift (SMS). An expression for the NDZ of this system in a load parameter space is derived and the effects of the ratio of the power capacity of the

20

inverters with AFD and SMS IDMs on the size of the NDZ are identified. The last case involves a system with two inverters equipped with the same type of active IDM (SMS) but with errors in the system's frequency measurements. The impact of the magnitude of this error on the NDZ of the system is analyzed. Both simulation and experiment results will be shown to demonstrate the effectiveness of the theoretical analysis at the end of this chapter.

2.2 NDZS OF MULTI-INVERTER SYSTEMS

From the previous chapter we learned that the phase criteria is the basic theory to analyze the islanded system in a Q_f vs. f_0 load parameter space. With it we can obtain the expression to caculate the NDZs for different IDMs of single inverter system. This theory is still applicative for the study of islanding of the multi-inverter system. The following approach is employed for assessing the islanding detection capabilities of multi-inverter systems with NDZs in the Q_f vs. f_0 load parameter space. All active IDM inverters are lumped together so that an angle for the current of an equivalent active IDM inverter can be calculated and then used for computing the NDZ applying the equation (1-14). On the other hand, the passive IDM inverters do not affect directly the NDZ curve of the multi-inverter system. They are combined with the local load, leading to an equivalent load with the same f_0 of the original local load but with a higher Q_f. The advantages of this approach can be demonstrated with the following case studies.

2.2.1 ACTIVE AND PASSIVE IDM INVERTERS SYSTEM

This system is composed of one active and one or more passive IDM inverters. The analysis of this configuration can be carried out by recognizing that the UPF passive IDM

21

inverter(s) only share the local load's active power with the inverter equipped with active frequency drifting IDM. The latter has to absorb (supply) all reactive power supplied (absorbed) by the local load, as the frequency of the island drifts from the rated value. Since the load power is shared by the passive and the active frequency drifting inverters,

$$P_{active} + P_{UPF} = P_{load} = \frac{V^2}{R} \tag{2-1}$$

Therefore, one can replace the UPF passive IDM inverter(s) with a negative resistance, resulting in an increase in the equivalent resistance of the local load. For the moment only active IDM inverter supplys the active power for the equivalent load.

$$P_{active} = P_{load} - P_{UPF} = \frac{V^2}{R_{eq}} \tag{2-2}$$

Comparing equation (2-1) with equation (2-2), one can get,

$$R_{eq} = \frac{R}{1 - \frac{P_{UPF}}{P_{load}}} = \frac{R}{1 - K_{UPF\,pu}} \tag{2-3}$$

where $K_{UPF\,pu} = \frac{P_{UPF}}{P_{load}}$, the ratio of the active power provided by UPF passive IDM inverter(s) to the total active power supplied for the load. Thus the equivalent resistance of the local load R_{eq} can be computed as a function of $K_{UPF\,pu}$.

With this equivalent resistance, the equivalent quality factor of the local load plus the passive inverter(s) is given by

$$
\begin{aligned}
Q_{f\,pu} &= R_{eq}\sqrt{\frac{C}{L}} \\
&= \frac{1}{1 - K_{UPF\,pu}} \cdot (R\sqrt{\frac{C}{L}}) \\
&= \frac{Q_f}{1 - K_{UPF\,pu}}
\end{aligned}
\tag{2-4}
$$

22

Thus, for the analysis of islanding detection capabilities, the active IDM inverter sees an equivalent load with the same f_0 as the original load but with a higher Q_f. The NDZ plots in the load parameter space developed for the single active IDM inverters can still be used provided that the value of Q_f for the equivalent load is recalculated as in (2-4). As an example, consider the case of a nonislanding active IDM inverter designed for a load with $Q_f \le 2.6$ and that operates in parallel with UPF inverters that supply half of the load's active power ($K_{UPF\,pu} = 0.5$). The equivalent load (UPF inverter + original load) presents a Q_f twice as large as that of the original load, what should increase the odds of islanding. In such a case, the active IDM inverter will only be able to prevent islanding for a local load with $Q_f \le 1.3$.

2.2.2 SYSTEM WITH AFD AND SMS IDM INVERTERS

In this analysis it is assumed that if more than one AFD IDM inverter exist, they have identical settings (δf). The same applies to the settings of the SMS inverter(s), i.e. θ_m and $f_m - f_g$. It is also assumed that the AFD IDM inverter(s) supply K_{AFDpu} of the load's active power while the SMS IDM inverter(s) supply $1 - K_{AFDpu}$. The currents of these IDMs are defined as

$$i_{AFD} = I_{AFD} \sin(2\pi f\, t) = I \cdot K_{AFD\ pu} \cdot \sin(2\pi f\, t + \theta_{AFD}) \tag{2-5}$$

$$i_{SMS} = I_{SMS} \sin(2\pi f\, t + \theta_{SMS}) = I \cdot (1 - K_{AFD\ pu}) \cdot \sin(2\pi f\, t + \theta_{SMS}) \tag{2-6}$$

where θ_{AFD} and θ_{SMS} are the phase angles of the AFD and SMS IDM inverters respectively, which are shown in the equation (1-3) and (1-5). The total current supplied by the inverters is,

$$\begin{aligned} i_{inv} &= i_{AFD} + i_{SMS} \\ &= I \cdot K_{AFD\ pu} \cdot \sin(2\pi f\, t + \theta_{AFD}) + I \cdot (1 - K_{AFD\ pu}) \cdot \sin(2\pi f\, t + \theta_{SMS}) \end{aligned} \tag{2-7}$$

23

Assume $\sin^2 \beta = K_{AFD\ pu}$, $(0 < k < 1, \beta \in (0, \pi/2))$, $\omega = 2\pi f$

$$i_{inv} = I \cdot [\sin^2(\beta) \cdot \sin(\omega t + \theta_{AFD}) + \cos^2(\beta) \cdot \sin(\omega t + \theta_{SMS})]$$
$$= I \cdot [\sin(\omega t) \cdot (\sin^2 \beta \cdot \cos \theta_{AFD} + \cos^2 \beta \cdot \cos \theta_{SMS})$$
$$+ \cos(\omega t) \cdot (\sin^2 \beta \cdot \sin \theta_{AFD} + \cos^2 \beta \cdot \sin \theta_{SMS})] \qquad (2\text{-}8)$$
$$= I \cdot \sqrt{A^2 + B^2} \cdot \sin(\omega t + \arctan \frac{B}{A})$$

Where $A = \sin^2 \beta \cdot \cos \theta_{AFD} + \cos^2 \beta \cdot \cos \theta_{SMS}$, $B = \sin^2 \beta \cdot \sin \theta_{AFD} + \cos^2 \beta \cdot \sin \theta_{SMS}$

$$\sqrt{A^2 + B^2}$$
$$= \sqrt{(\sin^2 \beta \cdot \cos \theta_{AFD} + \cos^2 \beta \cdot \cos \theta_{SMS})^2 + (\sin^2 \beta \cdot \sin \theta_{AFD} + \cos^2 \beta \cdot \sin \theta_{SMS})^2}$$
$$\qquad (2\text{-}9)$$
$$= \sqrt{1 - \frac{1}{2}\sin^2 2\beta \cdot [1 - \cos(\theta_{AFD} - \theta_{SMS})]}$$
$$\approx 1$$

The angle of the current of the equivalent active IDM inverter can be calculated as

$$\theta_{inv}(f) = \arctan \frac{B}{A}$$
$$= \arctan \frac{\sin^2 \beta \cdot \sin \theta_{AFD} + \cos^2 \beta \cdot \sin \theta_{SMS}}{\sin^2 \beta \cdot \cos \theta_{AFD} + \cos^2 \beta \cdot \cos \theta_{SMS}} \qquad (2\text{-}10)$$
$$= \arctan \frac{\tan^2 \beta \cdot \sin \theta_{AFD} + \sin \theta_{SMS}}{\tan^2 \beta \cdot \cos \theta_{AFD} + \cos \theta_{SMS}}$$

The NDZ for this system can be calculated using the phase criteria ($\theta_{inv} = \theta_{load}$) as described in the previous chapter. By substituting equation (2-10) into (1-14) and replacing the islanding frequency f_{is} by the frequency threshold f_{max} and f_{min}, the boundary of the NDZ for this system will be obtained as

$$f_{0\max} = \frac{f_{max}}{2Q_f}\left(-\tan \theta_{inv}\left(f_{max}, K_{AFD\ pu}\right) + \sqrt{\tan^2 \theta_{inv}\left(f_{max}, K_{AFD\ pu}\right) + 4Q_f^2}\right), (f_{0\max} > f_{0\min})$$

$$(2\text{-}11\text{a})$$

$$f_{0\min} = \frac{f_{min}}{2Q_f}\left(-\tan \theta_{inv}\left(f_{min}, K_{AFD\ pu}\right) + \sqrt{\tan^2 \theta_{inv}\left(f_{min}, K_{AFD\ pu}\right) + 4Q_f^2}\right), (f_{0\min} < f_{0\max})$$

$$(2\text{-}11\text{b})$$

24

Fig. 2-1 shows the resulting NDZs for a system with different shares of active power

supplied by SMS and AFD IDM inverters. The parameters of the IDMs are $\theta_m = 10°$, $f_m -$

$f_g = 3$Hz for the SMS and $\delta f = 1$ Hz for the AFD. It is worth mentioning that these two

inverters are nonislanding when they operate alone in a local system with net inductive

loads with $Q_f \leq 2.5$. Nonetheless, islanding can occur when the SMS and the AFD IDM

inverters operate together supplying inductive local loads with $Q_f \leq 2.5$. This also can be

explained by the fact that when local loads presents $f_0 < f_g$, the AFD IDM attempts to drift

the frequency up while the SMS IDM attempts to drift it down. As a result, they might

offset each other and the islanding frequency can remain within the normal frequency

range (59.3Hz $\leq f \leq 60.5$Hz) resulting in islanding.
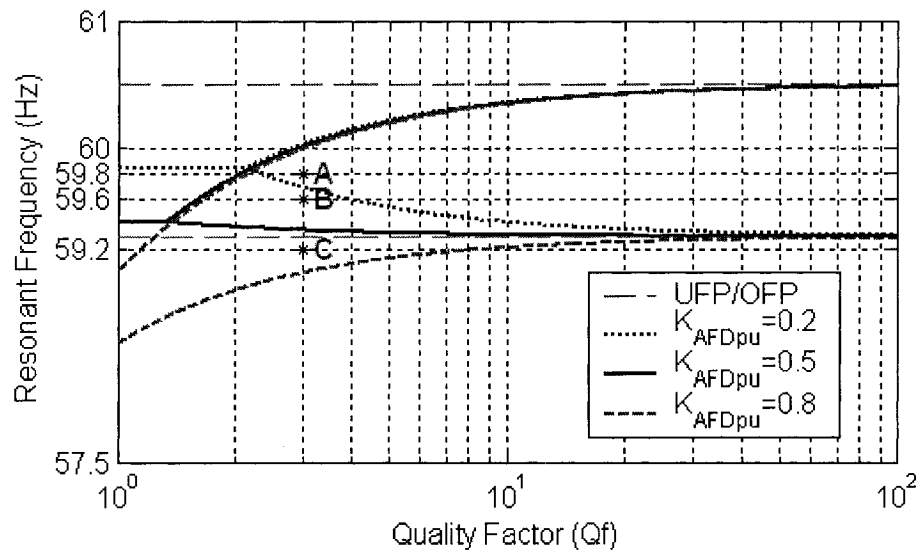
Fig. 2-1 NDZ of a multi-inverter system with both AFD and SMS IDMs.

Figure 2-1 shows three load cases (A, B and C) for which islanding detection

depends on the power ratings of the AFD and SMS IDM inverters. According to those

25

NDZs, load A would be islanded for the three inverter arrangements, load B would be islanded for two while load C only for one inverter combination.

2.2.3 SYSTEM WITH TWO SIMILAR ACTIVE (SMS) IDM INVERTERS BUT WITH FREQUENCY MEASUREMENT ERRORS

SMS IDM inverters have been chosen for this analysis because they have the potential for interfering with each other under certain conditions. It is assumed that there are frequency measuring errors Δf_e in both SMS IDMs caused by miscalibrated sensors. As a worst case scenario for inverters of same capacity, it is assumed that the errors present the same magnitude and opposite signs. To simplify the notation, $f_{v(k-1)}$ is replaced in this analysis by f. Thus, the frequencies of the output current from the two SMS IDM inverters become,

$$f_{SMS1} = f + \Delta f_e \tag{2-12}$$

$$f_{SMS2} = f - \Delta f_e \tag{2-13}$$

The problem in this case can arise due to the fact that whenever the measured voltage frequency (f) is above the central frequency (f_g) the SMS IDM attempts to increase the system's frequency by absorbing reactive power. Otherwise it attempts to decrease it. Therefore, for the conditions mentioned above and at nominal grid frequency, the two SMS IDMs tend to offset each other, possibly leading to islanding.

In this analysis, it is assumed that except the error in the frequency measurements, the inverters present the same capacity ($P_{SMS1} = P_{SMS2} = 0.5P_{load}$) and the same parameters for the SMS IDM ($\theta_m = 10°$, $f_m - f_g = 3Hz$). The NDZ of such a system is obtained for different values of frequency measurement error (Δf_e) to verify its impact on the variation of the size of the NDZ.

26

The current injected by the two inverters is given by

$$i_{inv} = i_{SMS1} + i_{SMS2}$$

$$= \frac{I}{2}\sin(2\pi f_{SMS1} t + \theta_{SMS1}) + \frac{I}{2}\sin(2\pi f_{SMS2} t + \theta_{SMS2}) \qquad (2\text{-}14)$$

$$\theta_{SMS1} = \theta_m \sin\left(\frac{\pi}{2}\frac{(f + \Delta f_e) - f_g}{f_m - f_g}\right) \qquad (2\text{-}15)$$

$$\theta_{SMS2} = \theta_m \sin\left(\frac{\pi}{2}\frac{(f - \Delta f_e) - f_g}{f_m - f_g}\right) \qquad (2\text{-}16)$$

For relatively small values of Δf_e the approximation below is valid.

$$i_{inv} \approx I \cos(\frac{\theta_{SMS1} - \theta_{SMS2}}{2})\sin(2\pi f t + \frac{\theta_{SMS1} + \theta_{SMS2}}{2}) \qquad (2\text{-}17)$$

The angle of the current of the equivalent SMS IDM inverter can be calculated as

$$\theta_{inv} = \frac{\theta_{SMS1} + \theta_{SMS2}}{2}$$

$$= \frac{1}{2}\theta_m \left[\sin\left(\frac{\pi}{2}\frac{(f + \Delta f_e) - f_g}{f_m - f_g}\right) + \sin\left(\frac{\pi}{2}\frac{(f - \Delta f_e) - f_g}{f_m - f_g}\right)\right]$$

$$= \frac{1}{2}\theta_m \cos\left(\frac{\pi}{2}\frac{\Delta f_e}{f_m - f_g}\right) \cdot \sin\left(\frac{\pi}{2}\frac{f - f_g}{f_m - f_g}\right) \qquad (2\text{-}18)$$

$$= \theta_{m\_eq} \sin\left(\frac{\pi}{2}\frac{f - f_g}{f_m - f_g}\right)$$

where, $$\theta_{m\_eq} = \theta_m \cos\left(\frac{\pi}{2}\frac{\Delta f_e}{f_m - f_g}\right) \qquad (2\text{-}19)$$

By comparing equation (2-18) and (2-19) to (1-11), one concludes that the frequency measurement error results in a reduction of the magnitude of the maximum phase shifting angle (θ_{m_eq}). As mentione in Section 1.3.3.3, the smaller the value of θ_m, the smaller is the largest value of Q_f for which islanding can be prevented with SMS IDM. However, even for relatively large values of error (~ 0.5 Hz), the magnitude of (θ_{m_eq}) decreases by

27

only 3.4 % for SMS IDMs with $f_m - f_g$ = 3Hz. Thus, the frequency measurement error should not affect much the NDZ of multi-inverter systems with SMS IDM. This can be seen in Fig. 2-2 that depicts the NDZs of the multi-inverter system with two SMS IDM inverters and different values for Δf_e.
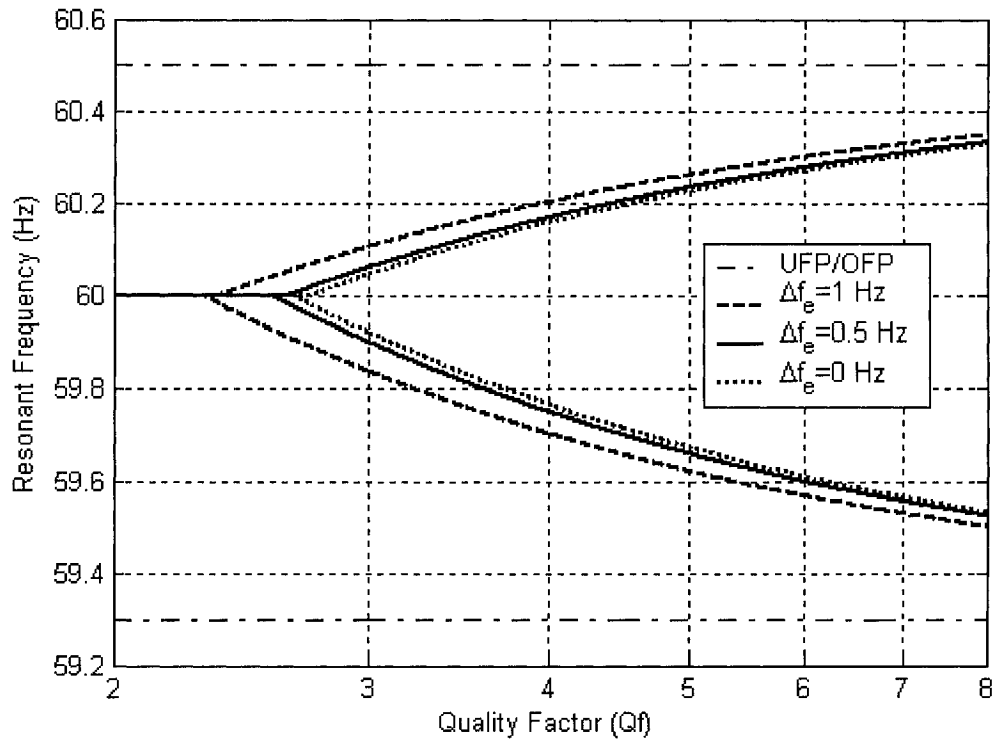
Fig. 2-2 NDZ of a multi-inverter system with 2 equal power SMS IDM inverters (θ_m =

$10°$ and $f_m - f_g$ = 3Hz) and frequency measurement error of Δf_e.

2.3 SIMULATION RESULT AND ANALYSIS

2.3.1 SIMULATION SCHEMATICS AND PARAMETERS SETUP

The theoretical analysis and NDZs derived in the previous sections are validated by means of simulation results by use of Matlab Simulink. The simulated multi-inverter

28

system is similar to that presented in Fig. 1-2 but comprises two or more PV inverter stations connected in parallel at the PCC, as shown from the Fig2-3.
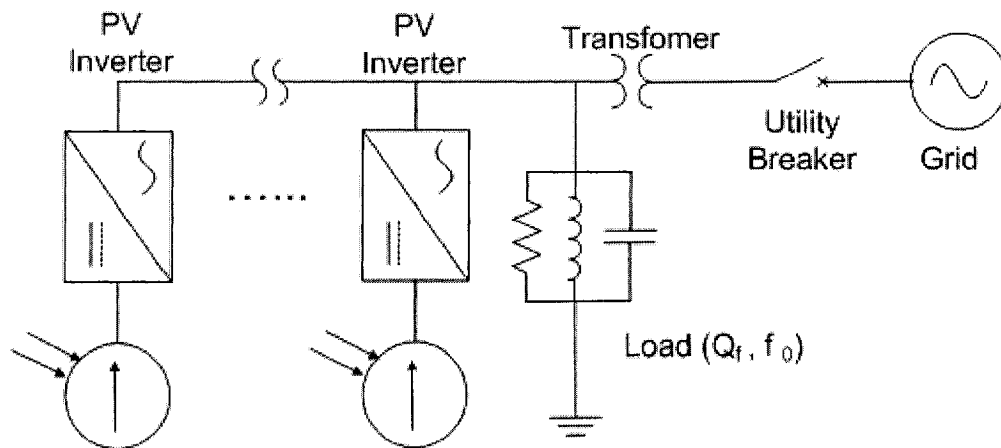
Fig. 2-3 The circuit for assessing anti-islanding features of grid-connected multi-inverter system

The system described in Fig. 2-3 was modeled with MATLAB Simulink as shown in Fig. 2-4. The PV array and current controlled voltage source inverters are simplified as two controllable current sources, which are connected to the PCC. The local load is represented by a parallel *RLC* block with variable resonant frequency and quality factor. The grid breaker, that connects the grid (AC voltage source) to the PCC, is preset to open at a prescribed time. The reference current with IDMs block is used to generate the inverter reference current with the islanding detection methods that match the local load's active power. There are two sets of reference currents provided for two PV inverters system respectively. By selecting the output terminal from the reference current block, one can switch different islanding detection methods for related simulation test conveniently. The frequency measurement block measures the frequency of the voltage at PCC, and UVP/OVP & UFP/OFP block would generate a fault signal to shut down the inverter if its frequency or voltage exceeds the IEEE Std. 929-2000 limits, shown in Table 1. The

29

manual switch is used to deactivate the frequency and the voltage protection thus allowing the measurement of the steady-state values of frequency and voltage across the load under islanding condition.

The Matlab Simulink model of the grid-connected PV system is discrete system sampled at simulation sampling rate of 3240 samples per cycle of $60\,Hz$, i.e. $T_s = 5.144 \times 10^{-6}\,s$. In the model, the value of the grid voltage is preset as $V_g = 120\,V$, $f_g = 60\,Hz$.
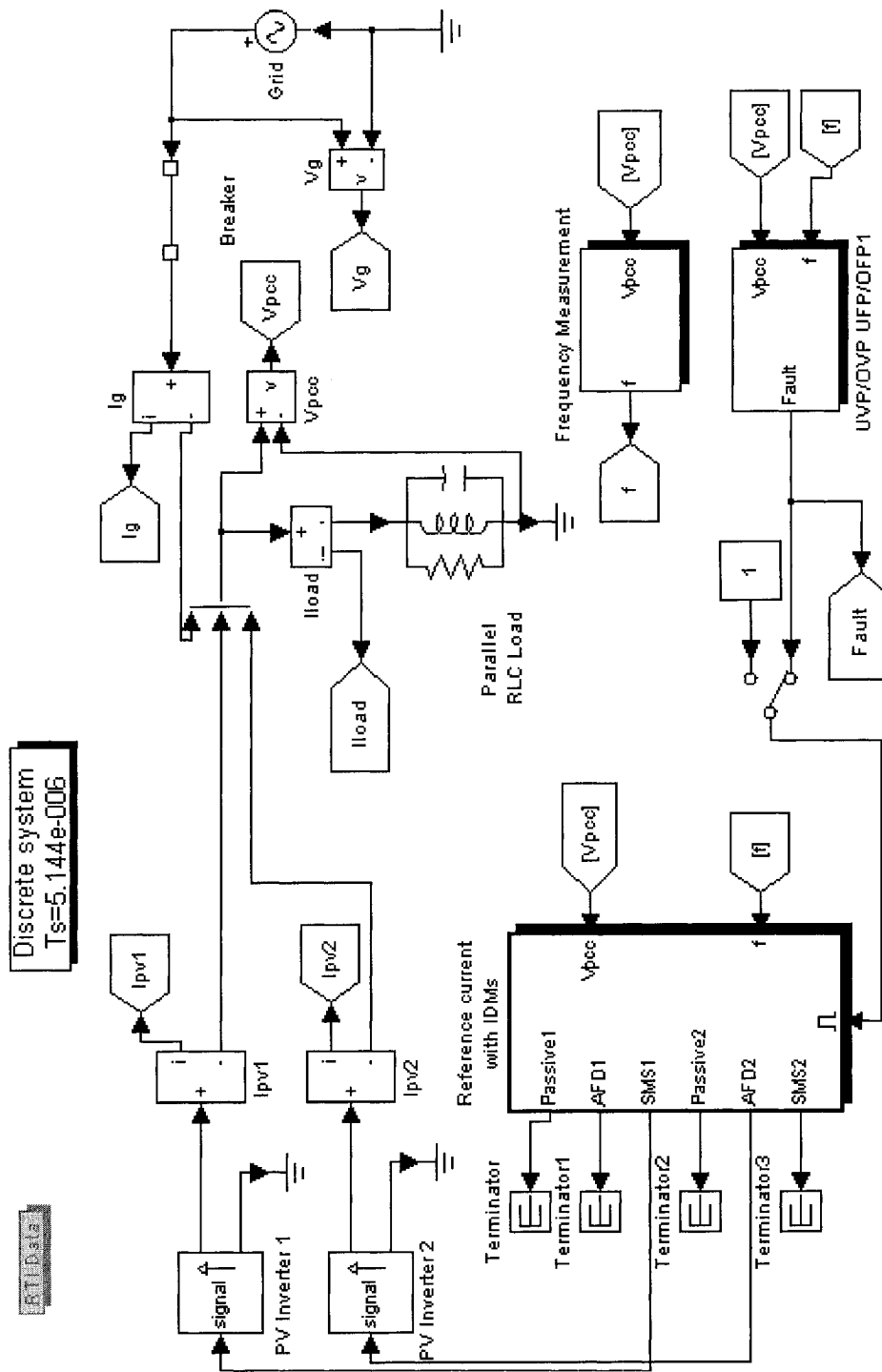
Fig. 2-4 MATLAB Simulink model of the grid-connected PV system.

31

2.3.1.1 Frequency Measurement Block [20]

Based upon the concept of zero crossings, the frequency of voltage at PCC can be measured and calculated. Considered the inconsistency between the lower estimation errors and shorter time delay by and large, one complete cycle usually is utilized for the calculation. The measurement method is based upon counting the number of samples in one complete cycle

Consider the following sinusoidal waveform for the purpose of the measurement:

$$v(t) = V_m \sin \omega t, \qquad (2\text{-}20)$$

where $\omega = 2\pi f$ is the angular frequency.

The frequency can be obtained by:

$$f = \frac{1}{NT_s}. \qquad (2\text{-}21)$$

where N is the number of samples per cycle, T_s is the sampling interval.

From the Fig. 2-5, one may find that the duration of one cycle of the waveform does not necessarily divide evenly over the sampling interval. In order to obtain a more accurate estimate of the frequency, a simple method is introduced as follow. Assume that $y_{-1}, y_0, \ldots, y_k, y_{k+1}$, shown in the Fig. 2-5, are the values of the sinusoidal waveform at the sampling time $t_{-1}, t_0, \cdots, t_k, t_{k+1}$ respectively. It is hereby assumed that the samples $y_0, \cdots, y_k$ are within interval of one complete cycle of the waveform, and that the two samples y_{-1}, y_{k+1} are outside this cycle.

32
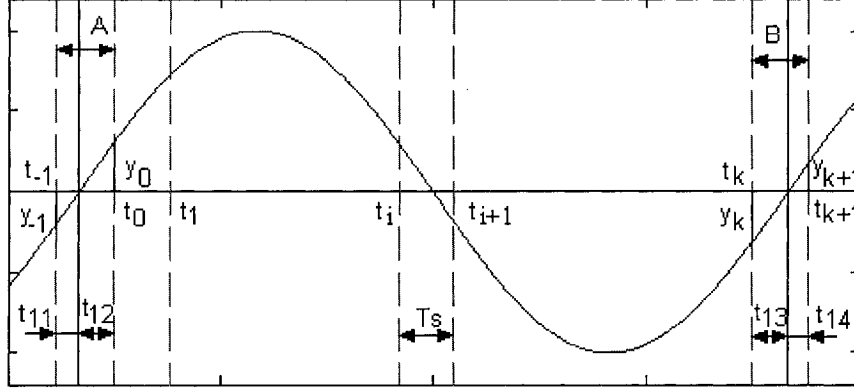
Fig. 2-5 Sine wave considered for measurement [20]

According to the notation in Fig. 2-5, the value of N is:

$$N = k + \frac{t_{12}}{T_s} + \frac{t_{13}}{T_s},$$ (2-22)

where k is the integer number of sampling periods in one cycle.

If the sample interval T_s is short enough, one can assume that the sine function in the range of a zero crossing is replaced approximately by a straight line, and by using the trigonometric identity, the number of the stripes in one cycle can be approximately by:

$$N \cong k + k' = k + \frac{|y_0|}{|y_0| + |y_{-1}|} + \frac{|y_k|}{|y_k| + |y_{k+1}|}.$$ (2-23)

With equation (2-21) and (2-23), one can see that the value of the frequency depends on the values of the two samples surrounding the first zero-crossing (y_0, y_1), the values of the two samples surrounding the last zero-crossing (y_k, y_{k+1}), the number of samples between these zero crossings (k) and the sampling interval (T_s).

The Frequency Measurement block is shown in Fig. 2-6. Fig. 2-6(a) shows the main circuit to measure the frequency of PCC voltage, and Fig. 2-6(b), (c) and (d) shows the detail of the 3 subsystems of the main circuit. This block has one input PCC voltage v_{PCC} and one output frequency of the PCC voltage f_{PCC}. The Hit Crossing block

33

compares the input signal to the hit crossing offset value, which is set as 0 here. If the input signal rises above the offset value, the block outputs 1, and Simulink takes a time step before and after the hit crossing time, which indicates the sampling interval, referred to the interval A or B in Fig. 2-5, when the default sample is larger than or equal to zero and the last sample is less than zero. The output of Hit Crossing activates the subsystem k', where the value $\dfrac{Y_k}{Y_k + Y_{k+1}}$ and $\dfrac{Y_{k+1}}{Y_k + Y_{k+1}}$ are calculated, as shown in Fig. 2-6(b). In this subsystem, the default value of the input signal is named Y_{k+1}, and the previous sample's value is named Y_k obtained by applying the Unit Delay block. After this interval, the subsystem Counter, shown in Fig. 2-6(d), starts to count the integer numbers of one cycle. The Enable and the Trigger blocks are placed to make this subsystem a enabled and triggered subsystem, and the Unit Delay used in this subsystem is used here to prevent the error of the ambiguous execution order due to use of subsystem in a loop during the simulation. The total integer number K_1 of one cycle and the value of $\dfrac{Y_{k+1}}{Y_k + Y_{k+1}}$ will be held in the subsystem Hold, shown in Fig. 2-6(c), and only update when Hold block is triggered by the Hit Crossing block output. Notice that $\dfrac{y_0}{y_0 + y_{-1}}$ in Equation (2-6), is obtained by applying a Unit Delay block to get the previous value of $\dfrac{y_{k+1}}{y_k + y_{k+1}}$, when Hold block is triggered. Thus, the value $N = K_1 + K_2 + K_3$, the frequency of the last cycle can be obtained by Equation (2-21). The Switch is used here to set the initial value of the frequency as $60\,Hz$.

34
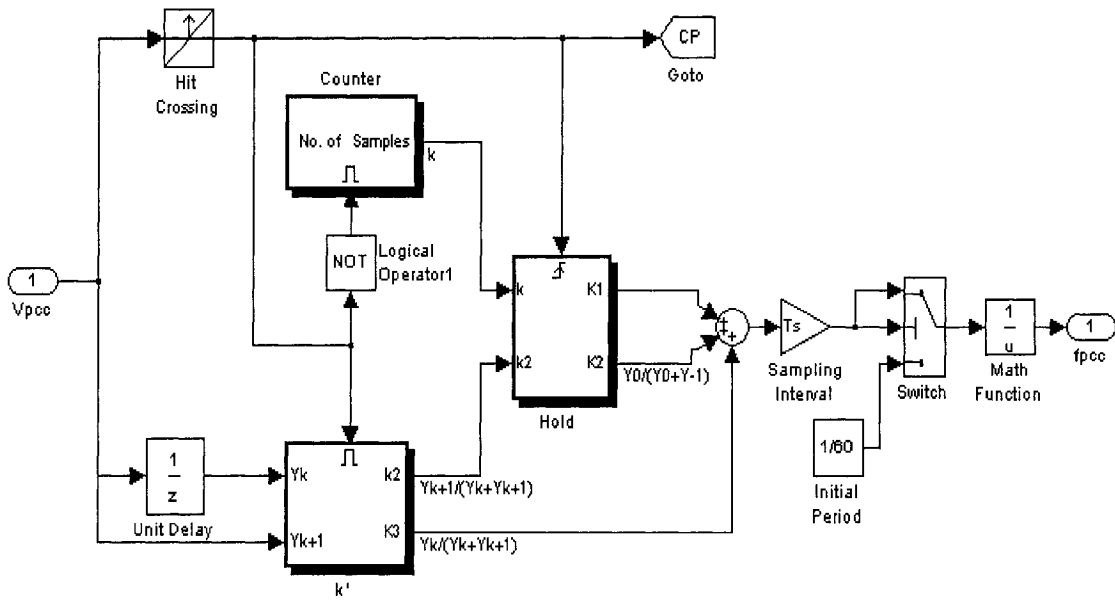
(a) Frequency measurement block main circuit
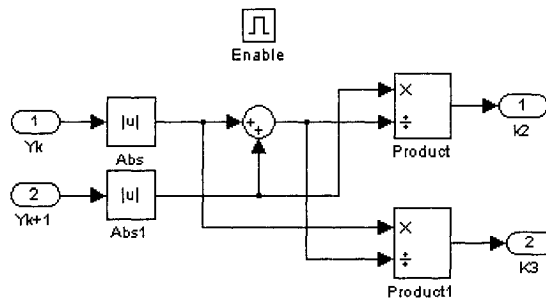
(b) k'
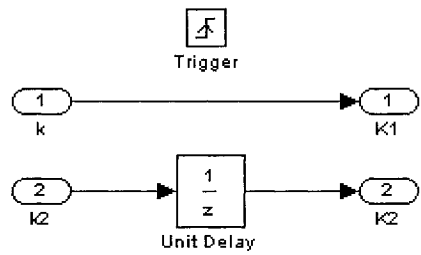
(c) Hold
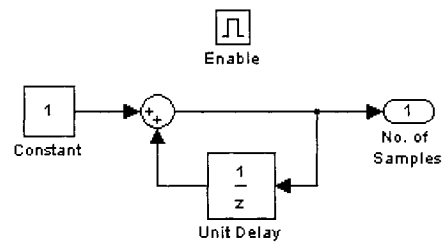
(d) Counter

Fig. 2-6 Frequency measurement block [20]

35

2.3.1.2UVP/OVP &UFP/OFP Block [20]

The UVP/OVP & UFP/OFP block is shown in Fig.2-7. The RMS value of the voltage is calculated using the definition of the RMS. The block Discrete Variable Frequency Mean Value is an existing block in Matlab Simulink, which computes the mean value of the input signal over a cycle of a specified frequency. The RMS value and the frequency of the PCC voltage are sent to the Voltage Thresholds and the Frequency Thresholds. If the RMS value or the frequency exceeds the limits, the Voltage Thresholds or Frequency Thresholds blocks will output 1 to enable the Abnormal Voltage Cycles Counter or Abnormal Frequency Cycles Counter, where the values of the cycles are different according to the Table 1. Then, the counter will be triggered to count the cycles of the continuous abnormal voltage at the zero crossing point which represents the start of one cycle. Once the number of continuous abnormal PCC voltage cycle exceeds the limitation of IEEE Std.929-2000, shown in Table 1, the resettable J-K Flip Flop, will be triggered, a low fault signal will be generated to turn off the inverter switches thereby ceasing the inverter to energize the utility. If the continuous normal voltage and frequency have been maintained by the utility for a minimum of five minutes, at the time the Normal Voltage Cycles Counter block will reset the J-K Flip Flop in order to automatically reconnect the PV system to the utility.

36
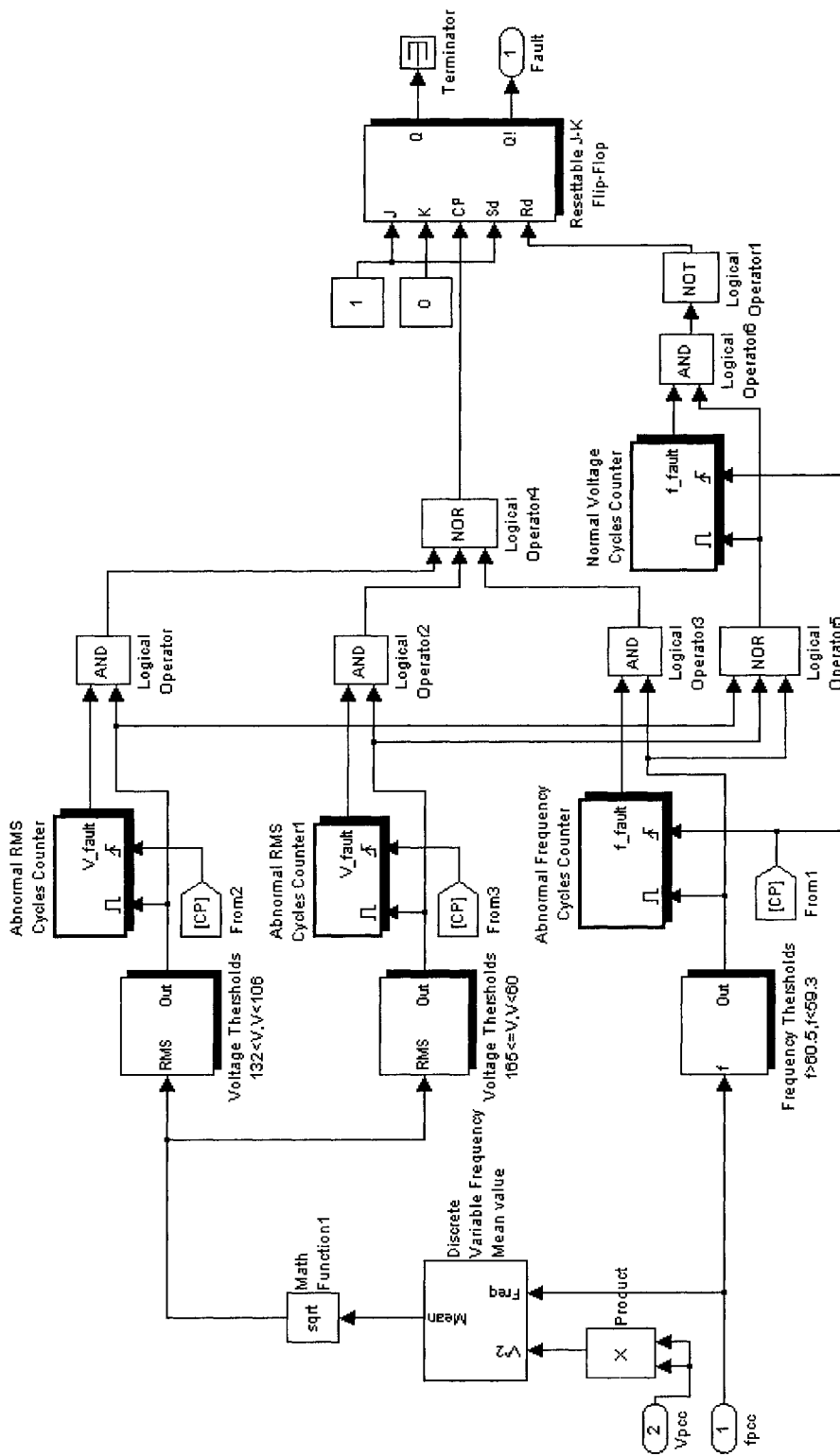
Fig. 2-7 UVP/OVP & UFP/OFP Block

37

2.3.1.3Reference Current Block

Fig. 2-8 shows the Reference Current block. The inputs of this block are the PCC voltage v_{PCC} and the frequency f_{PCC}. The outputs are the three reference currents: passive (UPF), AFD and SMS. The time t is obtained by use of the block Discrete-Time Integrator to integrate the input signal 1 per cycle, and this time t is reset when a new cycle starts.

For AFD, a fixed frequency drift df is added to the measured frequency of previous cycle of PCC voltage to obtain the current frequency $f = f_{PCC} + \delta f$. The Saturation block in this branch is to limit the input signal upper and lower saturation values. In this case, the lower limit is set to be 0, and the upper limit is set to be 2π. If the value of $2\pi(f_{PCC} + \delta f)t$ exceeds the upper limit, the Saturation block outputs the value 2π to create the zero current segment of the distorted AFD waveform, shown in Fig. 1-2. The distorted inverter output current of one cycle is

$$
\begin{aligned}
i_{AFD} &= I_{PV\max} \sin[2\pi(f_{PCC} + \delta f)t], &\text{when} \quad 0 \le t \le T_i; \\
i_{AFD} &= 0, &\text{when} \quad T_i < t \le T_{PCC}.
\end{aligned}
\tag{2-24}
$$

For SMS, an additional phase shift is added to the current cycle, and the value is

$\theta_{SMS} = \dfrac{\pi}{2} \dfrac{f_{PCC} - f_g}{3}$. The PV system inverter with SMS output current is

$$
i_{SMS} = I_{PV\max} \sin\left(2\pi f_{PCC} + \frac{2\pi}{360}\theta_{SMS}\right).
\tag{2-25}
$$

The reference current of a SMS IDM with a frequency measurement error is implemented utilizing the SMS model with an additional error constant Δf_e added to or subtracted from the correct measurement frequency. The Δf_e can be modified manually depending on different testing applications.

38
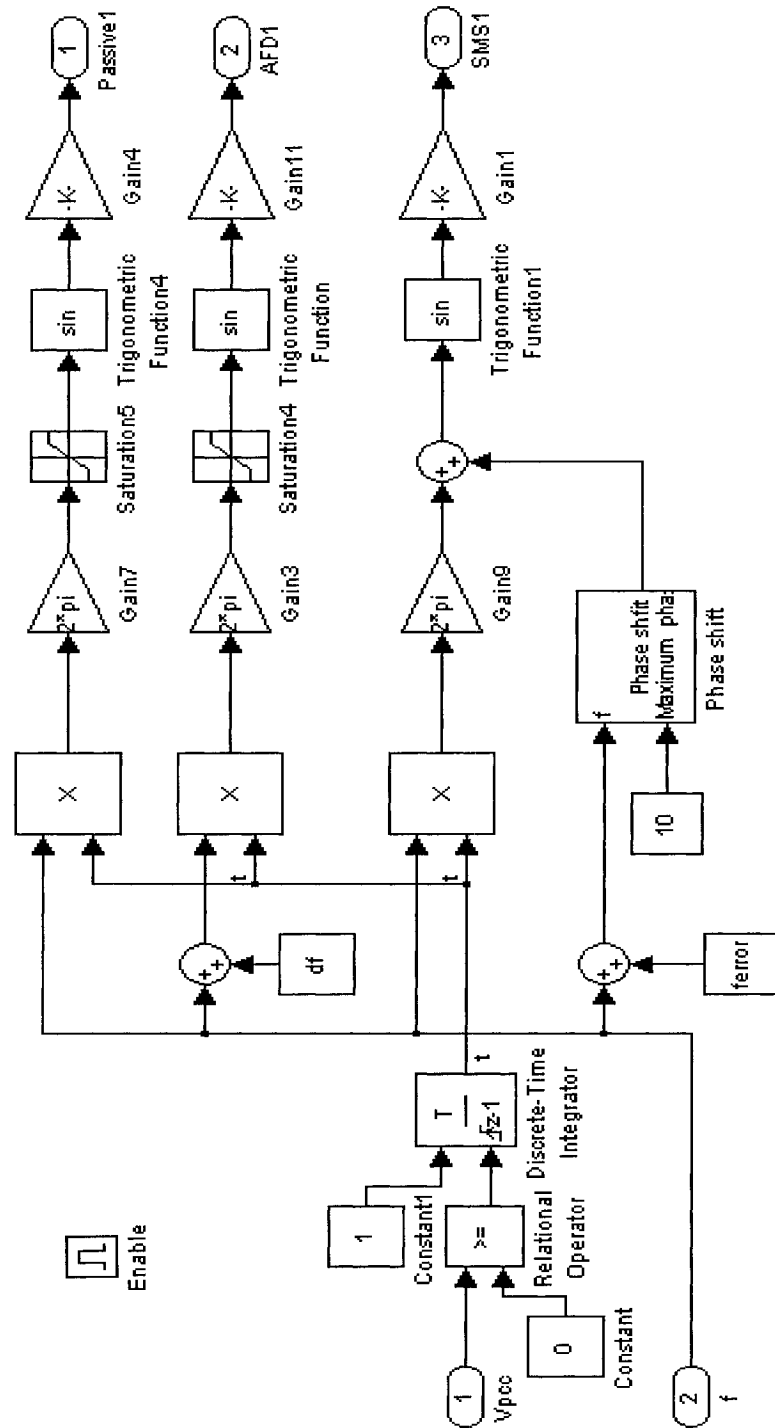
Fig. 2-8 Reference Current with IDMs Block.

39

2.3.2 SIMULATION RESULTS OF PASSIVE IDM AND SMS IDM INVERTERS SYSTEM

The first case to be investigated is a system composed of passive (UPF) and active frequency drifting IDM inverters. As we learned from Section 2.2.1 for a passive and active IDM invertes system, one can obtain $Q_{f_{eq}}$ by combining the UPF inverter with the load, and analyze the system utilizing the NDZ from that single active IDM. Without loss of generality, a nonislanding SMS IDM inverter, whose NDZ is shown in Fig. 1-6, for a local load with $Q_f \leq 2.6$ ($\theta_m = 10°$, $f_m - f_g = 3$Hz) is used in this study. Fig. 2-9 (a) shows the variation of the local system's frequency due to a single SMS IDM inverter supplying a 1 kW load with $Q_f = 2.58$ and $f_0 = 60.02$ Hz. As the grid breaker opens at t = 0.1 s, the frequency increases continuously until the UFP-OFP trips at 0.49 s, 6 line cycles after the system's frequency goes over 60.5 Hz. It is worth mentioning that for a passive UPF inverter, the system's voltage and frequency would remain unchanged due to the zero active and active power imbalance and islanding would occur. Fig. 2-9 (b) shows the variation of the local system's frequency when the 1 kW, $Q_f = 2.58$ and $f_0 = 60.02$ Hz local load is supplied by two inverters rated at 500 VA: One with SMS IDM ($\theta_m = 10°$, $f_m - f_g = 3$Hz) and the other with passive IDM. There one sees that the system frequency decreases very little remaining within the normal frequency range and leading to islanding. Fig.2-9 (c) shows the frequency variation of the previous system but with a local load with $Q_f = 1.19$. The frequency drifts outside the normal frequency range and islanding is detected. Thus, the analysis presented in Section 2.2.1 is validated.

40
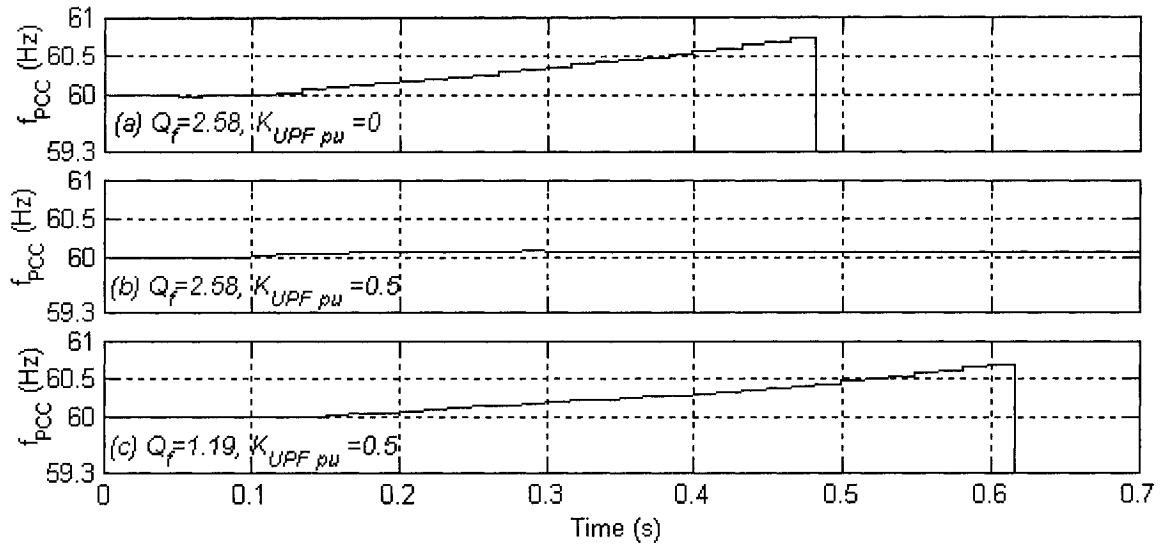
Fig. 2-9 Responses of systems with different power shares of active and passive inverters supplying local loads with different values of Q_f.

2.3.3 SIMULATION RESULTS OF AFD IDM AND SMS IDM INVERTERS SYSTEM

The second scenario includes only active frequency drifting IDM inverters: One with SMS IDM ($\theta_m = 10°$, $f_m - f_g = 3$Hz and the other with AFD IDM ($\delta f = 1$ Hz). The load power and quality factor are set to 1 kW and 3, respectively. The power shares of the AFD and SMS as well as the load's f_0 are varied so as to verify the validity of the NDZs defined in Section 2.2.2. The results shown in Fig. 2-10 refer to a load represented by point A in Fig.2-1. One sees that the system's frequency remains within the normal operating range for all three combinations of SMS and AFD inverters. Thus islanding occurs as anticipated, since this point lies in the NDZs of the three systems. Fig. 2-11 and Fig. 2-12 show the responses of the three systems to loads represented by points B and C in Fig. 2-1. The results also validate the analysis carried out with the NDZs. The system's

41

frequency remains in the normal frequency range for the cases where the loads are located in the NDZs of the inverter combinations.

It is worth mentioning that the use drift-down AFD IDM would not change the overall performance of the system significantly. In such a case there would be inductive loads ($f_0 > f_g$) for which islanding would occur. As explained before, the problem in this scenario is that one method always drifts the frequency in one direction (AFD) while the other (SMS) can drift it up or down depending on the load's f_0.
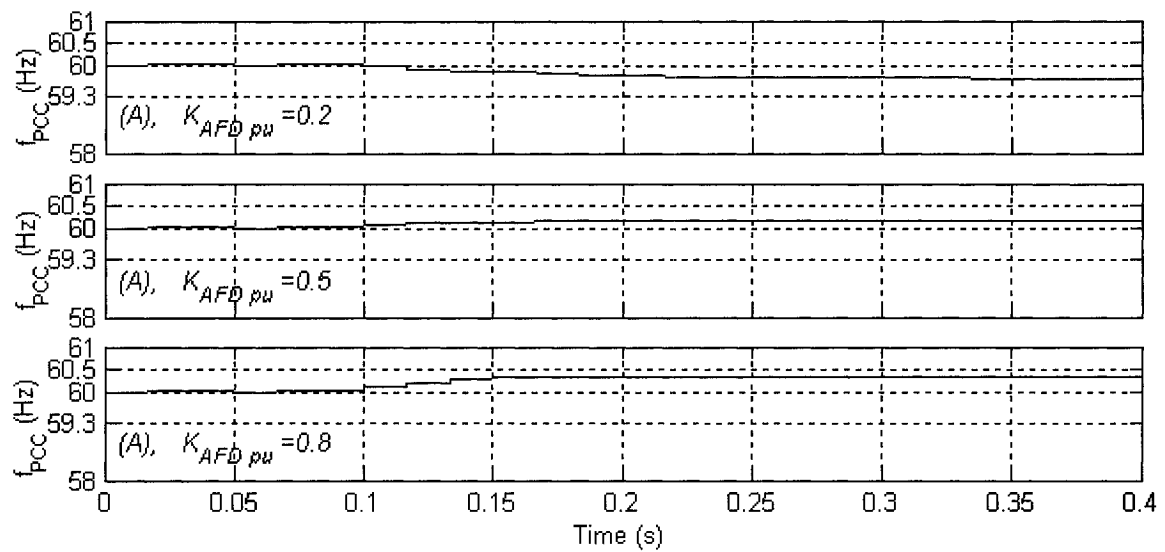
Fig. 2-10 Responses of systems with different power shares of SMS and AFD IDM

inverters (K$_{AFDpu}$) supplying a local load with Q_f=3 and f_0=59.8 Hz

42
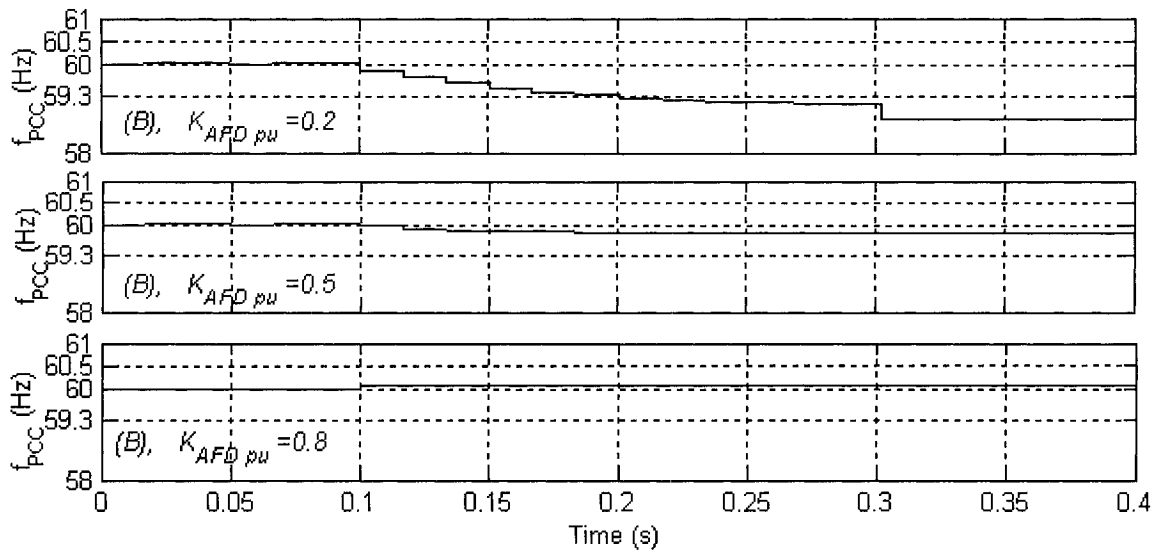
Fig. 2-11 Responses of systems with different power shares of SMS and AFD IDM

inverters (K$_{AFDpu}$) supplying a local load with Qf=3 and $f0$=59.6 Hz
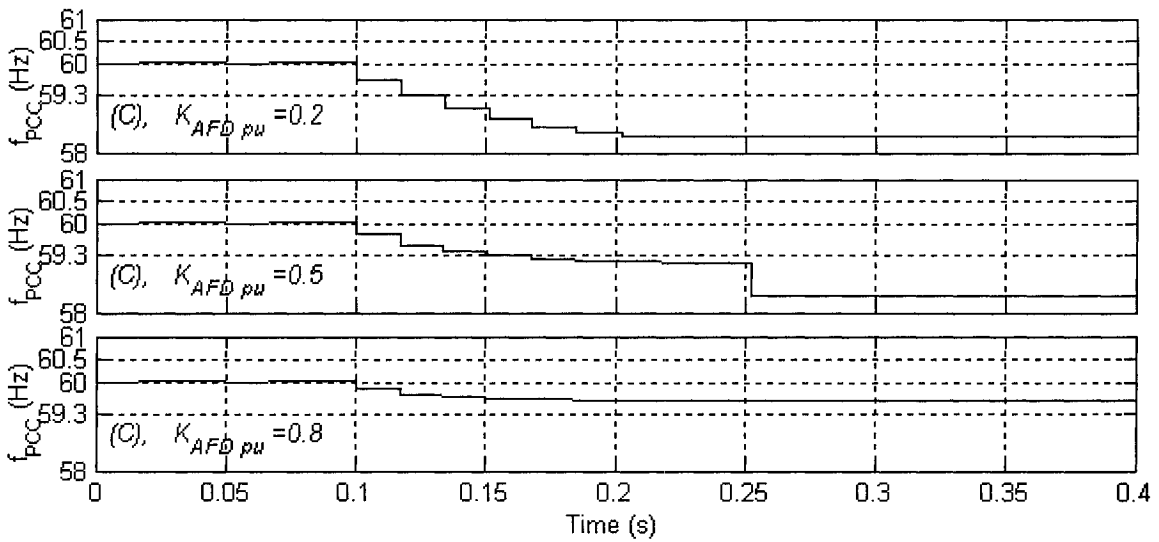
Fig. 2-12 Responses of systems with different power shares of SMS and AFD IDM

inverters (K$_{AFDpu}$) supplying a local load with Q_f=3 and f_0=59.2 Hz

43

2.3.4 SIMULATION RESULTS OF TWO SMS IDMs WITH MEASUREMENT ERRORS INVERTERS SYSTEM

The final case to be investigated is of a system with two SMS IDM inverters. If they are identical they would always attempt to drift the frequency in the same direction and the NDZ of the system would be the same as of a single unit. However as discussed in Section 2.2.3, they can in principle offset each other in the presence of opposite frequency measurement errors (Δf_e). Fig. 2-13 shows the response of the system's frequency for two 500 VA SMS IDM inverters with different values of Δf_e supplying a 1 kW load with $f_0 = 60.02$ Hz and 2.58, the point located between the two curves $\Delta f_e = 0$ and 0.5Hz shown in the Fig. 2-2. There one can see that the frequency drifts less for larger values of Δf_e because of the partial offset of the two SMS IDMs. Besides for a load $Q_f = 2.58$, islanding would only occur for very large values of Δf_e (~ 0.8 Hz) which are not very likely to happen in practical systems. Thus, one can say that SMS IDM inverters are appropriate for multi-inverter systems. They can be designed to be nonislanding for net inductive as well as net capacitive loads with a Q_f lower than a given value and they present low sensitivity for offsetting due to frequency measurement errors.
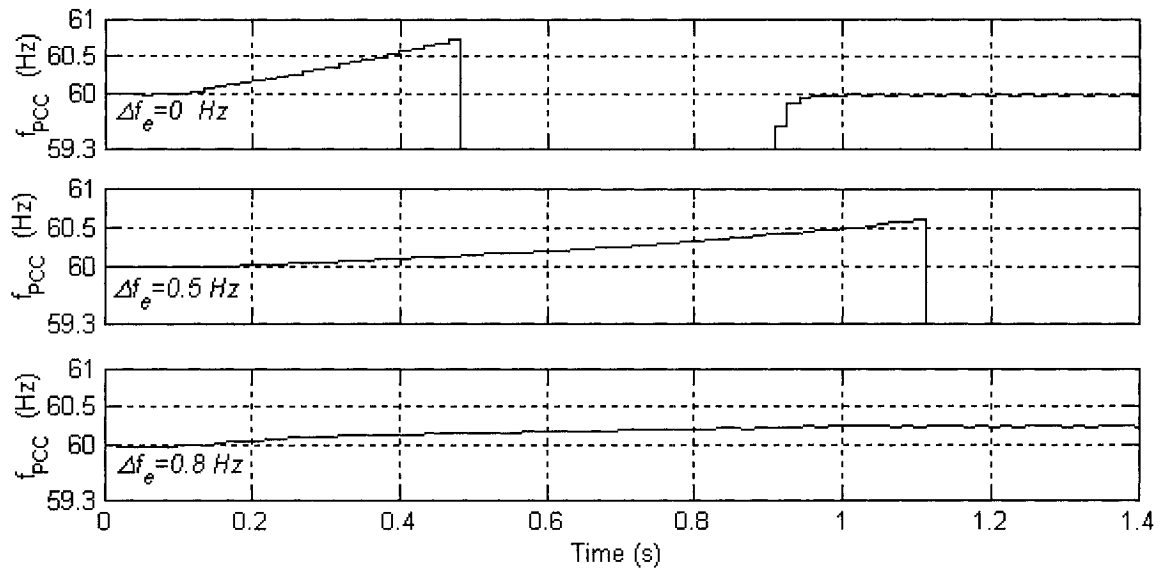
Fig. 2-13 Simulation results of two SMS IDM inverters supplying one local load

P_{load}=1kW , Q_f=2.58, f_0=60.02 Hz with different Δf_e

2.4 EXPERIMENT RESULT AND ANALYSIS

2.4.1 EXPERIMENT SETUP

A 1 kW topology system was implemented to validate the theoretical analysis. Fig. 2-14 depicts the configuration of the grid-connected PV multi-inverter system laboratory set-up [24,25].

Within the DC Part, a single phase diode bridge rectifier with a $600\,\mu F$ dc bus capacitor is utilized to emulate the PV array DC output. Usually a dc bus voltage regulating loop is included in a system like this to control the active power the inverter injects into the ac grid under transient conditions. However, since the worst case for islanding detection is when there is no variation of the power generated by the PV source and consumed by the local load, this feedback loop is omitted in this study. The PV inverters inject constant active power into the grid. Thus the PV source is assumed to

45

supply constant power to the Inverter Part. The dc bus voltage is controlled at 190 V via the VARIAC before the diode rectifier.

In the Inverter Part, the main element are two single phase voltage source inverters (VSIs), which are independently operating in parallel and connected to the PCC through 5 mH inductors. The inverters are built using a single-phase full bridge configuration with bipolar power transistors (FUJI EVK71-050, 75A 500V) and anti-parallel diodes as main switches. A digital signal processor (DSP) development kit (DS-1103, dSPACE) was employed to implement the reference current with the IDMs, including Passive, AFD and SMS. The real AC output current of each inverter is measured by Hall effect current sensors (LA55-P, LEM) and sent to hysteresis current controller. The gating signals generated by the three-level hysteresis current controller board, where the real measured inverter output current is compared with the reference current, are amplified and isolated by a gate drive system to control the inverter. The inner boundary and outer boundary of the hysteresis current controller are set as 0.2 A and 0.4 A respectively. The details of the three-level hysteresis current controller are shown in Appendix.

At the ac side the RLC local load is connected with the ac grid breaker and a single-phase $5\,kVA$ VARIAC (variable autotransformer) at PCC. An ac voltage sensor (LV100, LEM) is employed to monitor the PCC voltage. It provides synchronism for the reference current of the inverter and allows the measurement of the frequency and magnitude of the voltage at the PCC. The RMS value of the AC grid is set to 120 V by a single-phase 5 kVA variable autotransformer that represents the utility grid. It is worth mentioning that the dc bus voltage of the inverter has to be higher than the peak value of the ac grid voltage for full control of the power flow.

46
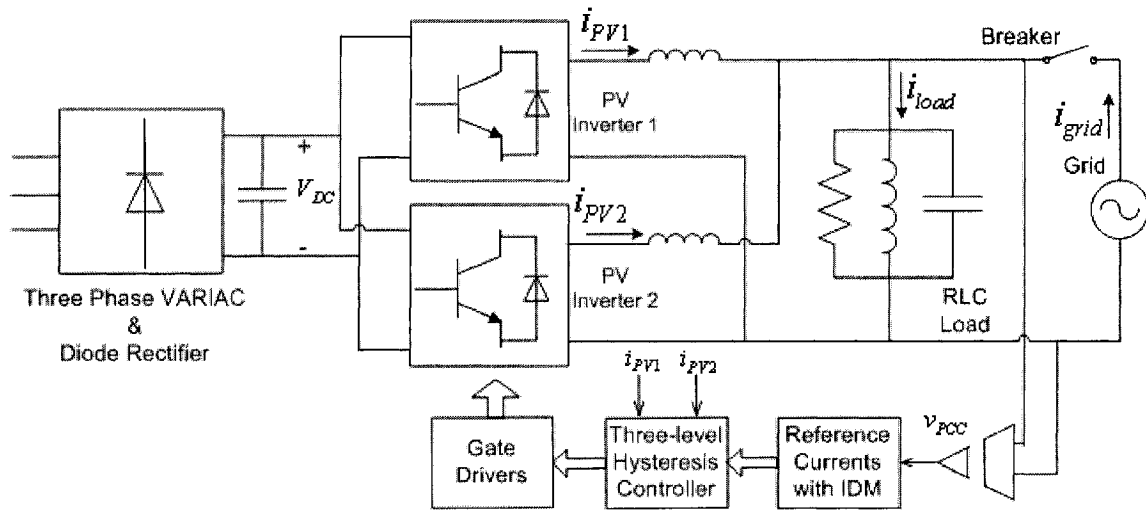
Fig. 2-14 Schematic of the grid-connected multi-inverter system laboratory set-up

2.4.2 LOCAL LOAD PARAMETERS SELECTION AND VALIDATION

In order to obtain the correct experiment results, the local load need be selected and validated correctly. The approach used in this section for calculating the load used in the experimental tests is based on the specification of the desired resonant frequency f_0 and quality factor Q_f. In the load parameter Q_f vs. f_0 space, there may exist several different combinations of L and C for a same resonant frequency f_0. However the inductor available in the laboratory has a maximum value of 32 mH and intermediary taps with inductances equal to 8 mH and 16 mH. We initially choose a value for the inductor and then calculate the value of the capacitor C that yields the desired resonant frequency since the values of capacitors available in the laboratory is more diverse than of inductors. At last the value of the resistor R is chosen so as to achieve a desired quality factor.

After deciding the theoretical value of the local load, one also need confirm the actual value of the resonant frequency and quality factor of a given *RLC* load by preliminary tests, because the actual value of most power components is not exactly the

47

nominal value. The manufactures usually provide a tolerance range, such as ± 10%, for each component. There are three steps in the preliminary test to adjust the load.

1) Without applying any active IDMs or UVP/OVP and UFP/OFP, open the utility disconnect switch, and let the system operate in islanding condition to achieve the load resonant frequency.

2) Once the system runs at steady state, the value of the resistance R can be verified through the preset value of the PV inverter current I_{PV} and the measurable islanding PCC voltage V_{PCC}.

3) The value of resonant frequency of the load can be read from ControlDesk, dSPACE's well-established experiment software, which provides all the functions to control, monitor and automate experiments.

Based on these three steps, the parameters of the local load, f_0 and Q_f, can be verified by the experimentally.

2.4.3 PASSIVE AND SMS IDM INVERTERS

There are two loads will be used in this test. Following the procedure described in Section 2.4.2, one can obtain the real value of the load parameters. One is f_0 =60.02 Hz and Q_f=2.58 (L=15.14 mH, C= 462 μF, R=14.86 Ω), the other is f_0 =60 Hz and Q_f=1.19 (L=32.9 mH, C= 214 μF, R=14.83 Ω). First test is for a single inverter equipped with SMS IDM (θ_m = 10°, $f_m - f_g$ = 3Hz) supplies power to the 1 kW load (f_0 =60.02 Hz, Q_f =2.58). The results can be seen in Fig. 2-15, which shows the four most relevant waveforms of the system, the grid current i_{grid}, the PCC voltage V_{PCC}, PV inverter current i_{SMS} and system frequency f. When the grid breaker opens at t=0.245 s, the frequency of the

48

voltage at PCC keeps decreasing and at t=0.522 s the island is detected and the inverter is shut down.

Fig. 2-16 shows that for the same load, two inverters rated at 500 VA supply the power simultaneously, one with SMS IDM ($\theta_m = 10°, f_m - f_g = 3\text{Hz}$) and the other with passive IDM. There one sees that after grid opens at t=0.18 s, the system frequency decreases very little remaining within the normal frequency range and leading to islanding. Fig.2-17 shows the frequency variation of the previous system but with a local load with Q_f =1.19. The frequency drifts outside the normal frequency range and islanding is detected at t=0.47 s after the utility is disconnected at t=0.18 s. Thus, the analysis presented in Section 2.2.1 is validated by the experiment.
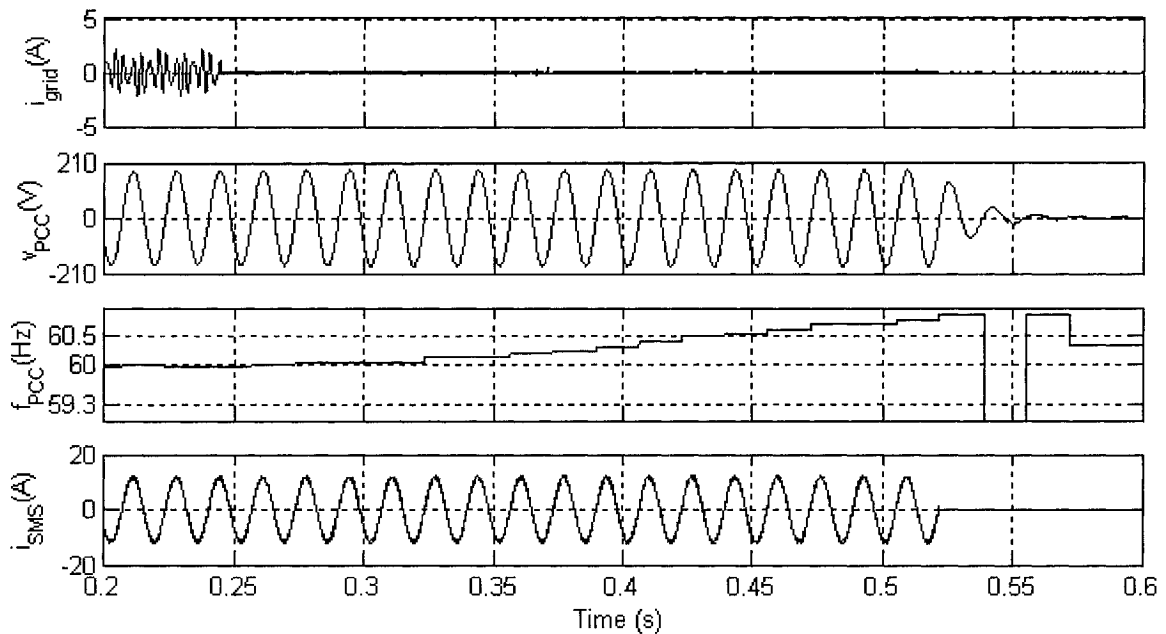
Fig. 2-15 Experiment results for a system with single SMS IDM inverter with load f_0

=60.02 Hz, Q_f=2.58

49
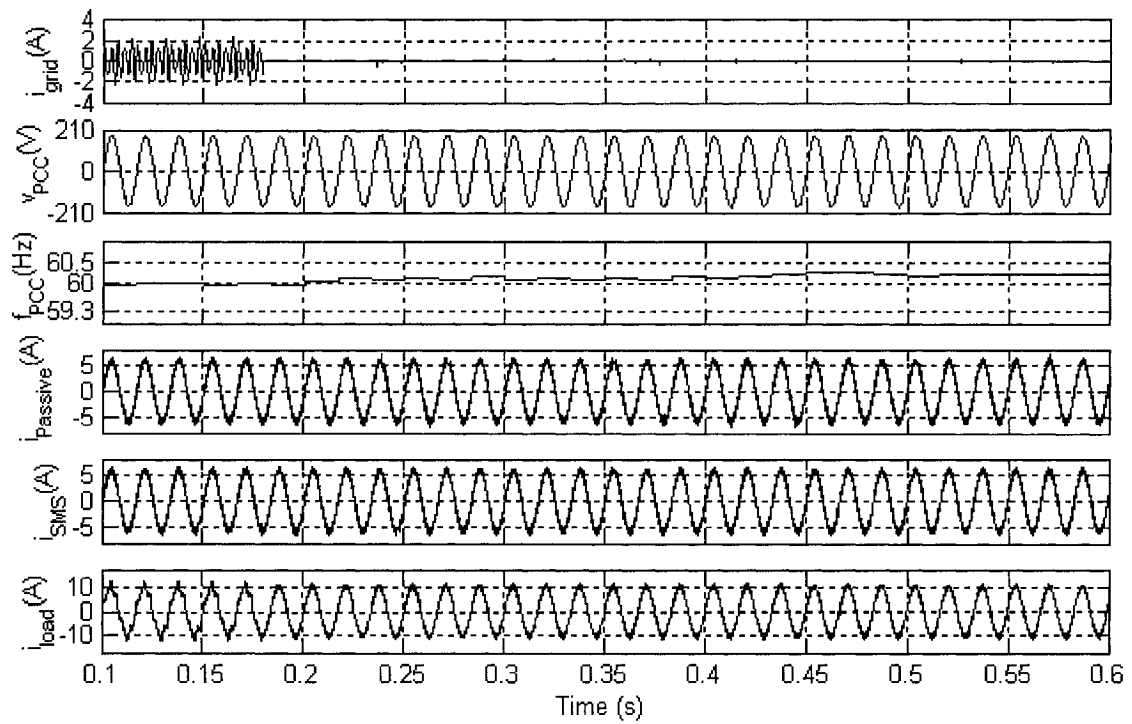
Fig. 2-16 Experiment results for a system with passive and SMS IDM inverters with load f_0 =60.02 Hz, Q_f =2.58
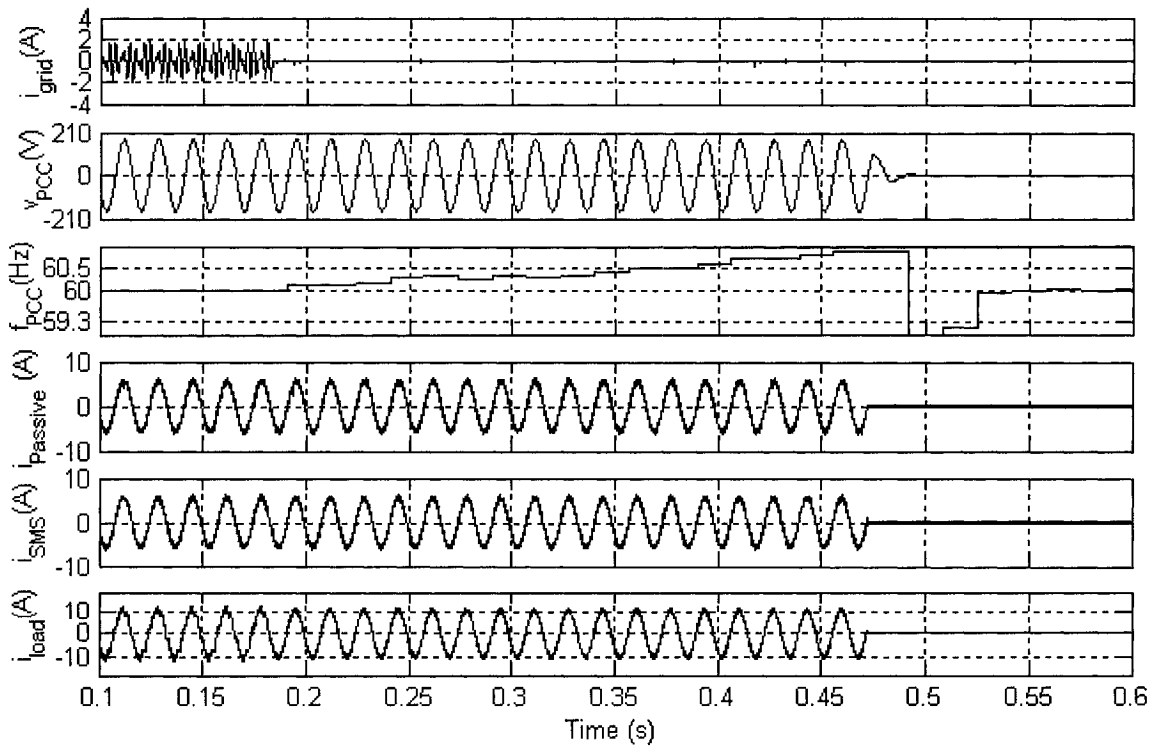
Fig. 2-17 Experiment results for a system with passive and SMS IDM inverters with load f_0 =60.02 Hz, Q_f =1.19

50

2.4.4 ONE AFD AND ONE SMS IDM INVERTERS

There are three different local loads involved in this test. The real values of the loads are listed in the Table 2 after verified by experiment.

Table 2-Parameters of the local *RLC* loads considered for the experimental tests.

LOAD	$L\,(mH)$	$C\,(\mu F)$	$R\,(\Omega)$	Q_{fcal}	$f_{0cal}\,(Hz)$
A	15.1	467	17.38	3	59.8
B	15.1	472	17.38	3	59.6
C	15.1	477	17.38	3	59.2

The 1 kW load is supplied by two active frequency drifting IDM inverters, SMS IDM ($\theta_m = 10°, f_m - f_g = 3$Hz) and AFD IDM ($\delta f = 1$ Hz). The Fig. 2-18 (a), (b) and (c) are the experiment results referred to a load represented by Point A in Fig. 2-1 for different power shares between SMS and AFD IDM inverters respectively. The difference in power injected by each inverter can be seen from the magnitudes of inverter output currents, i_{AFD} and i_{SMS}. One can find that the system frequency varies within the limitation f_{min} and f_{max}, thus the islanding detection fails for all cases as discussed at Section 2.2.2. Fig. 2-19 and Fig. 2-20 show the experiment results of the three systems with the loads represented by points B and C in Fig. 2-1. Islanding occurs when the loads are located in the NDZs mentioned in Section 2.2.2. The theoretical analysis is validated by the experiment.

51
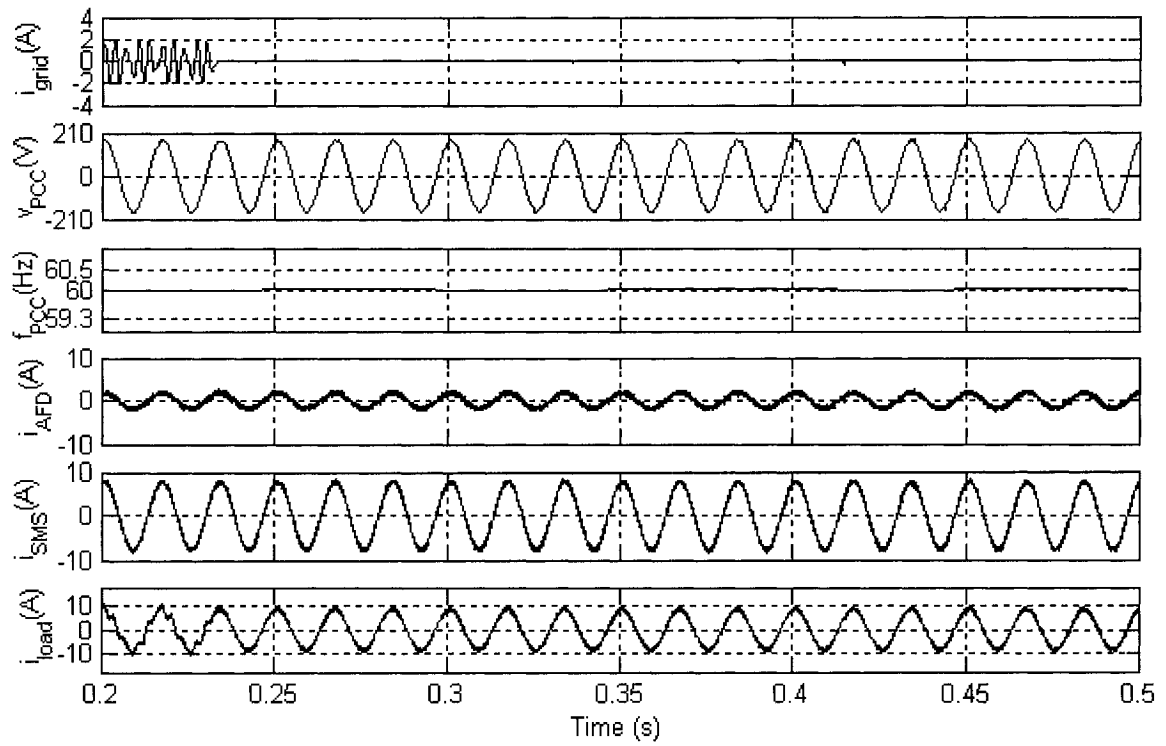
(a) $K_{AFD\ pu}$=0.2 for the load at testing point A

(b) $K_{AFD\ pu}$=0.5 for the load at testing point A

52
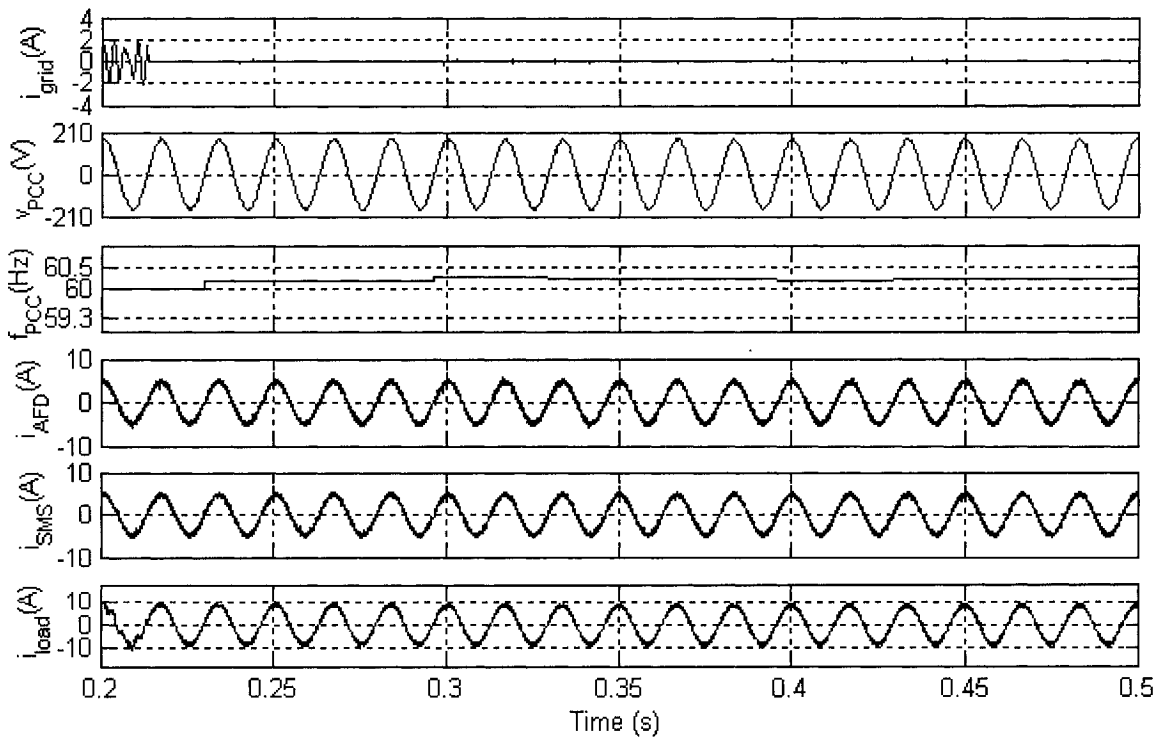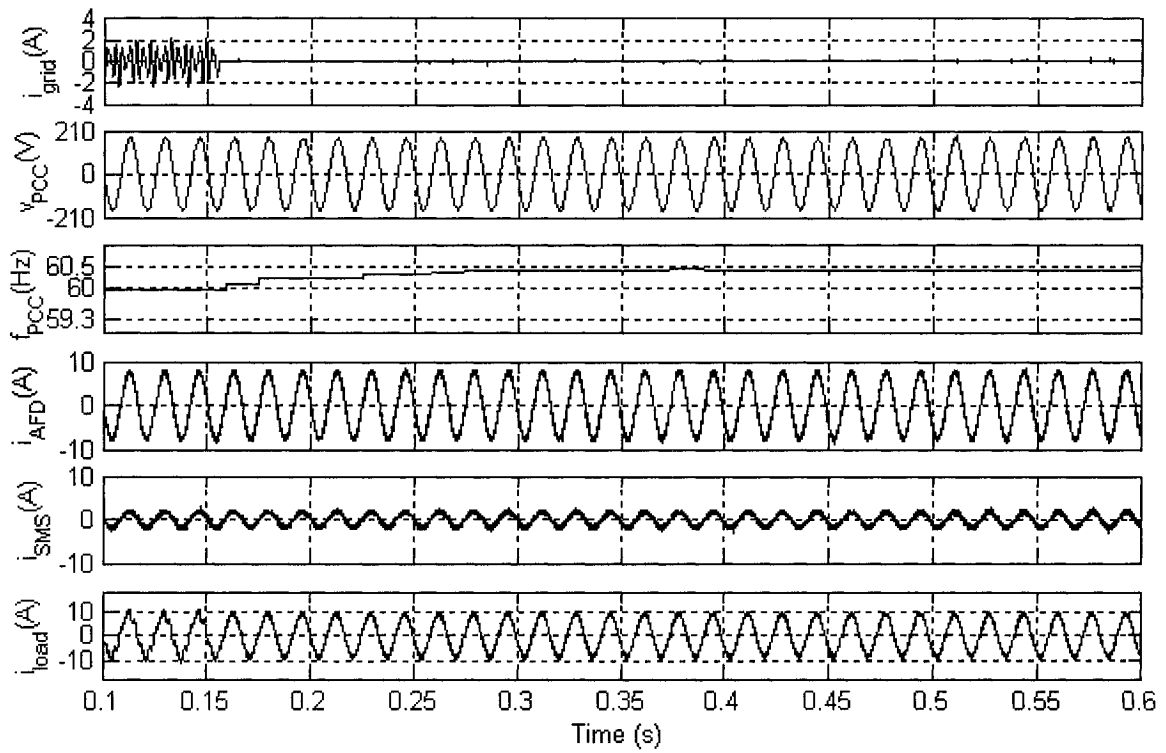
(c) $K_{AFD\,pu}$=0.8 for the load at testing point A

Fig. 2-18 Experiment results for a system with AFD and SMS IDM inverters with different power share $K_{AFD\,pu}$ with load f_0 =59.8 Hz, Q_f =3

53
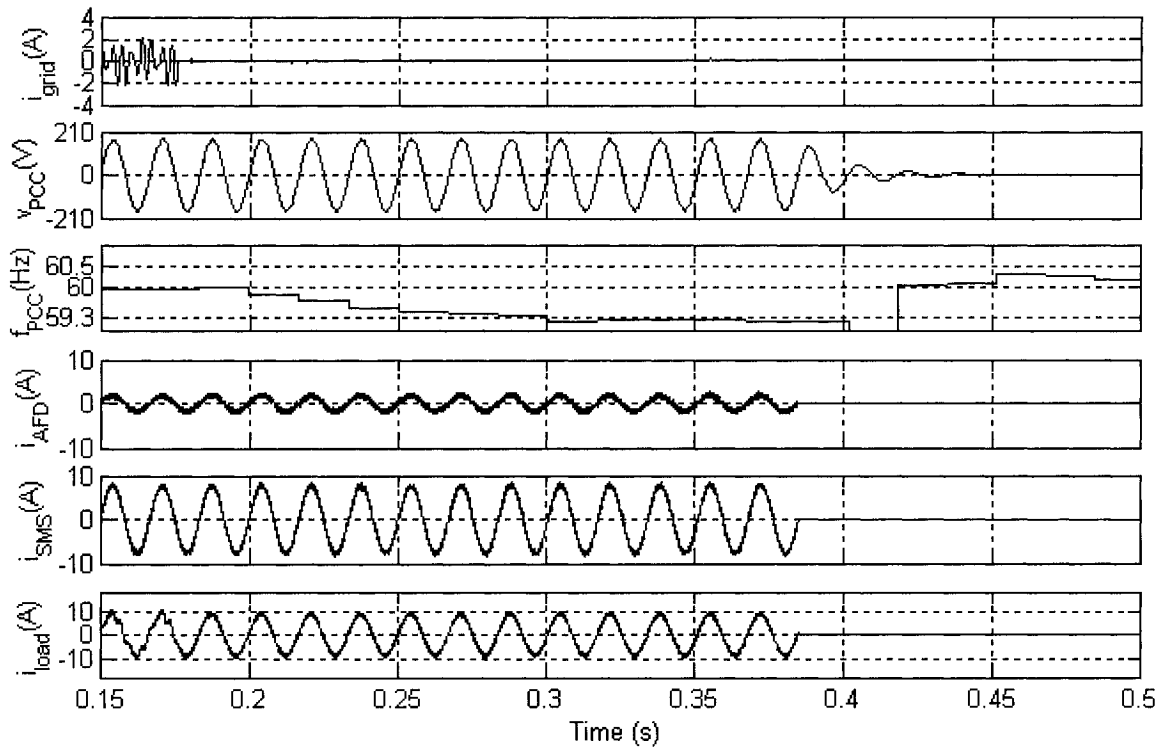
(a) $K_{AFD\ pu}$=0.2 for the load at testing point B

(b) $K_{AFD\ pu}$=0.5 for the load at testing point B

54
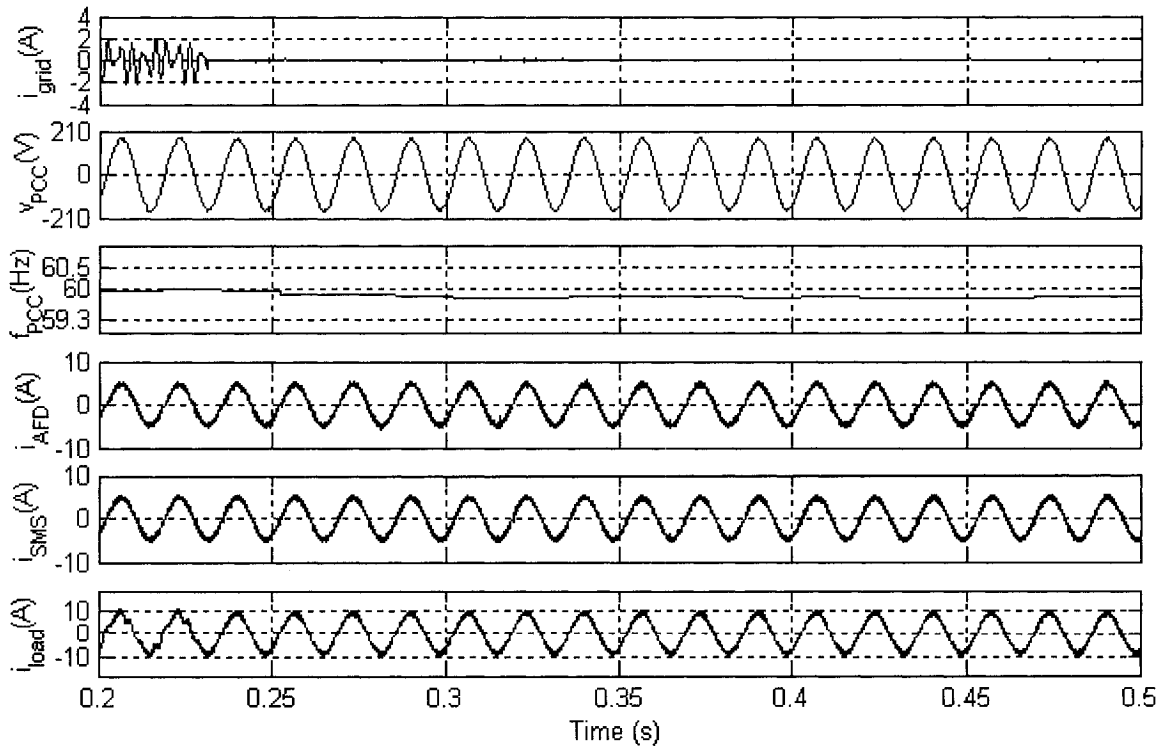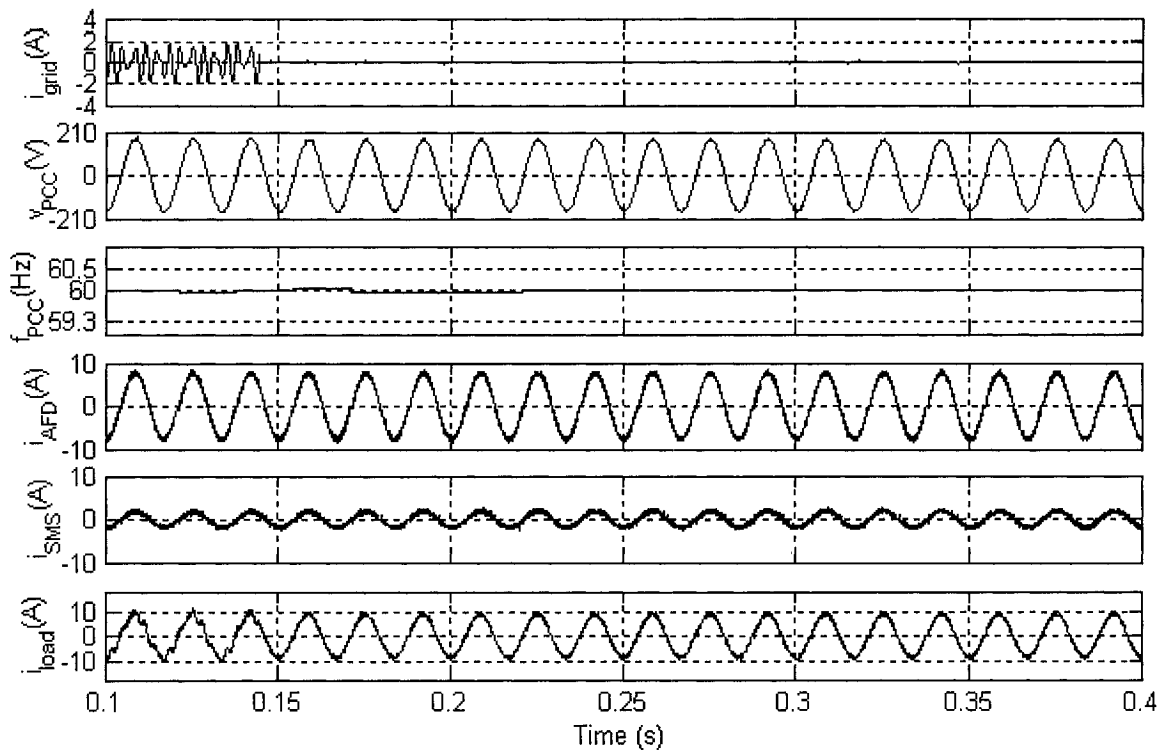
(c) $K_{AFD\ pu}$=0.8 for the load at testing point B

Fig. 2-19 Experimental results for a system with AFD and SMS IDM inverters with different power share $K_{AFD\ pu}$ with load f_0 =59.6 Hz, Q_f =3

55
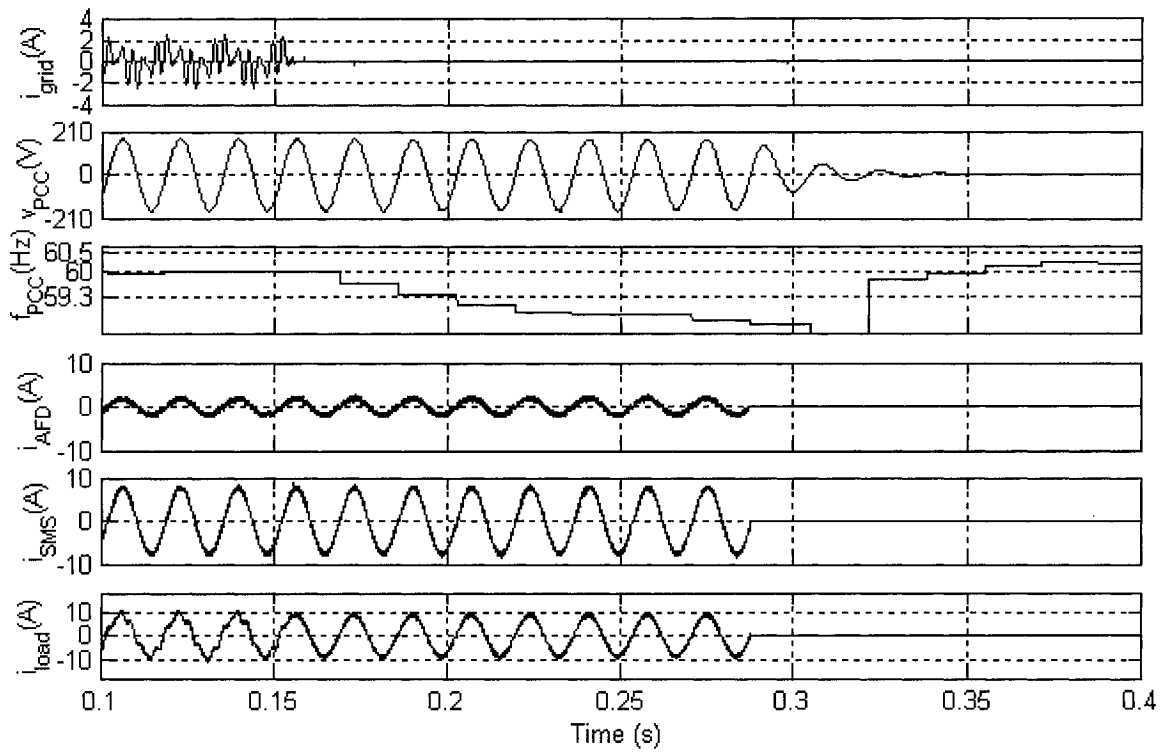
(a) $K_{AFD\ pu}$=0.2 for the load at testing point C

(b) $K_{AFD\ pu}$=0.5 for the load at testing point C

56
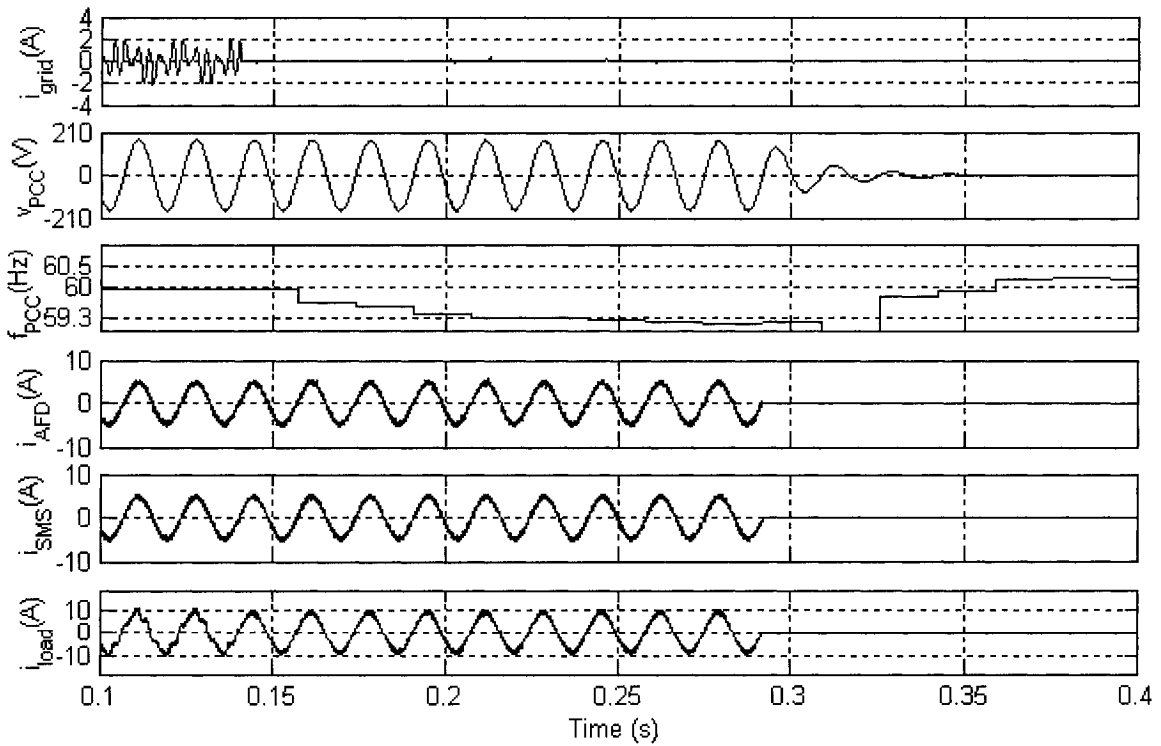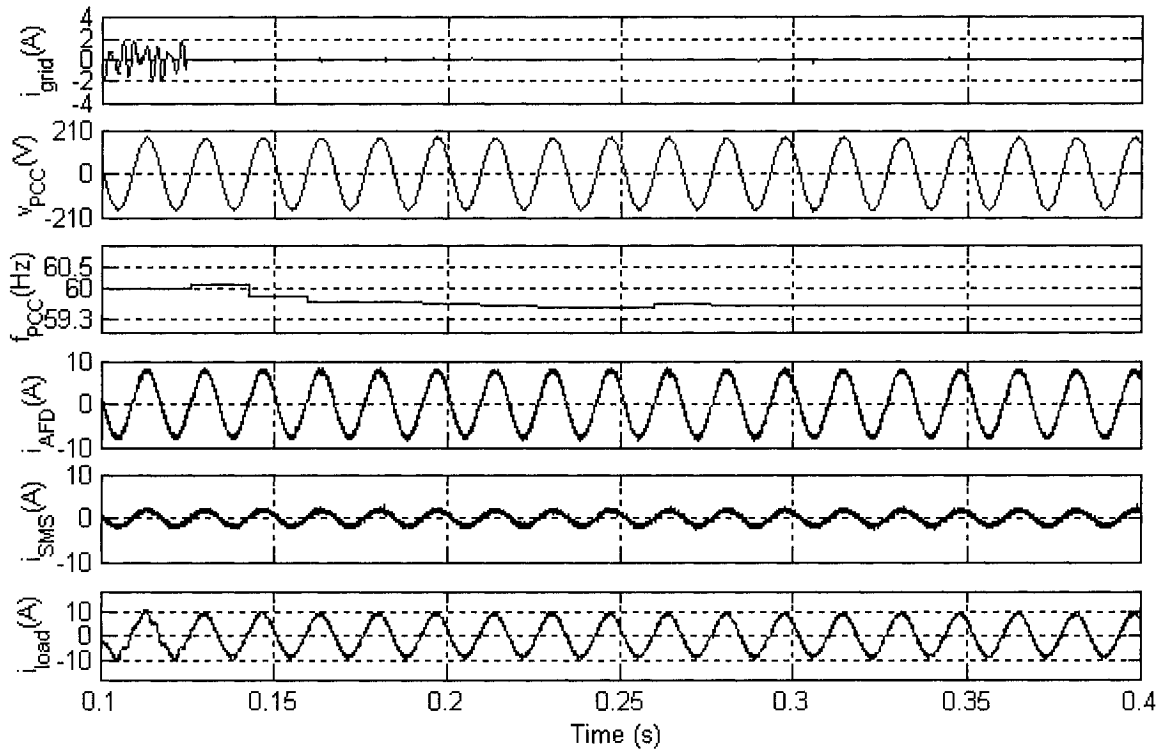
(c) $K_{AFD\ pu}$=0.8 for the load at testing point C

Fig. 2-20 Experimental results for a system with AFD and SMS IDM inverters with different power share $K_{AFD\ pu}$ with load f_0 =59.2 Hz, Q_f =3

2.4.5 TWO SMS IDM INVERTERS WITH FREQUENCY MEASUREMENT ERRORS

At the last test, the load is selected as f_0=60 Hz, Q_f=2.58 as same as the first load mentioned at Section 2.4.3. In the Fig. 2-21 one can see that when Δf_e =0.5 Hz, the system still can detect the islanding and shut down the system at t=1.01s. The results shown in the Fig. 2-22 for a Δf_e =0.8 Hz are accord with the NDZ boundaries theoretic calculation and simulation result.

57
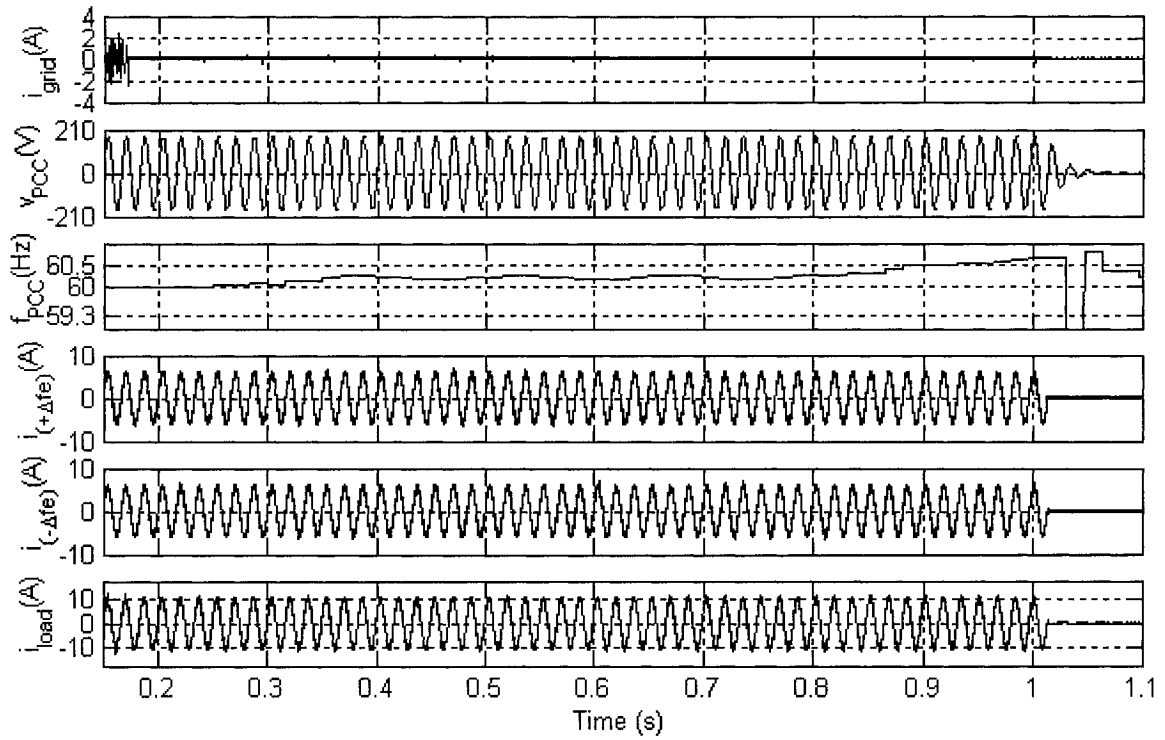
Fig. 2-21 Experimental results for the system with two SMS IDM inverters with Δf_e=0.5 Hz
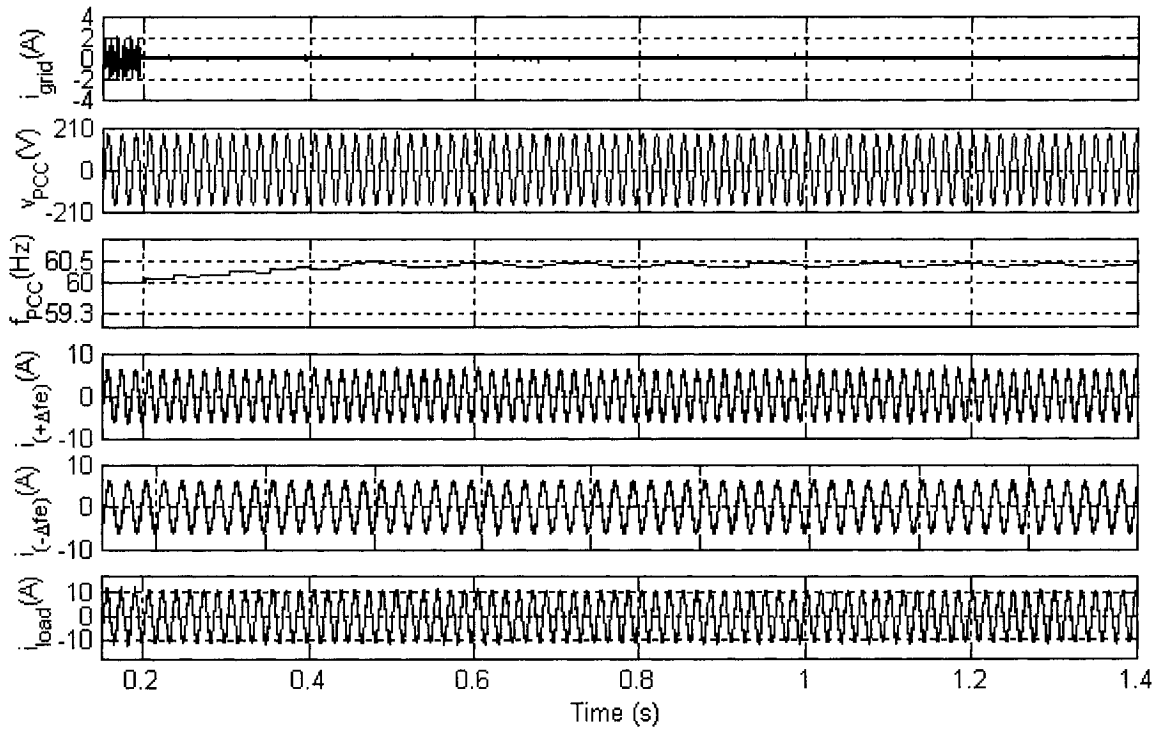
Fig. 2-22 Experimental results for the system with two SMS IDM inverters with Δf_e=0.8 Hz

58

2.5 CONCLUSION

The performance assessment of active frequency drifting IDMs of systems with a single inverter is usually done by means of NDZs in a load parameter space such as the Q_f vs. f_0 space. This chapter has shown that NDZs can also be defined for multi-inverter systems. For systems with multiple active IDM inverters, a new NDZ has to be defined as a function of the type, parameters and rated power of the inverters. On the other hand, the influence of the passive IDM inverters can be represented by an increase on the value of Q_f of the equivalent local load as a function of the share of the load's active power supplied by these inverters (participation factor).

Three cases were presented to demonstrate the use of the proposed approach. It was shown that for systems with one type of identical active IDM inverters plus passive IDM inverters, islanding becomes more likely to happen as the share of the load's active power supplied by passive inverters increases. The local load's maximum Q_f for which the active IDM inverter can provide islanding protection decreases proportionally to the participation factor of the passive IDM inverters. In systems with two different types of active IDMs, the NDZ of the combined inverters has to be redrawn. It was shown that when AFD and SMS IDM inverters are employed together, they can offset each other, increasing the NDZ and resulting in islanding for local load conditions which would be nonislanding if only one type of active IDM inverters were used. The effect of frequency measuring errors on the inslanding detection capabilities of a multi-inverter system was investigated for a system with SMS IDM inverters. In this case, the inverters could theoretically attempt to drift the frequency in opposite directions thus offsetting each

59

other and increasing the combined NDZ. It was shown that this is not an issue for practical frequency measuring errors in the order of 0.1 to 0.3 Hz.

CHAPTER 3
THE ISLANDING DETECTION ENHANCER

3.1 INTRODUCTION

The previous chapter has indicated that the assessment of the islanding detection capability of systems with multiple inverters equipped with active IDMs can become very complicated, mostly if they employ different techniques [6-9]. Non-islanding inverters certified for independent operation can interfere with each other averaging their effects out and failing to detect islanding.

A simple and effective way for preventing islanding in multi-inverter systems was proposed in [25]. A switched capacitor placed in parallel with a number of inverters with passive IDM is switched on by a signal supplied by a nearby substation when the grid is disconnected. As a result, the system frequency drifts down, tripping the inverters' UFP. Means for identifying grid disconnection are not clearly discussed. In principle a transfer circuit breaker could be used for a segment of the distribution system supplied by a single feeder. However, if the segment can be supplied by multiple feeders capacitors could be erroneously switched on, even when the power system was not islanded.

This chapter discusses the use of a small dedicated static synchronous compensator (STATCOM) to achieve enough reactive power imbalance, thus islanding detection, in a system with multiple inverters with passive IDM. It is called islanding detection enhancer (IDE) and its reactive power is varied as a function of the system frequency available locally. The NDZ for a system with one IDE and one unity power factor (UPF) inverter with passive IDM is derived analytically in a load parameter space. An IDE design

61

approach that eliminates the NDZ for loads with a quality factor smaller than a specified value is presented. The effectiveness of the IDE is demonstrated with experimental results for a system with one inverter and by simulation for a multi-inverter system.

3.2 PROPOSED ISLANDING DETECTION ENHANCER

The device proposed in this chapter, the IDE, was conceived for systems with multiple UPF inverters equipped with basic passive IDM. This approach works by changing the shape of the load angle curve so that no stable operating points occur within the normal frequency range. This can be done with a controllable reactive power source / sink such as a STATCOM placed in parallel with the local load.

Its reactive power is controlled with positive feedback as in a PV inverter with a frequency drifting IDM. However, since the STACOM is to be controlled independently of the inverter(s), it is not possible to define a phase angle that represents the active and reactive power injected into the islanded system. Recall that this was the inverter phase angle (θ_{inv}) in systems with an inverter with active IDM. Instead, one should define an modified equivalent load phase angle (θ_{load_eq}), for the STATCOM + local load, and compare it to a fixed inverter angle, $0°$ for UPF passive IDM inverters, for assessing the islanding detection capabilities of this system.

Operated as a STATCOM, the IDE does not consume any real power. Thus the equivalent impedance of IDE is

$$Z_{IDE} = jX_{IDE} = j\frac{V_{PCC}}{I_{IDE}(f)} \qquad (3\text{-}1)$$

where $I_{IDE}(f)$ is the RMS value of the IDE output current.

The equivalent load impedance is

62

$$Z_{load\_eq} = \frac{Z_{load}Z_{IDE}}{Z_{load} + Z_{IDE}} = \frac{1}{\dfrac{1}{R} - j\left(\dfrac{1}{\omega L} - \omega C + \dfrac{1}{X_{IDE}}\right)} = \frac{1}{\dfrac{1}{R} - j\left(\dfrac{1}{\omega L} - \omega C + \dfrac{I_{IDE}(f)}{V_{PCC}}\right)}. \quad (3\text{-}2)$$

Thus the equivalent load phase angle is

$$\phi_{load\_eq} = \arctan\left[R\left(\frac{1}{\omega L} - \omega C - \frac{I_{IDE}(f)}{V_{PCC}}\right)\right] = \arctan\left[Q_f\left(\frac{f_0}{f} - \frac{f}{f_0}\right) + R\frac{I_{IDE}(f)}{V_{PCC}}\right]. \quad (3\text{-}3)$$

The load current voltage (C-V) phase angle (θ_{load_eq}), that represents the angle by which the current leads the voltage, is given by

$$\theta_{load\_eq} = -\phi_{load\_eq} = -\arctan\left[Q_f\left(\frac{f_0}{f} - \frac{f}{f_0}\right) + R\frac{I_{IDE}(f)}{V_{PCC}}\right] \quad (3\text{-}4)$$

From the equation (3-4), one can see that the equivalent load phase angle (θ_{load_eq}) varies as a function of system frequency and different control methods of $I_{IDE}(f)$. Two schemes have been considered for controlling the IDE. These are the linear and the sinusoidal reactive current control methods. In both cases, the reactive current supplied or absorbed by the STATCOM varies with the frequency of the voltage at the bus where the IDE is located.

3.2.1 LINEAR REACTIVE CURRENT CONTROL

The RMS value of the inductive component of the IDE current is controlled according to

$$I_{IDE}(f) = k_{IDE}\left(f - f_g\right) \quad (3\text{-}5)$$

where k_{IDE} is a gain and f_g is the rated grid frequency.

Figure 3-1 shows the phase angle curves of a UPF inverter (0°) and of the modified local load (θ_{load_eq}) (RLC load in parallel with the linear IDE for different factors k_{IDE} and load Q_f, shown from the equation (3-4) For a load with $f_0 = 60$ Hz and $Q_f = 2.5$ that draws 1 kW at 120 V, the modified load angle curve changes from that of the original local load,

63

when $k_{IDE} = 0$, to one with a lower slope, as k_{IDE} increases. For k_{IDE} larger than a certain value, the slope of the equivalent load angle curve becomes negative and smaller than that of the UPF inverter (0°) in the normal frequency range (59.3 Hz to 60.5 Hz). Thus this becomes an unstable operation region when the grid is disconnected and islanding is prevented. The maximum reactive current that the IDE has to deal with continuously occurs at the lower end of the normal frequency range. For a gain $k_{IDE} = 0.75$, this current is 0.525 A. Figure 3-1 also shows the extreme cases ($k_{IDE} = 0$ and 0.75) for a load with $Q_f = 7.5$. Since the slope of this RLC load angle curve is larger than before, the reactive power absorbed by the inverter with the previous values of k_{IDE} is not enough to make the slope of the modified load angle curve become negative. Thus, for a local load with a higher Q_f, a higher value of k_{IDE} is required to make the normal frequency range unstable for islanded operation.

Fig. 3-1 Phase angle curves for the modified local load with the IDE operating with various values of k_{IDE} and loads with $Q_f = 2.5$ and 7. 5

64

3.2.2 SINUSOIDAL REACTIVE CURRENT CONTROL

The RMS value of the inductive component of the IDE current is controlled according to:

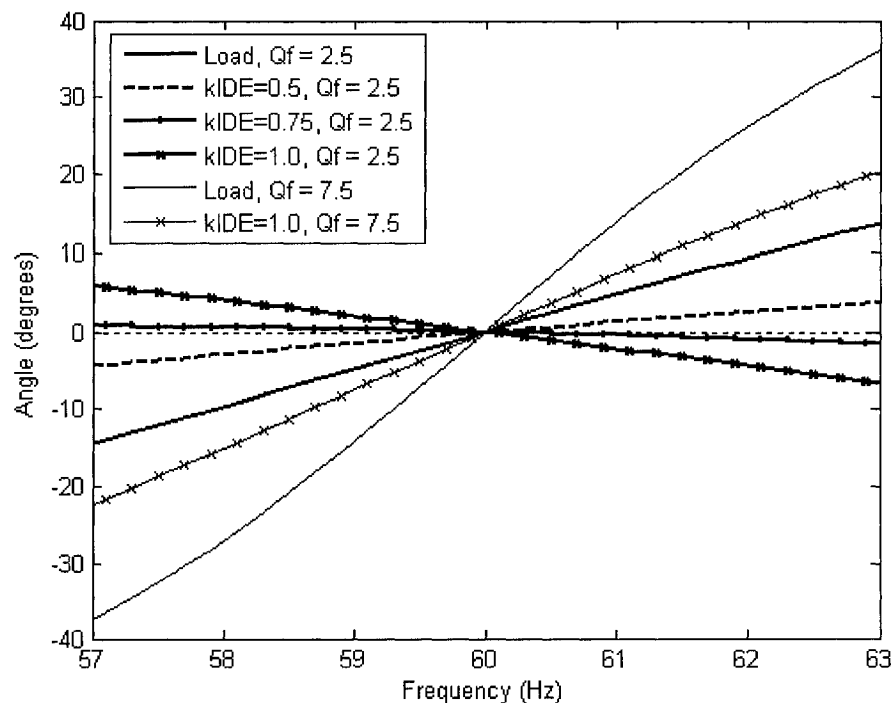$$I_{IDE}(f) = I_M \sin\left(\frac{\pi}{2} \frac{f - f_g}{f_m - f_g}\right)$$
(3-6)

where f_m is the frequency at which the maximum IDE current, I_M, occurs.

Figure 3-2 shows the phase angle curves of a UPF inverter (0°) and of the modified local load (θ_{load_eq}) for different factors I_M and load Q_f. Factor f_m- f_g is taken as 3 Hz as common in SMS IDM. For a load with $f_0 = 60$ Hz and $Q_f = 2.5$ that draws 1 kW at 120 V, the modified load angle curve changes from that of the original local load, when $I_M = 0$, to one with a lower slope, as I_M increases. It becomes negative at $f = 60$ Hz for I_M larger than 1.5 A, thus making the rated grid frequency an unstable operation point for a UPF inverter. For frequencies further above the rated grid frequency, the slope of the modified load angle curve becomes positive again and this curve intersects that of the UPF inverter. These operating points are stable ones but islanding is prevented when they occur outside the normal frequency range (59.3 Hz to 60.5 Hz) since the UFP or the OFP will shut the inverter down. Figure 3-2 also shows that the IDE needs to operate with larger values of I_M if islanding detection is required for a load with $Q_f = 7.5$.

This strategy yields a large $d\theta_{load\_eq}$ /df at rated grid frequency. At the same time, the current that the IDE has to provide at the lower end of the normal frequency is lower than that for a linear relation between I_{IDE} and f with the same $d\theta_{load\_eq}$ /df. Thus, one manages to reduce the power ratings of the IDE.

It should be noted that by reducing the slope of the modified load angle curve, the IDE allows inverters equipped with frequency drifting type active IDMs to detect islanding for

65

loads with Q_f larger than they were designed for. The reduction of the NDZ in such a case is discussed in Section3.5.
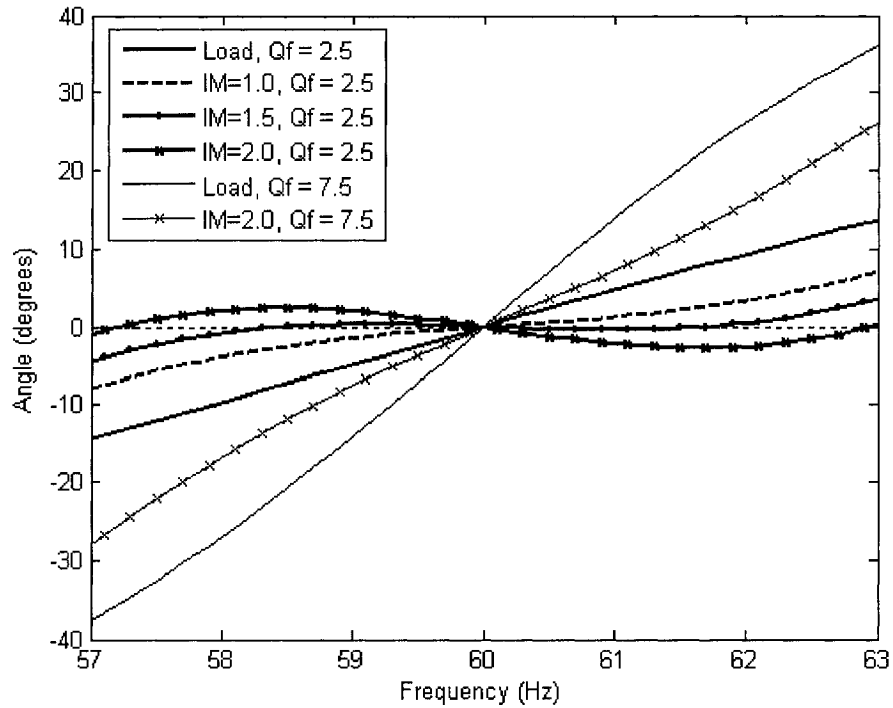
Fig. 3-2 Phase angle curves for the modified local load with the IDE operating with various values of I_M and loads with $Q_f = 2.5$ and 7. 5

3.3 DESIGN OF THE IDE

The design of the IDE consists primarily in determining the required value of the parameter I_M, used in the control strategy, and the rated power of the IDE. The main requirement for the selection of I_M is that all operating points within the normal frequency range of the inverters be made unstable. For inverter resident frequency drifting IDMs, this can be accomplished by making $d\theta_{inv}/df > d\theta_{load}/df$ at the frequencies where the inverter and load angle curves intersect in that range. Since the IDE is to be controlled independently of the inverter(s), one needs a criterion equivalent to $d\theta_{inv}/df > d\theta_{load\_eq}/df$ that is a function of the reactive current of the IDE. Given that the reactive current of UPF

66

inverter(s) is always zero and assuming that the magnitude of the voltages across all elements in the islanded system are the same, reference to the equation (3-4) the criterion can be stated as

$$\frac{d}{df}\left(-\arctan\left[Q_f\left(\frac{f_0}{f}-\frac{f}{f_0}\right)+R\frac{I_{IDE}(f)}{V_{PCC}}\right]\right)<0 \tag{3-7}$$

at the frequencies where the phase angle of the equivalent load is equal to zero.

Calculating the derivatives of (3-5) and substituting in (3-7) one gets

$$I_M>\frac{VQ_f}{R}\left(\frac{1}{f_0}+\frac{f_0}{f^2}\right)\frac{2(f_m-f_g)}{\cos\left(\frac{\pi}{2}\frac{f-f_g}{f_m-f_g}\right)\pi} \tag{3-8}$$

The critical operating point is $f=f_g$, where the reactive currents of the IDE and of a load with $f_0=f_g$ are zero. For f_m-$f_g=3$ Hz and $f_g=60$ Hz, the parameter I_M is given by

$$I_M>\frac{VQ_f}{5\pi R} \tag{3-9}$$

The rated reactive power of the IDE has to be chosen so that it can operate continuously while the grid is connected and the system frequency and voltage are within the normal range. As to (3-5), the highest magnitude of reactive current that the IDE has to deal with the system occurs at the low end frequency (59.3 Hz). This is the furthest point from the rated frequency where the control scheme is centered ($f_g=60$ Hz). Considering the trip point for the OVP of the inverter as 110 % of rated voltage, the rated power of the IDE is given by

$$S_{IDE}\geq 0.028 PQ_f \tag{3-10}$$

Figure 3-3 shows the reactive power of the IDE normalized with respect to the rated load active power, for loads with different resonant frequencies and with $Q_f=2.5$ when $V_g=1.1$ pu. As per the IEEE Std. 929-2000, the inverter's OVP should trip after 120 line

67

cycles at this voltage level. The IDE operates with maximum reactive power for a load with

$f_0 = 60^-$ Hz (59.99 Hz). The normalized reactive power is approximately 0.064 pu and

varies linearly with Q_f. The discontinuity point at 60 Hz is due to the fact that in principle,

the IDE will attempt to drift the system frequency downwards when f_0 of the local load is

smaller than f_g and upwards otherwise. Since the amount of frequency drifting from the

vicinity of the rated frequency required to trip the UFP is larger than to trip the OFP, the

magnitude of I_{IDE} is larger in the first case than in the second.
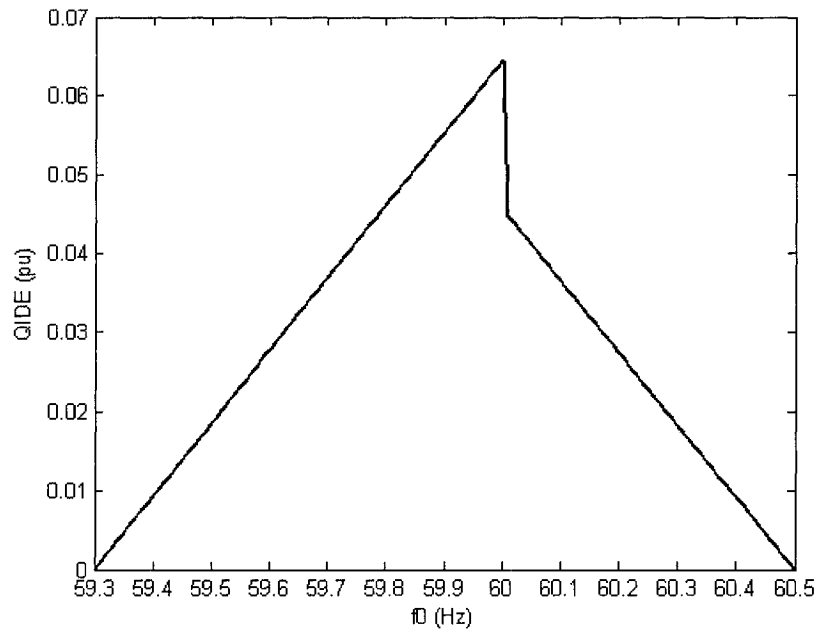
Fig. 3-3 Normalized reactive power of the IDE for loads with $Q_f = 2.5$

As a design example, consider a system where a UPF inverter and a local load with

$P_{rated} = 1$kW, $Q_f = 2.5$ and $f_0 = 60$ Hz are connected to a $V_g = 120$V and $f_g = 60$ Hz grid. One

calculates I_M from (3-9) as 1.46 A, (using a grid voltage of 1.1 pu). The power rating of the

IDE according to (3-10) is approximately 70 VAr or 0.07 pu.

68

3.4 PERFORMANCE ASSESSMENT OF THE IDE

The performance enhancement provided by the IDE can be demonstrated by comparing the NDZ of two cases in a $Q_f \times f_0$ load parameter space [18]. The first case deals with an UPF inverter while the second deals with an inverter equipped with the SMS frequency drifting IDM.

3.4.1 UNITY POWER FACTOR INVERTER AND THE IDE

For the IDE operating with sinusoidal current variation, there will always be a stable operating point. This occurs where the phase angle of the equivalent load is equal to zero. Thus by equating (3-4)

$$I_{IDE}(f) = \frac{VQ_f}{R}\left(\frac{f}{f_0} - \frac{f_0}{f}\right)$$ (3-11)

The boundaries of the NDZ of a system with a UPF inverter and the IDE in the $Q_f \times f_0$ space can be calculated the following way. For a given value of Q_f one computes the values of f_0 for which f equals the limits of the normal line frequency range (f_{min} and then f_{max}) used in (3-11). The operation is repeated for other values of Q_f until the entire range of interest is covered.

Since the NDZ of the proposed scheme is located in the vicinity of the normal line frequency range, one can linearize (3-11) around the limit values of the normal frequency range (f_{min} and f_{max}). By applying the Taylor series to the right hand side term of (3-11)

$$y = \frac{f_{min\_max}}{f_0} - \frac{f_0}{f_{min\_max}}$$ (3-12)

and ignoring quadratic and higher order terms, one finds

$$\Delta y = \frac{dy}{df_{min\_max}} \Delta f_{min\_max} .$$ (3-13)

69

where

$$\left.\frac{dy}{df_{min\_max}}\right|_{f_{min\_max}=f_0} = \frac{1}{f_0} + \left.\frac{f_0}{f_{min\_max}}\right|_{f_{min\_max}=f_0} = \frac{2}{f_0}.$$ (3-14)

Thus, one can simplify the Equation (3-11) by

$$\frac{2}{f_0}\left(f_{min\_max} - f_0\right) = \frac{I_{IDE}\left(f_{min\_max}\right)R}{V\,Q_f}$$ (3-15)

Solving for f_0, one can obtain the following expressions for the maximum and minimum values of the load resonant frequency at the threshold of the NDZ as

$$f_{0\,max} = \frac{2Q_f f_{max}}{2Q_f + \dfrac{I_{IDE}\left(f_{max}\right)R}{V}} \quad \text{when} \quad f_0 > f_g$$ (3-16)

$$f_{0\,min} = \frac{2Q_f f_{min}}{2Q_f + \dfrac{I_{IDE}\left(f_{min}\right)R}{V}} \quad \text{when} \quad f_0 < f_g.$$ (3-17)

3.4.2 INVERTER WITH SMS IDM AND THE IDE

The performance improvement of the proposed IDE to a system with an inverter equipped with an active IDM can also be analyzed and demonstrated in the $Q_f \times f_0$ space. The inverter-resident active IDM considered in this case was the SMS.

Utilizing the phase criteria and assuming that there is no active power imbalance prior to the opening of the grid and that the phase angle of the inverter is small enough, one can obtain,

$$Q_f\left(\frac{f_0}{f} - \frac{f}{f_0}\right) + R\frac{I_{IDE}\left(f\right)}{V_{PCC}} = \theta_{SMS}$$ (3-18)

From the equation (3-12) and (3-13), one can simplify the equation (3-18) by

$$f_0 = \frac{2Q_f f}{2Q_f + \left[\dfrac{RI_{IDE}\left(f\right)}{V_{PCC}} + \theta_{SMS}\right]}$$ (3-19)

70

Thus the following expressions can be used to calculate the NDZ of such a system in the $Q_f \times f_0$ space

$$f_{0\max} = \frac{2Q_f f_{\max}}{2Q_f + \left[\dfrac{I_{IDE}(f_{\max})R}{V} + \theta_{Iinv}(f_{\max})\right]} \qquad (3\text{-}20)$$

$$f_{0\min} = \frac{2Q_f f_{\min}}{2Q_f + \left[\dfrac{I_{IDE}(f_{\min})R}{V} + \theta_{inv}(f_{\min})\right]} \qquad (3\text{-}21)$$
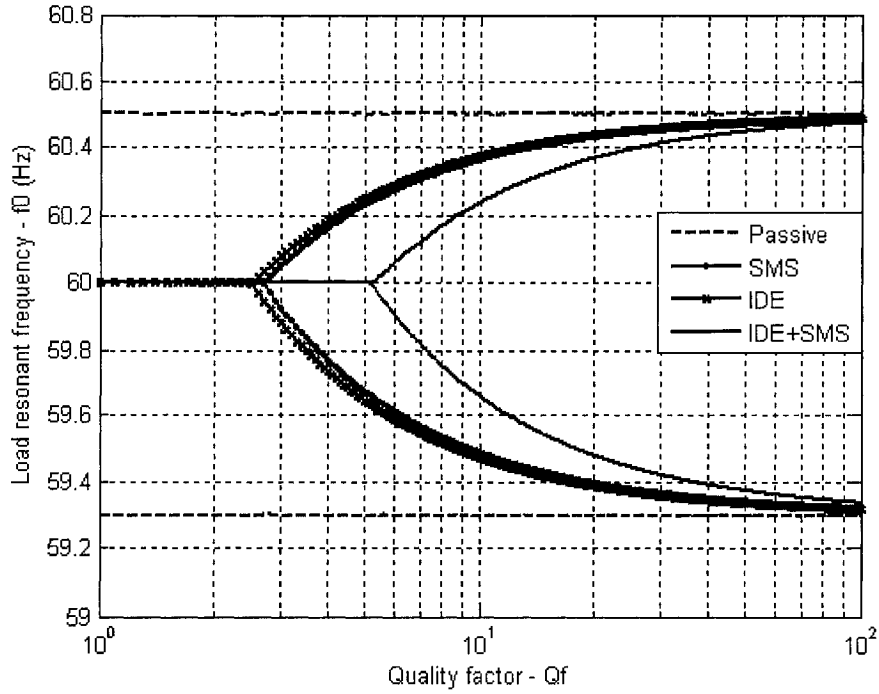
Fig. 3-4 The NDZs of systems with one inverter and different types of IDMs

Figure 3-4 shows the resulting NDZs of four cases. In the first one, there is no IDE, only an inverter with SMS IDM designed for preventing islanding for a load with $Q_f \le$ 2.5 ($\theta_m = 10°$) [18]. The second case refers to a system with a UPF inverter and the IDE designed as in Section3.4. One sees in Fig. 3-4 that the NDZs of these two cases are very similar and null for loads with $Q_f < 2.5$. The NDZ of a system with passive IDM only can

71

be obtained from (3-16) and (3-17) by making $I_{IDE} = 0$. As Fig. 3-4 shows, any loads with resonant frequency in the normal range of line frequency (59.3Hz to 60.5Hz) will result in islanding, irrespectively of the Q_f. Finally, one can see the NDZ of a system where the IDE and the inverter with the SMS IDM are used together. It shows that the IDE can increase the islanding detection capability of the SMS inverter to loads with Q_f of up to 5.1.

3.5 SIMULATION AND EXPERIMENTAL RESULTS

The effectiveness of the IDE is verified by simulation and by a prototype for a system with one inverter and by simulation for a multi-inverter system.

3.5.1 THE IDE IN A SYSTEM WITH ONE INVERTER

The single inverter system described in Fig. 1-2 with an IDE connected in parallel with the RLC load was modeled with MATLAB Simulink as shown in Fig. 3-5. The IDE is represented by a current source that is controlled with a sinusoidal function of the voltage frequency. The reference current block is used to output the inverter's reference current. The UFP/OFP & UVP/OVP block measures the frequency and the RMS value of the PCC voltage, and shuts down the inverter if either the frequency or the voltage at the PCC exceeds the IEEE Std. 929-2000 limits for 6 line cycles.

72
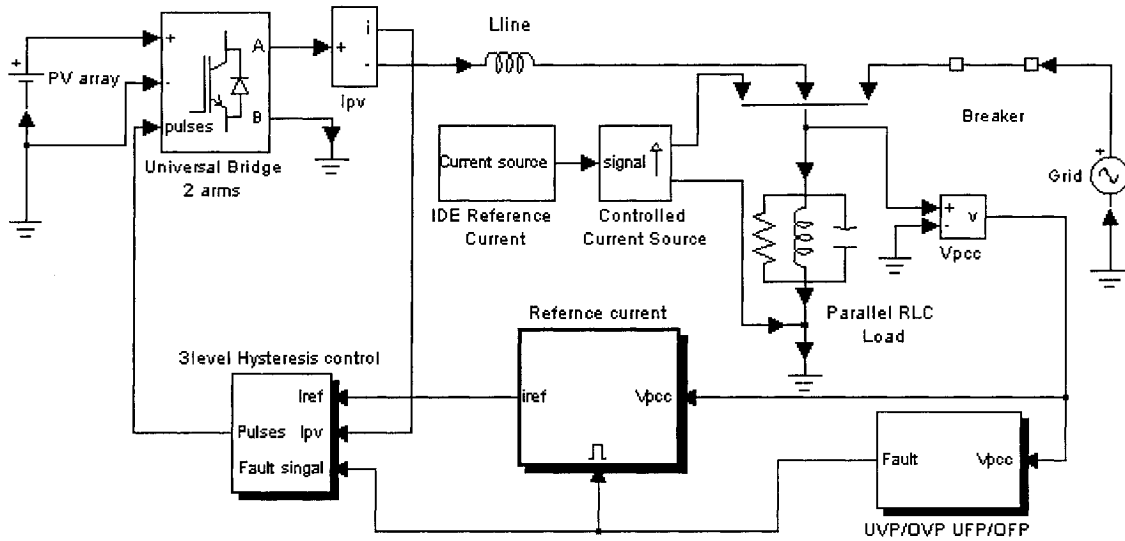
Fig. 3-5 MATLAB-Simulink model of the grid-connected PV system with IDE
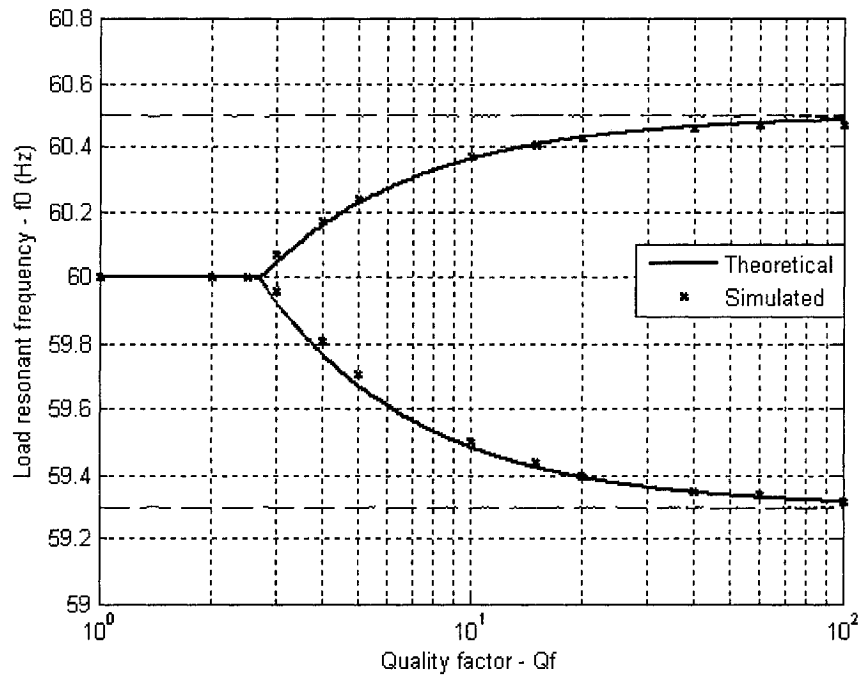
Fig. 3-6 Comparison of the theoretical and simulated NDZs for a system with the IDE and a unity power factor inverter

The validation of the theoretical NDZ of the IDE plus UPF inverter system was carried out by simulating the system designed in Section 3.3 and that was also used to generate

73

Fig. 3-4. Figure 3-6 shows a comparison of the theoretical and simulated NDZs for the case when there is a perfect match between the active power consumed by the load and that supplied by the inverter. The values of L and C used in the simulation were calculated to yield values of f_0 and Q_f close to those predicted by the theoretical analysis for failure of the IDM. As one sees from Fig.3-6, the agreement between the theoretical and the simulation results is very good.

A 1 kW system was implemented to validate the theoretical analysis. The UPF inverter and the IDE are implemented with power transistors and are connected to the PCC through 5 mH inductors. The RMS value of the ac grid is set to 120 V by a single-phase 5 kVA variable autotransformer that represents the utility grid. Both converters use three-level hysteresis current control with 0.4 and 0.2 A tolerance bands, respectively. The control functions of the inverter and IDE are implemented in a digital signal processor (DSP) development kit (DS-1103, dSPACE) that operates with a sampling frequency of 18 kHz. The local load used in the experiment presents $f_0 = 59.8$ Hz and $Q_f = 2.53$ and consumes around 1 kW at rated voltage and frequency. The inverter operates with unit power factor injecting 8.3 A into the PCC and the factor I_M of the IDE is equal to 1.5 A. Figure 3-7 shows some relevant waveforms. The grid current is mostly composed of low order harmonics that flow through the load (capacitor) while the grid is connected. When the grid breaker opens at t = 0.3 s, the magnitude of the IDE current starts to increase, drifting the frequency downwards until the inverter and IDE shut down at t = 0.47 s. It has been seen in other tests that the system frequency drops to 59.8 Hz when the UVP/OVP & UFP/OFP block and IDE are disabled, which is the load's resonance frequency.

74
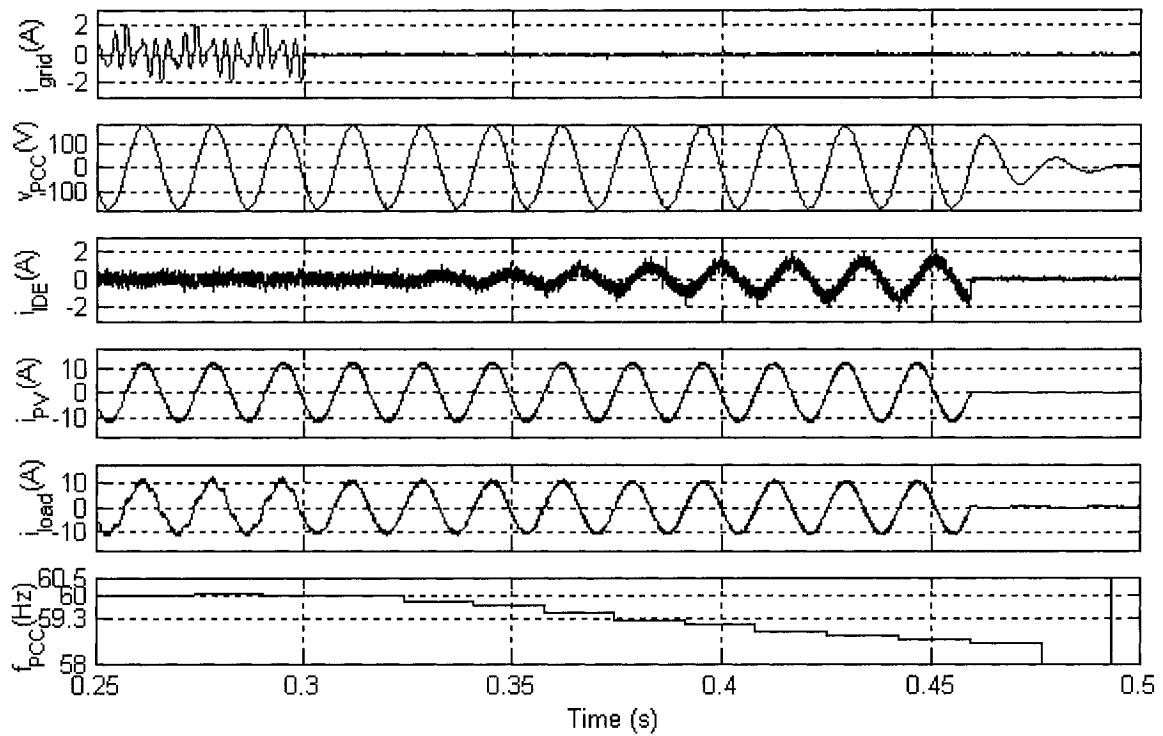
Fig. 3-7 Experimental results for a system with one inverter and the IDE

3.5.2 THE IDE IN A SYSTEM WITH MULTIPLE UPF INVERTERS

The system considered for verifying the performance of the IDE when multiple independently-controlled UPF inverters are used is shown in Fig. 3-8. It represents the low voltage side of a radial residential distribution system supplying five homes from a 50 kVA, 14.4/25kV – 120/240 V, 60 Hz pole-mounted transformer. The parameters of the transformer and conductors were obtained from [26]. The lengths of the secondary circuits and of the service drops were assumed to be 100 m and 50 m respectively. The inverter and load characteristics assumed for the houses are shown in Table 3. There one can see cases with shortage and others with surplus of active power. The IDE (I_M = 20 A, f_m- f_g = 3 Hz and Q_{IDE} = 1050 VAr) was designed for a 15 kW power system with Q_f = 2.5.

Figure 3-9 shows some relevant waveforms including the currents of the inverter (i_{PV5}), load (i_{load5}) and service drop (i_5) of house #5. The voltage at all buses is

75

approximately at rated value before the grid breaker opens. After the grid is disconnected, the voltage magnitude decreases to 92% of rated value at all buses because of the overall shortage of active power, and so do the load currents. Nonetheless, i_{load5} is still larger than i_{PV5} with additional active power coming from other inverters through i_5. The IDE starts to supply an increasing amount of reactive power drifting the system frequency downwards. The magnitude of i_5 increases slightly due to the reactive power supplied by the IDE, showing that the IDE affects all inverters in the island. The system frequency keeps decreasing until the OFPs of the inverters trip 6 line cycles after it falls below 59.3 Hz. The energy stored in the load capacitors and inductors is consumed by the load resistors and the load voltage decreases to zero. The measured value of system frequency is irrelevant after the inverters shut down.

A number of cases such as surplus of active power and equivalent loads with resonant frequencies above and below the rated line frequency were simulated. The results were always the same. The IDE was able to drift the frequency of the island outside the normal frequency range when the system power and the quality factor of the equivalent load were below those used in the design of the IDE.

Table 3-Parameters of the inverters and loads of Fig. 3-8

House #	P_{INV} (kW)	P_{load} (kW)	f_0 (Hz)	Q_f
1	1.0	1.0	59.90	2.50
2	5.0	4.0	60.20	2.40
3	3.5	5.0	59.90	2.40
4	2.2	2.0	59.80	2.50
5	2.1	3.0	60.00	1.50
Total	13.8	15	59.95	2.21

76
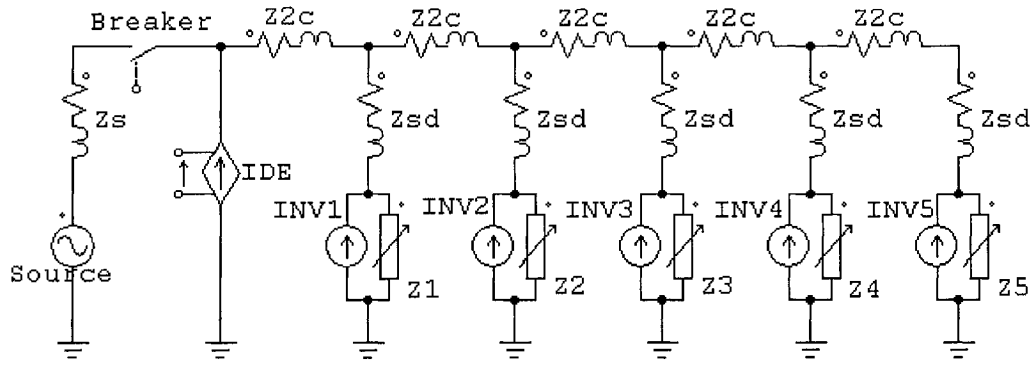
Fig. 3-8 Equivalent circuit of the multi-inverter system
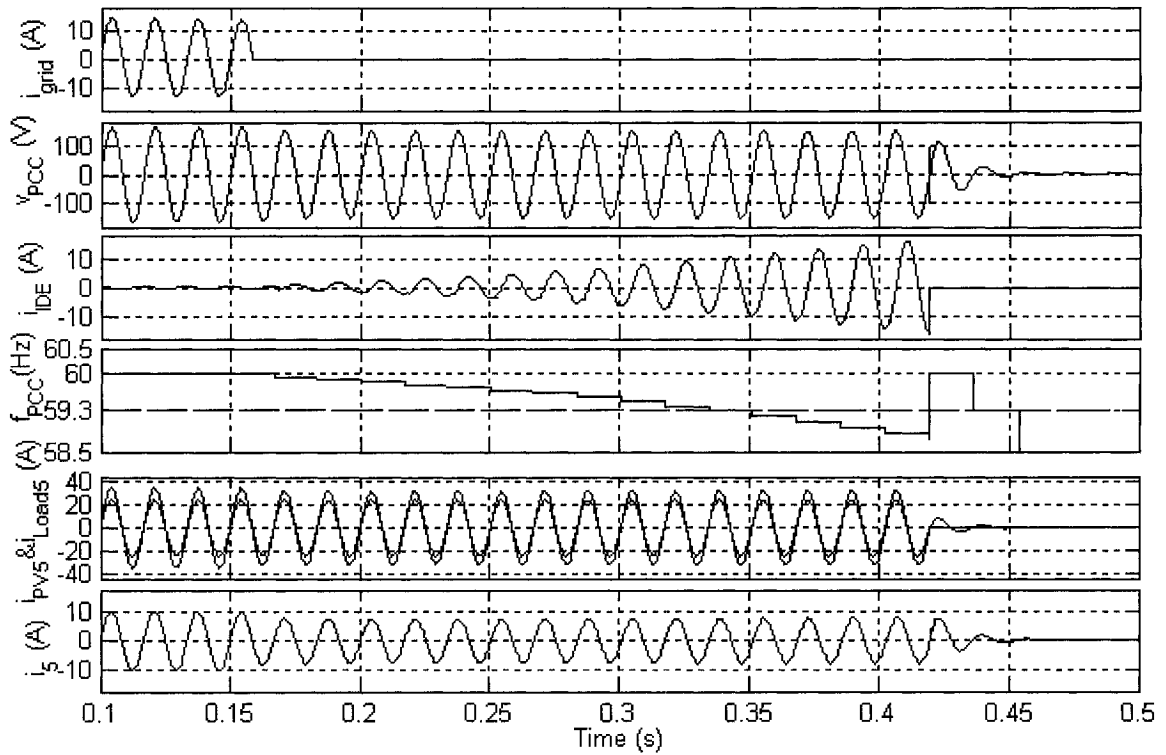
Fig. 3-9 Simulation results for a multi-UPF-inverter system with one IDE

77

3.6 LIMITATIONS OF THE PROPOSED TECHNIQUE

The approach of using a single active frequency drifting device to prevent islanding in a system with multiple passive IDM inverters presents some limitations. The IDE can only cause the shut down, by tripping of the UFP-OFP, of the passive IDM inverters that are connected to it during an islanding condition. For instance, if a breaker/fuse opens in the service line of house #5, that is downstream to the IDE, an island can result if the power imbalances there are small. By small it is meant less than those required for tripping the UVP-OVP and the UFP-OFP of the passive UPF inverter(s). Therefore, the IDE should be located in a position that includes as many possible islands with small power imbalances as possible. In fact, the ideal environment for the IDE would be a building with multiple ac photovoltaic modules [24], some on the roof top others in the façade, and a single load bus.

Another issue is the cost and ownership of the IDE in a system as that of Fig. 3-8. As mentioned in Section3.3, the required size of the IDE depends on the power rating of the active power injecting inverters. It is envisioned that the IDE be deployed in a modular fashion such as in UPSs for telecommunication applications. If more inverters are added to the system, the capacity of the IDE can be easily increased. The cost of the upgrading the IDE could be charged to the owners of the new inverters along with the utility inspection fee that takes place prior to the commissioning of the inverters.

Two of the main concerns of the utilities with inverter based distributed resources are islanding and power quality. There are a few measures that can reduce the harmonic distortion caused by inverters: Operation at high switching frequencies, output filters with large reactors and small capacitors and current references generated internally and not an image of the grid voltage [27]. Although the reference current for some active IDMs, such

78

as AFD, is not a pure sinusoid, the chopping factor (d_f) is selected so that the total harmonic distortion of the injected current (THD$_i$) is very low [10]. The IDE should not present any extra burden on the power quality of the system for a number of reasons. It does not inject any active power into the grid so it will not cause voltage surges. It is implemented with a high frequency self-commutated converter using an internally generated sinusoidal reference current yielding a THD$_i$ lower than that of AFD IDM inverters. Finally, due to its reduced power rating, as compared to the inverters (~ 7%), the magnitude of the current harmonics it injects into the grid is very small and so should be the voltage distortion it causes.

3.7 CONCLUSION

This chapter has discussed the use of a STATCOM as an islanding detection enhancer (IDE) for a system with multiple inverter based distributed resources. It shows that the IDE can be designed to drift outside the normal frequency range the frequency of an islanded system with UPF inverters and load with a quality factor lower than a specified value. Thus a non-islanding multi-inverter system can be implemented with inverters equipped with standard under and over frequency protections. By employing inverters with passive, technology neutral IDM, possible interactions between active IDMs that might interfere with each other, averaging their effects out and thus failing to detect islanding are prevented. The power rating of the IDE is very small, around 7 % of the total active power generated in the island and for a load with quality factor smaller than 2.5 , as considered in the test circuit of the IEEE Std. 929-2000. For compliance with IEEE Std. 1547-2003, where the quality factor of the test load is 1, the power rating of the IDE would be 2.8 %.

Limitations of this technique and issues concerning ownership, upgrade of the IDE and its impact on the power quality were briefly discussed.

CHAPTER 4

CONCLUSION

4.1 SUMMARY

Grid interconnection of photovoltaic (PV) power generation systems has the advantage of effective utilization of generated power. However, the technical requirements from the utility power system side need to be satisfied to ensure the safety of the PV system installer and the reliability of the utility grid. The "Islanding Detection" topic has undergone extensive study and discussion.

This thesis firstly reviews some commonly used IDMs. In order to assess the islanding detection performances of different IDMs, the concept of NDZs was introduced subsequently. The performance of islanding detection of two frequency drifting methods AFD and SMS in a single-inverter system were assessed in detail, utilizing NDZ in the $Q_f \times f_0$ load parameter space based on the phase criteria.

It is believed that in systems with multiple inverters equipped with active IDMs, non-islanding inverters certified for independent operation can interfere with each other averaging their effects out and failing to detect islanding. With increased deployment or even expansion of PV systems, it is very likely that actual islands will contain multiple inverters. Therefore, the second Chapter extends the concept of phase criteria from single-inverter system to multi-inverter system. It shows that NDZ in $Q_f \times f_0$ load parameter space can still be defined for systems with multiple inverters equipped with different types of IDMs. Three possible scenarios that can be found in a system with multiple PV inverters were studied to show how the frequency drift methods average

81

their effects out and fail to detect islanding. It was shown that passive IDM inverters reduce the effectiveness of active IDMs' as their share of the total load power increases. Besides, certain IDMs, such as AFD and SMS, tend to interfere with each other reducing their effectiveness. The shape of the NDZ of this type of system, as well as its size, varies with the power share of the inverters. Finally, it was shown that inverters with the same type of active IDMs present very little interference on each other, thus enabling the shape and size of the individual's NDZ to be extended to the multi-inverter system. The simulation and experiment results were presented to validate the theoretical analysis.

The last issue discussed in this thesis was how to design an islanding detection enhancer for a system with multiple inverters to eliminate the potential islanding in the multi-inverter systems. The performance assessment of the IDE was given. A prototype of the proposed grid connected inverters system has been implemented with a digital signal processing (DSP) and two three-level hysteresis logic controllers. A number of tests that demonstrate the effectiveness of the proposed scheme have been presented.

4.2 SUGGESTIONS FOR FUTURE WORK

1) The assessment of the performance of active frequency drifting islanding detection methods (IDMs) is done by means of non-detection zones (NDZs) in a load parameter space. The phase criterion tells only if the frequency of an islanded system will drift out of the normal frequency range. However, it does not provide any information regarding how long the transient period lasts. The development of a means for calculating this time interval would be very important for the design of fast acting IDMs.

2) The procedure for investigating the interaction of active frequency drifting IDMs could be applied for other combinations of IDMs such as AFD – SFS and SFS – SMS.

82

3) The IDE can only drift the frequency of those inverters that are connected to it during an islanding condition. Therefore, it is important to develop a method for selecting the most appropriate location of the IDE in a system with multiple sources, loads and breakers would. Such a method should be based on known profiles of power generation and consumption in each node of the system.

REFERENCES

[1] Wilsun Xu; Konrad Mauch; Sylvain Martel, "An Assessment of Distributed Generation Islanding Detection Methods and Issues for Canada", CETC Number 2004-074 / 2004-08-03

[2] Nigim, K.A.; Hegazy, Y.G., "Intention islanding of distributed generation for reliability enhancement", PES, IEEE 2003, Volume 4, 13-17 July 2003

[3] W. Bower and M. Ropp, "Evaluation of islanding detection methods for photovoltaic utility-interactive power systems", Task V, Report IEA-PVPS T5-09: 2002, March 2002.

[4] N. Cullen, J. Thornycroft, A. Collinson, "Risk Analysis of Islanding of Photovoltaic Power Systems Within Low Voltage Distribution Networks", International Energy Agency, Report IEA PVPS T5-08:2002, March 2002.

[5] IEEE Std. 929-2000, "IEEE Recommended Practice for Utility Interface of Photovoltaic (PV) systems".

[6] IEEE Std. 1547-2003, "IEEE Standard for Interconnecting Distributed Resources with Electric Power Systems".

[7] Ropp, M.E.; Aaker, K.; Haigh, J.; Sabbah, N.; "Using power line carrier communications to prevent islanding [of PV power systems]", Photovoltaic Specialists Conference, 2000. Conference Record of the Twenty-Eighth IEEE 15-22 Sept. 2000

[8] Kern, G.A., "SunSine300, utility interactive AC module anti-islanding test results," Photovoltaic Specialists Conference, 1997, Conference Record of the Twenty-Sixth IEEE, 29 Sept.-3 Oct. 1997

[9] Ropp, M.E.; Begovic, M.; Rohatgi, A., "Analysis and performance assessment of the active frequency drift method of islanding prevention", Energy Conversion, IEEE Transactions on, Volume: 14, Issue: 3, Sept. 1999

[10] M. Ropp, M. Begovic, A. Rohatgi, G.A. Kern, R.H. Bonn and Gonzalez, "Determining the relative effectiveness of islanding detection methods using phase criteria and nondetection zones", IEEE Transactions on Energy Conversion, vol. 15, Issue: 3, Sept. 2000.

[11] John, V.; Zhihong Ye; Kolwalkar, A.; "Investigation of anti-islanding protection of power converter based distributed generators using frequency domain analysis", Power Electronics, IEEE Transactions on, Volume: 19, Issue: 5 , Sept. 2004

[12] Youngseok Jung; Junghun Sol; Gwonjong Yu; Jaeho Choj; "Modelling and analysis of active islanding detection methods for photovoltaic power conditioning systems", Electrical and Computer Engineering, 2004. Canadian Conference on , Volume: 2 , 2-5 May 2004, Pages:979 - 982 Vol.2

[13] Z. Ye, A. Kolwalkar, Y. Zhang, P. Du and R. Walling, "Evaluation of anti-islanding schemes based on nondetection zone concept," Proceedings of the 34th IEEE Power Electronics Specialist (PESC 2003), vol. 4, 15-19 June 2003, Pages: 1735 – 1741.

[14] Sung-Il Jang; Kwang-Ho Kim, "An islanding detection method for distributed generations using voltage unbalance and total harmonic distortion of current", Power Delivery, IEEE Transactions on Volume 19, Issue 2, April 2004

[15] Vieira, J.C.M.; Freitas, W.; Xu, W.; Morelato, A., "Evaluation of the distributed generators frequency protection due to changes in the anti-islanding requirements", Power Engineering Society General Meeting, 2006. IEEE 18-22 June 2006

85

[16] Jin Beom Jeong; Hee Jun Kim; Soo Hyun Back; Kang Soon Ahn, "An improved method for anti-islanding by reactive power control", Electrical Machines and Systems, 2005. ICEMS 2005. Proceedings of the Eighth International Conference on Volume 2, 27-29 Sept. 2005

[17] Zeineldin, H.; El-Saadany, E.F.; Salama, M.M.A., "Impact of DG interface control on islanding detection", Power Engineering Society General Meeting, 2005. IEEE, 12-16 June 2005 Page(s):1489 - 1495 Vol. 2

[18] Lopes, L.A.C.; Huili Sun, "Performance assessment of active frequency drifting islanding detection methods", Energy Conversion, IEEE Transactions on Volume 21, Issue 1, March 2006

[19] Gwon-jong Yu; Jeong-Hoon So; Young-Seok Jung; Ju-yeop Choi; Seung-Gi Jeong; Ki-Hyun Kim; Ki-ok Lee, "Boundary conditions of reactive-power-variation method and active-frequency-drift method for islanding detection of grid-connected photovoltaic inverters", Photovoltaic Specialists Conference, 2005. Conference Record of the Thirty-first IEEE, 3-7 Jan. 2005 Page(s):1785 - 1787

[20] Huili Sun, "Performance Assessment of Islanding Detection Methods Using the Concept of Non-Detection Zones", Thesis (M.A.Sc.)--Dept. of Electrical and Computer Engineering, Concordia University, 2005

[21] Jeraputra, C.; Aeloiza, E.C.; Enjeti, P.N.; Choi, S., "An improved anti-islanding algorithm for utility interconnection of multiple distributed fuel cell powered generations", Applied Power Electronics Conference and Exposition, 2005. APEC 2005. Twentieth Annual IEEE Volume 1, 6-10 March 2005 Page(s):103 - 108 Vol. 1

[22] Noda, Y.; Mizuno, T.; Koizumi, H.; Nagasaka, K.; Kurokawa, K., "The development of a scaled-down simulator for distribution grids and its application for verifying interference behavior among a number of module integrated converters (MIC)", Photovoltaic Specialists Conference, 2002. Conference Record of the Twenty-Ninth IEEE, 19-24 May 2002 Page(s):1545 - 1548

[23] Woyte, A.; Belmans, R.; Njis, J., "Testing the islanding protection function of photovoltaic inverters", Power Engineering Society General Meeting, 2003, IEEE, Volume 4, 13-17 July 2003

[24] Knaupp, W.; Schekulin, D.; Voigtlander, I.; Bleil, A.; Binder, C., "Operation of a 10 kW PV facade with 100 W AC photovoltaic modules", Photovoltaic Specialists Conference, 1996., Conference Record of the Twenty Fifth IEEE, 13-17 May 1996 Page(s):1235 - 1238

[25] H. Kobayashi, K. Tanigawa, E. Hashimoto, A. Kitamura and H. Matsuda "Method for preventing islanding phenomenon on utility grid with a number of small scale PV systems", Proceedings of the 22nd IEEE Photovoltaic Specialists Conference, 1991, pp. 695 – 700.

[26] Oury, A.; Bergeron, R.; Laperriere, A., "Source impedances of the Canadian distribution systems (residential and industrial)", Electricity Distribution. Part 1. Contributions. 14th International Conference and Exhibition on (IEE Conf. Publ. No. 438), Volume 1, 2-5 June 1997 Page(s):34/1 - 34/8 vol.2

[27] Enslin, J.H.R.; Heskes, P.J.M.; "Harmonic interaction between a large number of distributed power inverters and the distribution network", Power Electronics, IEEE Transactions on, Volume 19, Issue 6, Nov. 2004 Page(s):1586 - 1593

[28] Bode, G.H.; Holmes, D.G., "Implementation of three level hysteresis current control for a single phase voltage source inverter", Power Electronics Specialists Conference, 2000. PESC 00. 2000 IEEE 31st Annual, Volume 1, 18-23 June 2000 Page(s):33 - 38 vol.1

[29] Kato, T.; Miyao, K., "Modified hysteresis control with minor loops for single-phase full-bridge inverters", Industry Applications Society Annual Meeting, 1988., Conference Record of the 1988 IEEE, 2-7 Oct. 1988 Page(s):689 - 693 vol.1

APPENDIX

## THREE-LEVEL HYSTERESIS CURRENT CONTROLLER

A1. INTRODUCTION

Hysteresis current control (HCC) is well-known for its excellent transient response, inherent peak current limiting, stability and robustness under varying load conditions. However, the average switching frequency of the classical two-level HCC is high since at any switching instant, four switches of the bridge switch simultaneously. It has been shown in [28, 29] that three-level HCC can be implemented with the use of zero states when the converter free-wheels the ac current. It is worth mentioning that the reduction in the switching frequency for the HCC due to the use of the zero state(s) is typically larger than that achieved by the unipolar PWM control, which also uses zero states, with respect to the bipolar one.

A2. CONTROL STRATEGY

Figure A-1 shows a full-bridge single-phase voltage source converter (VSC). The switching functions for the converter legs S_A and S_B are defined according to the state of the upper switch of each leg. If U_A (U_B) is ON, S_A (S_B) is 1, otherwise it is 0. The lower switches of each leg operate complementarily to the upper switches to prevent a dc bus short-circuit.

Unlike conventional two-level HCC where the converter switches between the positive state ($S_A S_B = 01$), when the ac current (i) is to increase, and the negative state ($S_A S_B = 10$), when the ac current is to decrease, three-level HCCs also use the zero state

89

$(S_AS_B = 00$ or $11)$. In such a state, the converter flywheels the AC side current whose gradient is determined by the ac source voltage (v_o) and inductor (L).
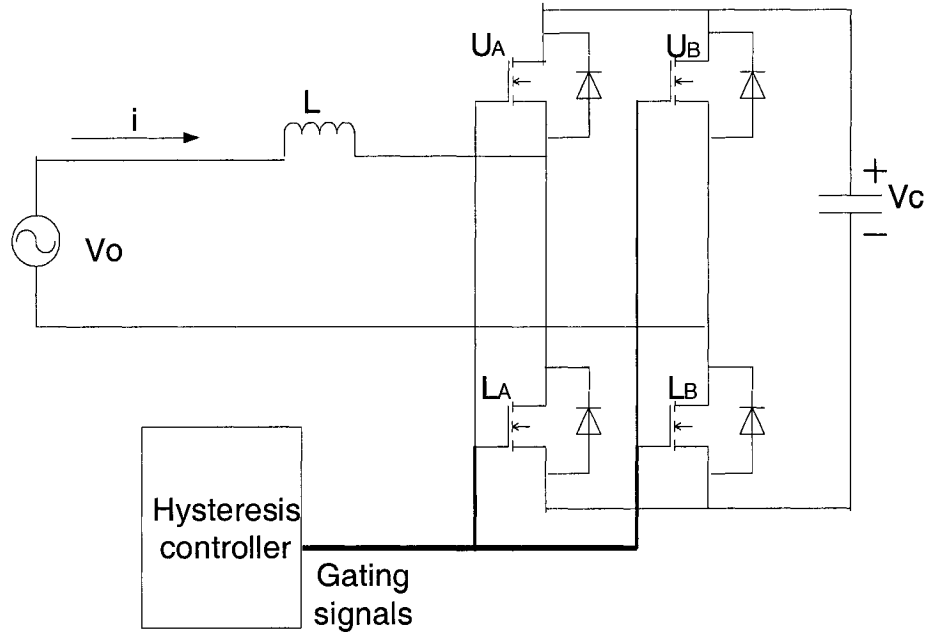
Fig. A-1 Single-phase Voltage Source Converter

The change rate of the ac side current at each converter state is given by

$$\frac{di}{dt} = \begin{cases} \dfrac{v_o + v_c}{L} \text{ at the positive state} \\ \dfrac{v_o - v_c}{L} \text{ at the negative state} \\ \dfrac{v_o}{L} \quad \text{at a zero state.} \end{cases}$$ (A-1)

Recall that for this boost type converter the magnitude of the dc bus voltage must be larger than the peak value of the ac voltage source. As shown by trajectory IJ in Fig.A-2, during a zero state, the trajectory of the ac side current will move towards the upper boundary $(i_{ref} + h)$ when $v_o - L\dfrac{di_{ref}}{dt} > 0$, since the gradient of the ac side current is bigger than that of the reference current i_{ref}. It is worth noting that this statement applies even

90

when $v_o < 0$ and $L\dfrac{di_{ref}}{dt} < 0$ as illustrated by trajectory GH. Similarly, i will move towards

the lower boundary (i_{ref} - h) during a zero state when $v_o - L\dfrac{di_{ref}}{dt} < 0$, as illustrated by

trajectory BC. The three-level hysteresis control logic contemplates four possible crossings

or transitions as shown in Fig.A-2.

- The ac side current increases and crosses the inner upper hysteresis boundary (i_{ref}

+ h). If the converter is in the positive state ($S_A S_B = 01$), the converter will be set to a zero

state (as shown in points B and G). Otherwise, the converter will be set to a negative state

($S_A, S_B = 10$), as shown in point J.

- The ac side current decreases and crosses the inner lower hysteresis boundary (i_{ref}

- h). If the converter is in the negative state ($S_A S_B = 10$), the converter will be set to the zero

state (as shown in point I). Otherwise, the converter will be set to the positive state ($S_A S_B$

= 01), as shown in points A and C.

- The ac side current increases and crosses the outer upper hysteresis boundary (i_{ref}

+ ho). The converter will be set to the negative state ($S_A S_B = 10$), as shown in point H.

- The ac side current decreases and crosses the outer lower hysteresis boundary (i_{ref}

- ho). The converter will be set to the positive state ($S_A S_B = 01$).

It is worth noting that the converter has two zero states: $S_A S_B = 00$ and $S_A S_B = 11$, and

they should occur alternately to prevent that one leg remains idle while the other leg

switches at all transitions. In other words, the HCC control logic should output '00' if the

previous zero state was '11', and vice-versa. In this way, the switching of the four switches

is balanced.

91
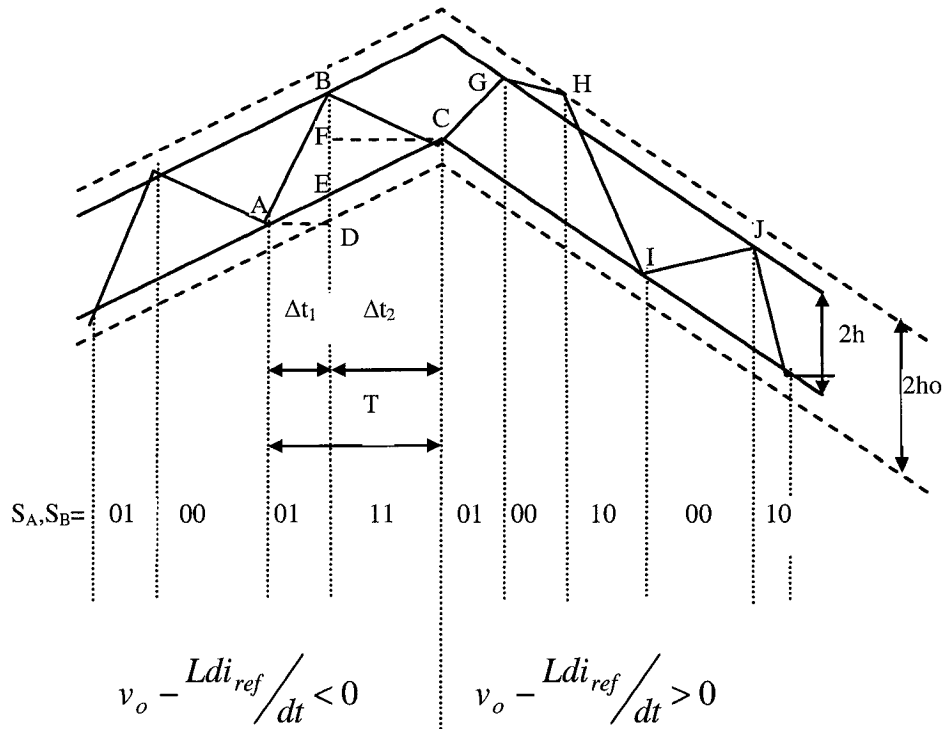
Fig. A-2 Current trajectory of the proposed three-level HCC

A3. IMPLEMENTATION OF THE CONTROL LOGIC

Based on the proposed three-level hysteresis control logic, a sequential state machine has been used to represent this three-level controller, as shown in Fig.A-3. There are two inputs for the state machine: C_{in} and C_{out} which are the logical outputs of the inner and outer hysteresis comparators, respectively. The configuration of the comparators is as follows: C_{in} changes to "1" when the current error reaches the inner upper hysteresis boundary, and changes to "0" when it reaches the inner lower hysteresis boundary. C_{out} changes to "0" when the current error reaches the outer upper hysteresis boundary, and changes to "1" when it reaches the outer lower hysteresis boundary. The output U_A and U_B define the switching states of the converter legs. Moreover they also indicate the next switching state ($S_A S_B$) of the converter. In addition, another state variable S_Z is

92

introduced to denote the latest zero state of the system: $S_Z = 1$: when the latest zero state $S_A S_B = 11$ and $S_Z = 0$: when the latest zero state $S_A S_B = 00$

System States: $S_Z S_A S_B$
Input/Output: $C_{in} C_{out}/U_A U_B$
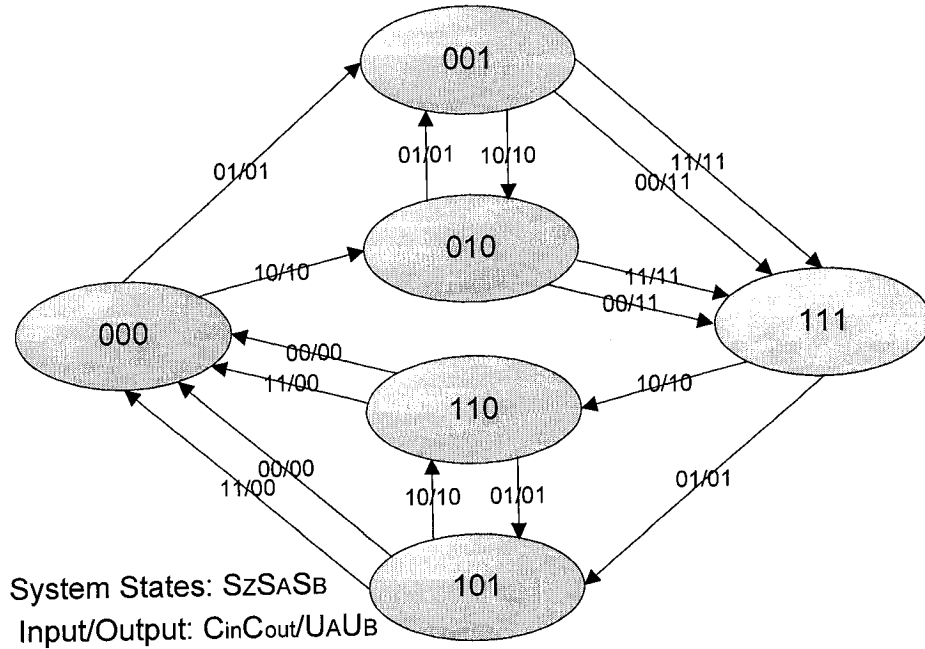
Fig. A-3 Proposed three-level HCC state transition diagram

There are six states in the proposed system. The logic expression of state variable S_Z and output U_A, U_B can be calculated from.

$$S_Z^{n+1} = \overline{C_{in} \oplus C_{out}} \cdot \overline{S_Z^n} + (C_{in} \oplus C_{out}) \cdot S_Z^n$$

$$U_A^{n+1} = \overline{C_{in} \oplus C_{out}} \cdot \overline{S_Z^n} + (C_{in} \oplus C_{out}) \cdot C_{in} \qquad (A-2)$$

$$U_B^{n+1} = \overline{C_{in} \oplus C_{out}} \cdot \overline{S_Z^n} + (C_{in} \oplus C_{out}) \cdot C_{out}$$

The state variable S_Z remains unchanged when the input signals C_{in} and C_{out} are the same; once the two inputs are different, the state S_Z inverses from the previous state to ensure that the two zero states appear alternately. A D-type flip-flop implements this function and balance the switching frequency of the two legs.

93

According to the state and output equations, a simple logic circuit composed of a D-type flip flop, two comparators along with a few logic gates can be used to implement the proposed logic as shown in Fig. A-4.
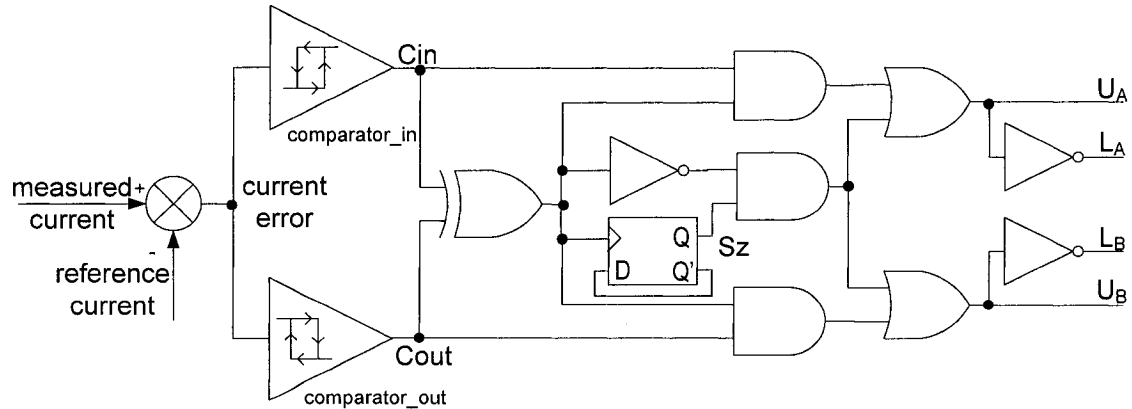

Fig. A-4 Proposed implementation for a three-level HCC

A4. SIMULATION RESULT

A unity power factor rectifier controlled with the three-level hysteresis current controller is tested by simulation using MATLAB/Simulink. The switches are modeled as ideal devices, so the dead time circuits are not used. Fig. A-5 shows the simulation results, including the current waveforms, gating signals generated for the switches U_A and U_B and the resulting operating states of the converter. Here one sees that the gating signals are balanced. This means that the switching balance circuit works as expected and opposite zero states appear alternately. There one can also see that the converter operates alternately with the zero state and negative state between points N and O and the ac side current follows the reference current. At point O, when the ac current reaches the lower inner boundary, the state of the inverter changes from 10 to 11. Between points O and P, the slope of the reference current becomes less negative and the actual current does not reach the upper inner boundary as before. The next crossing between ac current and one of the

94

inner boundaries is again with the lower boundary at point P. Since the outputs of the hysteresis comparators remain unchanged from the previous crossing, no commutations occur at point P and the ac current keeps decreasing. Then, it reaches the lower outer boundary, when the positive state is used to quickly increase the ac current. Similarly, inner boundary crossings without commutations also occur when the reference current is increasing (point M).
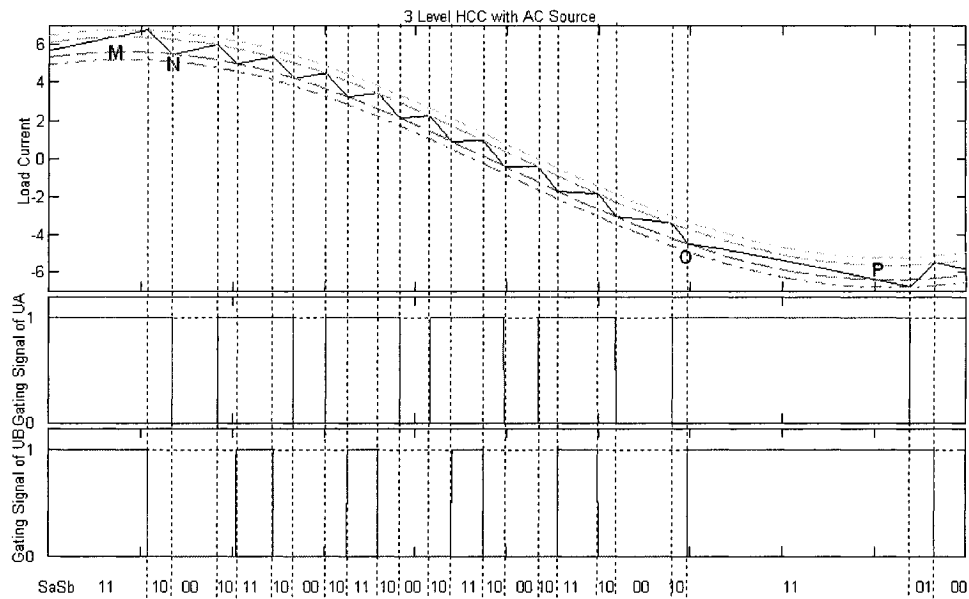
Fig. A-5 Switching patterns for the APF with the three-level HCC